

Storke Memorial Field Course to Peru 2019

Field Guide

Lamont-Doherty Earth Observatory/Columbia University

Organizers:

Bar Oryan Elise M. Myers

Table of Contents

| <i>Title</i> | <i>Page Number</i> |
|--|--------------------|
| Ancient Andean Culture ~ <i>Elise M. Myers</i> | 3 |
| Tectonics & Earthquakes in Peru ~ <i>Lucy Tweed</i> | 10 |
| Mountain Building and the Altiplano ~ <i>Kelvin Tian</i> | 14 |
| Lake Titicaca ~ <i>Jonathan Lambert</i> | 21 |
| Marine Life in Peru ~ <i>Elise M. Myers</i> | 26 |
| Terrestrial Biodiversity in Peru ~ <i>Joshua Russell</i> | 33 |
| El Niño/La Niña & Peru ~ <i>Thomas Weiss</i> | 39 |
| Coastal Upwelling & Productivity ~ <i>Nicholas O'Mara</i> | 48 |
| Arc Volcanism in Peru ~ <i>Henry Towbin</i> | 55 |
| Rainbow (Vinicunca) Mountain ~ <i>Jonathan Lambert</i> | 56 |
| Tropical Glaciers ~ <i>Jonathan Kingslake</i> | 61 |
| Peru's Desert and Sand Dunes ~ <i>Bar Oryan</i> | 69 |
| Coastal Geomorphology in Peru ~ <i>Lloyd Anderson</i> | 75 |
| Peruvian Thermal Springs & Salt Mining ~ <i>Chris Carchedi</i> | 81 |

Ancient Andean Culture

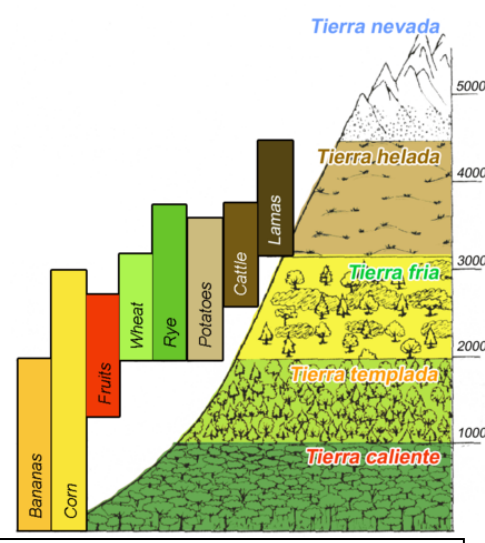
Elise M. Myers

Humans have lived in the Andean region, characterized by proximity to the Andean mountains, for millenia. The general theory for human migration is passage via the Bering Strait from Siberia into North America (Dryomov *et al.* 2015). Divergence between groups of North America and South America occurred around 14.75 kyr (Lindo *et al.* 2018).

In South America, the earliest indication of hunter-gatherers was found to be 12 kyr (*e.g.* Gnecco *et al.* 1997, Aceituno *et al.* 2013). The populations in this area are believed to have transitioned to permanent occupation of the region in the early Holocene (Pearsall 2008), by 7 kyr (Haas *et al.* 2017), signified by a shift to cultivation of plants and the presence of women and children in higher altitude archaeological remains. According to a study by Lindo *et al.* 2018, on ancient human DNA near Lake Titicaca, there was another divergence in populations, this time between low- and high-elevation populations at around 8.75 kyr (Lindo *et al.* 2018). By 7 kyr, there were notable distinctions between the populations, particularly that the high-elevation populations had bigger hearts, slightly higher blood pressure, and the ability to digest starch, a common food at higher elevations (Lindo *et al.* 2018). Despite the genetic divergence, there was frequent contact between highland and lowland peoples, especially as empires shifted over time.

Ancient Andean history is divided into 7 horizons by archaeologists, which are characterized by food sources, population organization, arts, architecture, and geographic ranges (Maestri 2019). Overall, ancient Andean peoples generally had political centers located at higher altitudes, with the kinsmen or citizens settling between a 3-10 days' walk (Paterson *et al.* 2019). The communities outside of the political centrals were often multi-ethnic (*i.e.* belonging to different cultural groups), yet individuals practicing certain professions were shared among various communities, such as salt miners, fishers, gatherers, and cultivators. The system of barter and exchange of good is known as trueque (Moseley 1992). These populations also relied on “minga”, which was a shared labor system that was based on reciprocity (Moseley 200). It is still unknown how there could have been established centers that traded peacefully and allowed for safe caravan transport through different lands (Paterson *et al.* 2019).

To survive the harsh environmental conditions in this region, ancient Andean people also organized themselves in what John Victor Murra coined a “vertical archipelago” or “ecological complementarity” (Murra & Rowe 1984). Different regions along the strong vertical gradient of the Andes had distinct contributions. The coastal desert area was dominated by fishers (of fish, marine mammals, and other marine organisms) and cotton cultivation, some of which was used for nets for fishing (*e.g.* Murra 1985; van Burgen 1995). In these lower altitudes, there was also cultivation of bananas and corn. Higher up in the puna (plateau), at an altitude of 3800 m and higher, there were highly productive



Vertical Archipelago - Wikipedia

fields and terraces, especially near Lake Titicaca. Many tubers were grown here, including the globally known potatoes. In this agricultural region, there were 6-, 8-, and 10-year crop rotations, which replenished nutrients and allowed for continued cultivation. Further up the mountains, llama herders roamed at altitudes above 3900-4000 m. These altitudes did not allow for cultivation, so herders relied on shelf-stable charqui (jerky) and chuño (freeze-dried potato). Black chuño is formed over a 5-day process by exposing frost-resistant potatoes to low night temperatures in the Altiplano to freeze them and then exposing them to intense sunlight. Sometimes the potatoes were crushed to release water and allowed to further dehydrate and become a starchy powder that could be used to thicken stews (Paterson *et al.* 2019). White chuño instead is made by soaking potatoes in icy water for days before sun-drying them. Both forms of chuño were able to keep for years, making them valuable for alpaca herders who would often be far from the puna level where food was cultivated. Charqui was made from a variety of animals, including llamas, and was similarly shelf-stable. Through the vertical archipelago, risks were diversified among the different groups and trade was prevalent. This system of different ethnic groups and multi-ethnic groups was eventually replaced by larger polities like the Inca Empire.

Late Preceramic – 3500 BCE

The Late Preceramic period is the first horizon of pre-Incan populations designated by historians and began in 3500 BCE. Within this period, people began cultivating food, fishing with nets and hooks, building huts, creation of stone tools, milling seeds. There is also evidence of llama and guinea pig domestication during this period. This society initially was split between fishing villages and winter camps. Winter camps were located in the lomas, patches of vegetation outside of the values that received water in the winter season via fog. Lomas were used for cultivation of food and for hunting prey. Eventually, due to climate shifts, the winter camps were abandoned and populations were based only in fishing villages (Paterson *et al.* 2019).



Late Preceramic Empire –
Howling Pixel

Initial (Lower Formative) Period – 1800 or 2100 BCE

The second horizon, the Initial period, is characterized by the earliest ceramics, particularly jars, bottles, and bowls. Timing for this period is defined as either 1800 or 2100, with the range being due to differences in radiocarbon dates. This period saw the first recorded appearance of the double-spouted bottle, common in ancient Andean pottery. Ceramics in this period were decorated with incisions, hatching, stamped circles, and feline figures. There were also ceramics found that were possibly urns for cassava beer. During the period, populations increased reliance on cultivated plants and cotton cloth. Key architectural feats from this time period are La Florida pyramid, the Tank at Ancon, and Las Haldas (Paterson *et al.* 2019).

Early Horizon – 1400 or 850 BCE

In the third horizon, the Early Horizon, art styles changed significantly, expressing the Chavín art styles throughout various populations along the northern coast of Peru. The widespread nature of this art style represented an end of regional isolation for populations and is viewed as a cult

expression (Saikia 2016; Paterson *et al.* 2019). This style of art is seen in painted textiles, pottery, and stone carvings. At about 1000 BCE, Andean highlanders invaded the coastal Carma Valley, allowing them to unify the coast. The Chavín art style linked together the north and center of Peru, from the highlands to the coast.

In the southern Peruvian coast, there was a distinct population, noted by their lack of incorporating the Chavín art style. Pottery found in Paracas from this horizon was unique, characterized by the common closed globular vessels with a flattened base. Further, artifacts from this time period in the south include embroidered textiles and wide-ranging weaving techniques (Paterson *et al.* 2019).

Early Intermediate Period – 200 or 400 BCE

The decline of Chavín's cultural influence marked the beginning of the next horizon where significant artistic and technological advancement occurred. In the coastal regions, Paracas pottery evolved to become Nazca pottery, which incorporated basic life forms, complex demons, and, commonly, exaggerated life forms. In this southern region, the Nazca people wove intricate textiles and also created largescale marvels with their pyramids and Lines (Paterson *et al.* 2019; Saikia 2016). The ceremonial center of 6 pyramids, Cahuachi, still stands today.

Nazca Lines are one of Peru's most famous features. These Lines are found in a region that is 500 square kilometers in area (Paterson *et al.* 2019). By removing the top layers of iron-oxide soil (red/brown), yellow-grey subsoil is left peeking through. The trenches made are 10-15 cm in depth and still can be viewed today (Aveni 1986; Silverman & Brown 1991), primarily because of the aridity of the region. The Nazca Lines depict various life forms, including the condor, a spider, a monkey and a flower. Each of these Lines ranges between 0.4 to 1.1 km in length. Because of the size of these Lines, they are best seen from a plane or helicopter.

During this time period, Moche culture also thrived in the northern region. Architectural feats like adobe pyramids distinguished this culture. Within paintings on pottery and in the architectural layouts, hierarchical states were evident (Saikia 2016). Archaeologists suggest that the dispersed communities were connected through their dependence on the well-irrigated ceremonial centers.



Cahuachi, the ceremonial center of 6 pyramids. *Reuters*



Aerial images of the condor (left, *Wikipedia*) and spider (right, *Aaron Oberlander*) Nazca Lines.



The Doorway God (aka The Smiling God) on an arch at Tiwanaku.
Greg Gerster

Notable changes in populations living in the highland regions also marked the Early Intermediate Period. In the north, the very unique and independently derived Recuay pottery style was developed. Some pottery featured painted running-scroll designs, which hinted at the use of writing. In the southern region, more development was seen in large ceremonial centers near Lake Titicaca. The highly popular attraction Tiwanaku ceremonial center was built during this period. This period also saw the development of semi-subterranean temples with stone heads. The advanced masonry work during this time was held together by very precisely carved notches or by copper clamps in grooves.

Middle Horizon – 600 AD

Massive expansion to 2 major centers of multi-valley political rule marked the Middle Horizon. The Huari (Wari) Empire spread from the north of modern day Peru to Cusco, while the Tiwanaku Empire extended from Cusco through northern Chile. The Huari art styles dominated Nazca and Moche cultures, especially notable in the significant textile work of this period. One of the most notable features is Pachacamac, a great temple that was likely a large town with decent independence within the empire until its fall to the Incan Empire.



Extent of the Huari and Tiwanaku Empires during the Middle Horizon. (*Wikipedia*)

Later Intermediate Period – 1000 AD

Following the Huari Empire, the Chimú state took over the northern region. At this time, bronze and tin production increased, with a tendency towards mass production with simpler designs. Settlements began to include walls, signifying an increased need for defense, and also demonstrated command of canals. Some compounds were scattered throughout large, irrigated areas. One notable feature in Chan Chan, the capital of the Chimú state, was that the ground was lowered in troughs to reach the water table. This was done likely either for water supply or for sustaining plant growth. This period represented a large empire expansion to the coast and south, which was shortly after taken over by the Inca in about the 1460s.



Extent of the Chimú state during the Late Intermediate Period (*LatinAmericanStudies.org*)

The Inca Empire – Tawantinsuyu

The Inca Empire began in about the 1460s and is also known as Tawantinsuyu, which translates to “The Four Parts Together”. The empire extended from modern day Ecuador, Bolivia, and Peru, as well as the highlands of Argentina and Chile. The empire included a large range of multi-ethnic peoples and also encompassed people on both the humid coasts and those in the highlands. By 1532, there were an estimated 12 million people in the empire who spoke 20 different languages.

Largescale projects requiring significant labor distinguished the Inca Empire. For the Cuzco Valley Reclamation, rivers were channeled, the valley floor was leveled, and agricultural terraces were added. This project significantly increased the agricultural production in the empire. Corvée labor was employed for largescale projects like this, as well as military operations and public work projects (e.g. roads, aqueducts, and storage buildings). Laborers would be fed and provided corn beer for the duration of their service (McGovern 2019). The agricultural terraces in Moray (near Cuzco) were created by the Inca Empire for growing various crop types and suggested ecozone optimization for crops (Paterson *et al.* 2019). Machu Picchu, now a World Heritage Site (UNESCO) was constructed around 1450 using this same labor system (Sapp 2015).

The Inca Empire also created their own version of the Pan-American Highway that exists in modern Peru. This highway was over 15,500 miles of roads and is built along the coast and high in the puna grasslands. Along the road, there were thousands of storehouses (*tambos* or *qollqa*) that help food for humans and alpacas, pottery, textiles, etc. Tambos were also used to feed and clothe troops during battle marches, which aided in swift and efficient deployment of armies (“Inca Warfare”).

The Inca Empire employed forced resettlement of populations, which likely was used to ensure Inca support from the people. Populations were thought to be moved to unknown land, taught to accept and value Inca rule before being returned to their lands. Guiding the Inca emperors was a rule that no rulers could inherit property from their predecessor. The new emperor then had to acquire land and labor during their rule (Paterson *et al.* 2019).

Fibers were an essential part of the Incan Empire, both for records and for infrastructure. The quipu (khipi), rope records were used to provide quantitative and historical records. The length of rope, knot placement and size, and



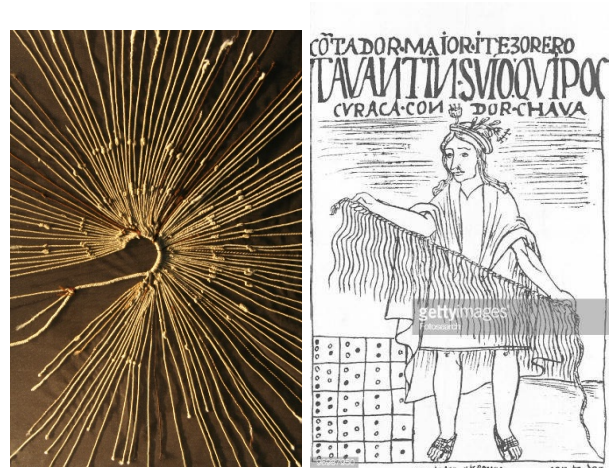
The Inca Empire extended throughout the coastal region and highlands of South America.
Britannica



An example of a recently constructed fiber bridge using the Incan technique.

color of the rope were used as distinctions. Quipus were a portable technology said to document storehouse inventory, population, debts, and more. In Cuzco, quipu bookkeeping records were used by the Spanish to divide the country and populations systematically (Domenici & Domenici 1996; Neuman 2016). Fibers were also used in the construction of suspension bridges. Bridges during this time period could extend over 150 feet, which were much longer than the stone bridges built in Europe at that time. These bridges were built over deep gorges using braided fiber cables of cotton, grasses, saplings, and alpaca wool (Bauer 2006; Wilford 2007).

Ancient Andean populations were highly advanced and proceeded through multiple organizations during their long human history. Prior to the arrival of the Spanish, the Inca Empire was the largest empire in South America (Cartwright 2014) and is an empire to be added to the more commonly known ancient empires: Roman, Ottoman, and Byzantine.



Quipus (left, *Museo Chileno de Arte Precolombino*) and quipu readers (right, *Getty Images*) were essential for bookkeeping in Incan cities.

References

- “Inca Warfare: Battle Tactics.” *How to Peru*, 14 Mar. 2019, <https://www.howtoperu.com/inca-warfare-battle-tactics/>.
- “Vertical Archipelago.” *Everipedia*, Everipedia International, 30 July 2016, https://everipedia.org/wiki/lang_en/Vertical_archipelago/.
- Aceituno, Francisco J., et al. “The initial human settlement of Northwest South America during the Pleistocene/Holocene transition: synthesis and perspectives.” *Quaternary International* 301 (2013): 23-33.
- Aveni, Anthony F. “The Nazca lines: Patterns in the desert.” *Archaeology* 39.4 (1986): 32-39.
- Bauer, Brian S. “Suspension bridges of the Inca Empire.” *Andean Archaeology III*. Springer, Boston, MA, 2006. 468-493.
- Cartwright, Mark. “Inca Civilization.” *Ancient History Encyclopedia*, Ancient History Encyclopedia, 15 Sept. 2014, https://www.ancient.eu/Inca_Civilization/.
- Centre, UNESCO World Heritage. “Historic Sanctuary of Machu Picchu.” *UNESCO World Heritage Centre*, United Nations, <https://whc.unesco.org/en/list/274>.
- Domenici, Viviano, and Davide Domenici. “Talking knots of the Inka.” *Archaeology* 49.6 (1996): 50-56.
- Dryomov, Stanislav V., et al. “Mitochondrial genome diversity at the Bering Strait area highlights prehistoric human migrations from Siberia to northern North America.” *European Journal of Human Genetics* 23.10 (2015): 1399.
- Gnecco, Cristóbal, and Santiago Mora. “Late pleistocene/early holocene tropical forest occupations at San Isidro and Pena Roja, Colombia.” *Antiquity* 71.273 (1997): 683-690.

- Haas, Randall, et al. "Humans permanently occupied the Andean highlands by at least 7 ka." *Royal Society Open Science* 4.6 (2017): 170331.
- Lindo, John, et al. "The genetic prehistory of the Andean highlands 7000 years BP through European contact." *Science advances* 4.11 (2018): eaau4921.
- Maestri, Nicoletta. "Timeline of the Andean Cultures of South America." ThoughtCo, Feb. 18, 2019, thoughtco.com/initial-period-through-late-horizon-172678.
- McGovern, Patrick, professor of anthropology at University of Pennsylvania Museum in Philadelphia www.penn.museum/sites/biomoleculararchaeology/?page_id=147
- Moseley, Michael Edward. *The Incas and their ancestors: the archaeology of Peru*. London: Thames and Hudson, 1992.
- Murra, John V. "The limits and limitations of the 'vertical archipelago' in the Andes." *Andean ecology and civilization: An interdisciplinary perspective on Andean ecological complementarity* 91 (1985): 15.
- Murra, John V., and John Howland Rowe. "An Interview with John V. Murra." *The Hispanic American Historical Review* 64.4 (1984): 633-653.
- Neuman, William. "Untangling an Accounting Tool and an Ancient Incan Mystery." *The New York Times*, The New York Times, 2 Jan. 2016, <https://www.nytimes.com/2016/01/03/world/americas/untangling-an-accounting-tool-and-an-ancient-incan-mystery.html>.
- Pearsall, Deborah M. "Plant domestication and the shift to agriculture in the Andes." *The handbook of South American archaeology*. Springer, New York, NY, 2008. 105-120.
- Saikia, Arnav. "Andean Civilization." *Ancient Civilizations | History Simplified*, AncientCivilizations.com, 29 Jan. 2016, <http://www.ancient-civilizations.com/andean-civilization/>.
- Sapp, William D. "Design, Construction, and Measurement in the Inka Empire." *Architecture and Mathematics from Antiquity to the Future*. Birkhäuser, Cham, 2015. 361-372.
- Silverman, Helaine, and David Browne. "New evidence for the date of the Nazca lines." *Antiquity* 65.247 (1991): 208-220.
- Van Buren, Mary. "Rethinking the vertical archipelago: ethnicity, exchange, and history in the south central Andes." *American Anthropologist* 98.2 (1996): 338-351.
- Wilford, John Noble. "How the Inca Leapt Canyons." *The New York Times*, The New York Times, 8 May 2007, <https://www.nytimes.com/2007/05/08/science/08bridg.html>.

Tectonics and Earthquakes

Lucy Tweed

Andean subduction zone

Peru lies along the convergent margin where the Nazca plate is subducting beneath the South American plate at a rate of 7-8 cm/yr. Subduction begins at the Peru-Chile trench (a.k.a. the Atacama trench), located about 100km off the coast of Peru which reaches a depth of 8km. In front of the trench, but still off-shore is the Pliocene-Quaternary accretionary prism, formed as sediments are scraped off the down-going plate. Peru itself can be divided into three major regions: the Coastal region, the Andes, and the sub-Andes region. These divisions are principally made on the basis of their climatic regimes, however they are also tectonically distinct. The Coastal region is made of the coastal cordillera in the north and south, behind which lies the low-lying central depression which is a fore-arc basin. The Andes are split into the Western Cordillera, the Antiplano, in the south, and the Eastern cordillera. Subduction of the Nazca plate has been active for over 200Ma and is responsible for many geologic features including the Andes mountains, arc volcanism, and

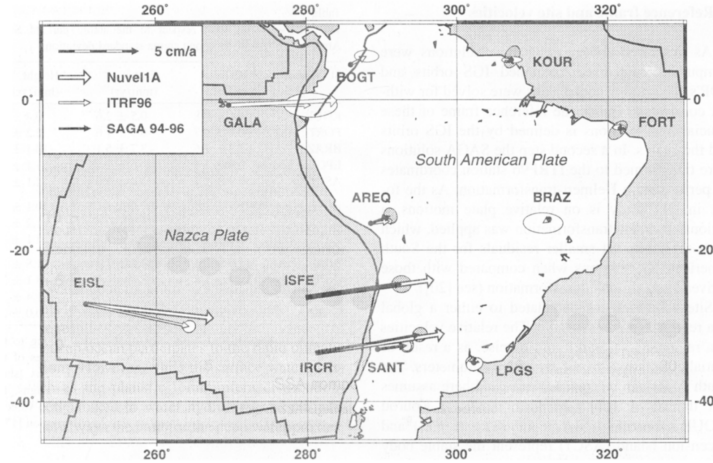


Figure 1: GPS data from four sites in the Nazca Plate (Easter Island, Galapagos, Robinson Crusoe and San Felix Islands) & from five sites in the stable core of the South American Plate used to calculate convergence rate [Angerman et. al., 1999] seismicity.

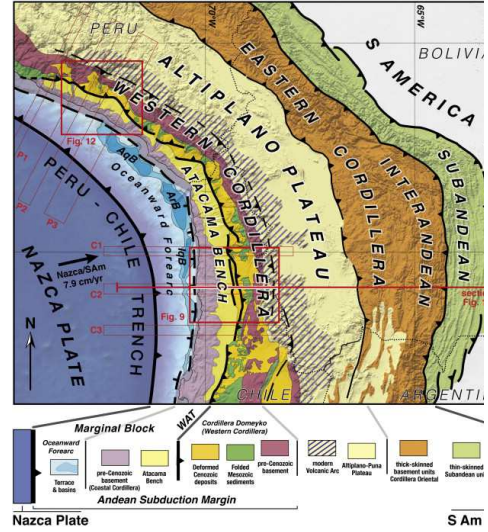


Figure 2: Map showing different tectonic/geological regions in the south of Peru [Armijo et al., 2015]

Peru's subduction zone is anomalous in that in north and central Peru, it is characterized by flat slab subduction where the slab initially subducts beneath the lithosphere, before flattening out into a plateau (Fig. 2), in a stair-step geometry. This transitions into more typical steep slab subduction beneath Ecuador and southern Peru. Unlike steep slab subduction, flat slab regions lack any associated active arc volcanism, and have increased interplate coupling and deformation in the overlying crust. This creates a volcanic gap between 3°S - 15°S where no extrusive magmatism is observed. The causes of flat slab subduction are still debated. One suggestion is that the abnormally thick oceanic crust of the Nazca ridge and the now subducted Inca plateau

contribute additional buoyancy which effectively prop up the subducting plate (Fig. 3). Another

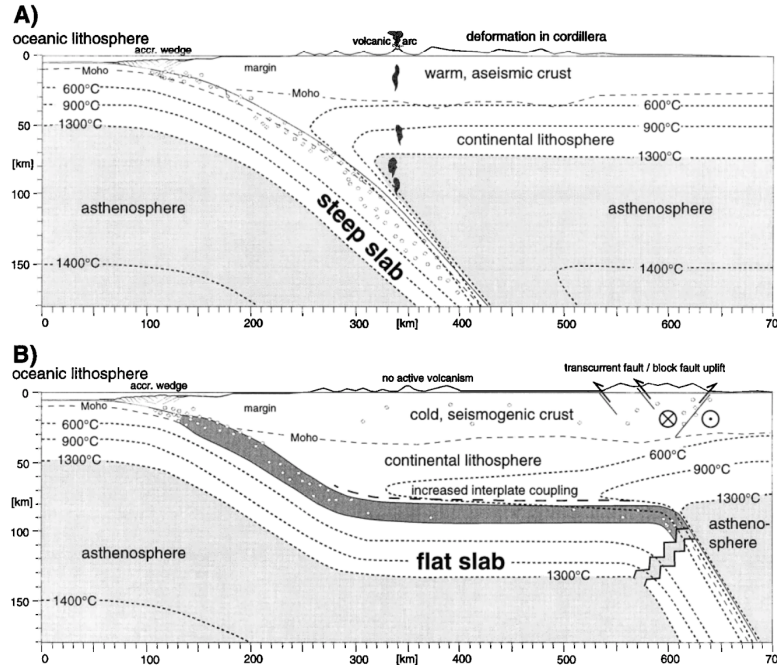


Figure 3: A - geometry and features of typical steep slab subduction. B - Geometry and features of flat slab subduction [Gutscher et. al., 2000]

model is that the flat geometry is a result of roll-back of the slab due to trenchward motion of the thick Amazonia craton. Over time, this roll-back closes the mantle wedge.

Megathrust seismicity

Most of the plate convergence is taken up by slip on the megathrust at the interface between the downgoing slab and the overriding continental lithosphere. Slip is accommodated by a combination of rapid stick-slip earthquakes, episodic slow-slip events, and quasi-static creep. Asperities are regions of the fault that are coupled to the overlying plate, where strain is accumulated (Fig. 5). Eventually these regions rupture causing coseismic slip and the release seismic energy. Coupled regions can be constrained from inversion of high-resolution GPS data. Currently coupled regions, which should correspond to the locations of future earthquakes, are shown in Fig. 6. Interestingly, the Nazca ridge has never been known to rupture in an earthquake and

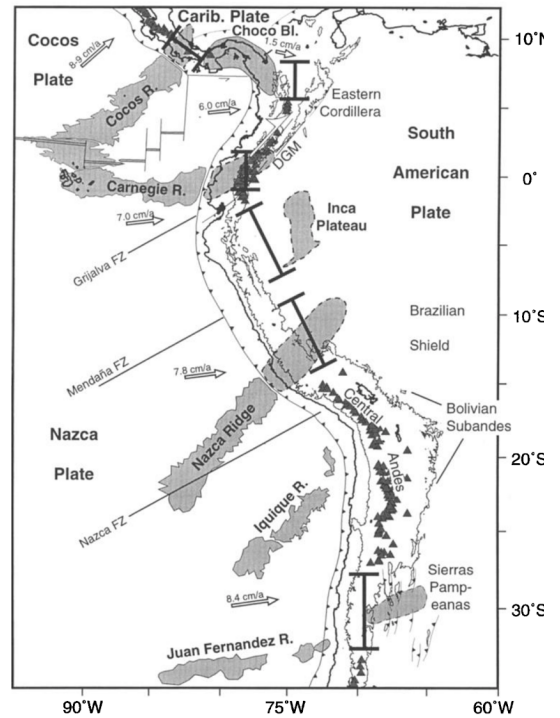


Figure 4: Tectonic setting of the Andean margin with flat slab segments indicated by thick brackets and subducting oceanic plateaus shaded gray [Gutscher et. al., 2000]

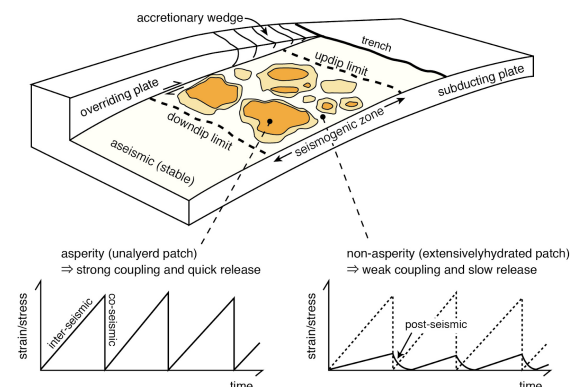


Figure 5: Diagram showing difference in behaviour of coupled (asperities) and uncoupled regions of the subduction zone megathrust

behaves as a barrier to the seismic rupture propagation.

The Andes subduction zone has produced some of the largest known historical earthquakes. Fig. 7 shows some of the largest recent Peruvian earthquakes with many exceeding a 7.5 on the richter scale. These present a major seismic and tsunami hazard, and often result in major fatalities and infrastructure damage. The M8.0 2007 earthquake, which had an epicenter south of Lima, caused 519 fatalities, many of these in the city of Pisco, where 85% of buildings were destroyed, including the cathedral. This was considered to be a once-in-100-years event.

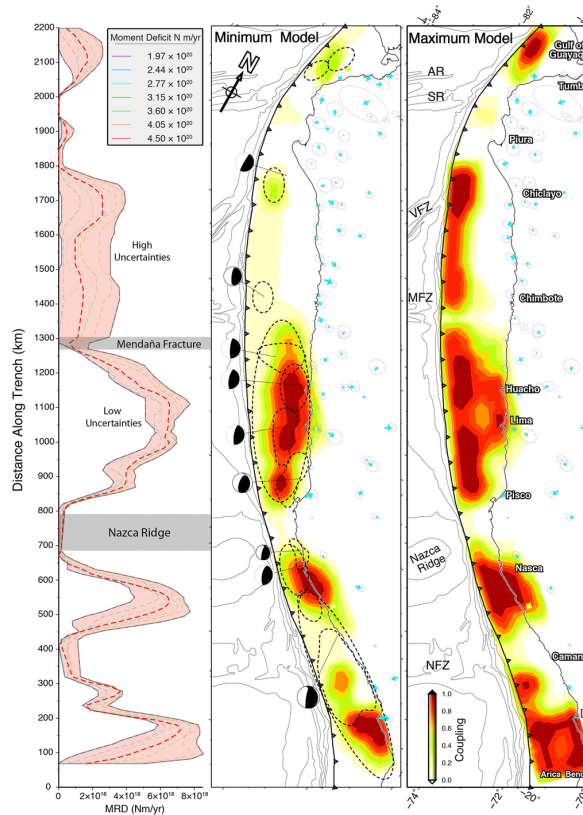


Figure 6: Inferred coupled regions of megathrust with estimated moment deficit (strain energy that has been built up during interseismic deformation) for different slip distribution models [Villegas-Lanza et. al., 2016]

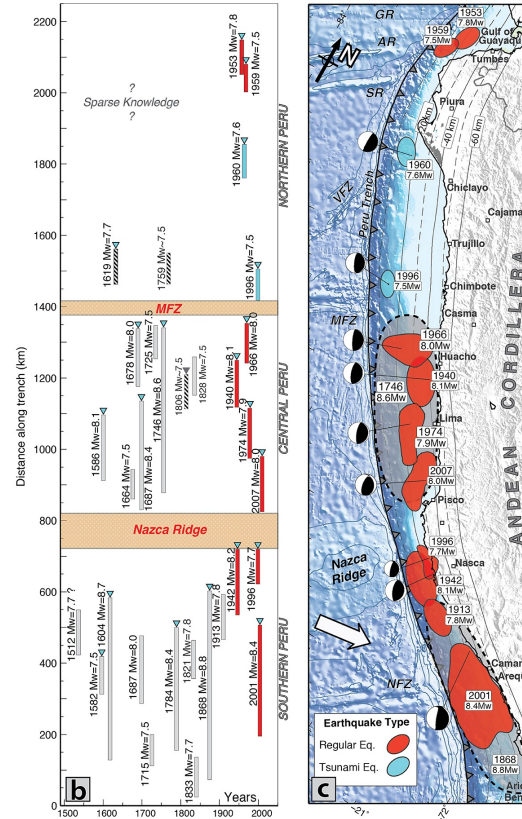


Figure 7: Recent major megathrust earthquakes and tsunamigenic earthquakes and their approximate slip distributions [Villegas-Lanza et. al., 2016]

Interplate seismicity

The Andes subduction zone is a compressive subduction zone in which there is extensive deformation in the overlying plate. Over time this has led to the creation of the Andes mountains. It has been noted that there is increased seismicity above flat-slab regions compared to adjacent steep-slab regions. This has been attributed to the greater contact area between the plates and the cooler temperatures.

Earthquakes in the crust of the upper plate are typically smaller than earthquakes on the megathrust (rarely exceeding M6.0). This relates to the fact that faults are smaller, and less strain is built up. 5% of the total convergence between the plates is taken up by interplate deformation. Earthquakes in the upper crust also show a greater diversity of focal mechanisms, including thrust, strike-slip and normal faults. This is a result of distributed strain partitioning.

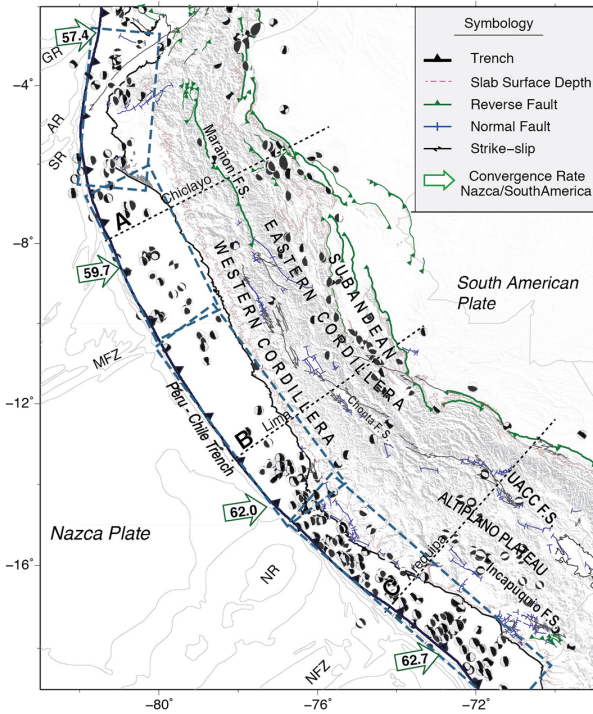


Figure 8: Neotectonic setting of the Peruvian margin showing focal mechanisms for $M > 5$ earthquakes [Villegas-Lanza et. al., 2016]

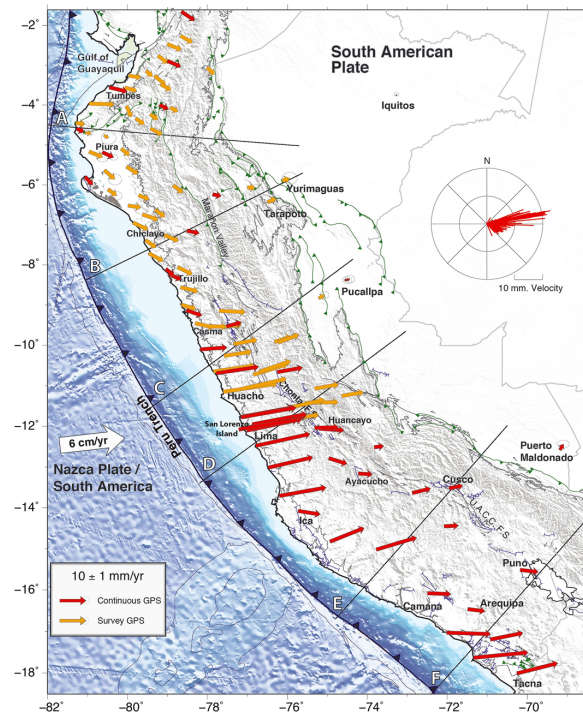


Figure 9: GPS velocity field expressed with respect to the SSA reference frame. [Villegas-Lanza et. al., 2016]

References

- Angermann, D., Klotz, J. and Reigber, C., 1999. Space-geodetic estimation of the Nazca-South America Euler vector. *Earth and Planetary Science Letters*, 171(3), pp.329-334.
- Armijo, R., Lacassin, R., Coudurier-Curveur, A. and Carrizo, D., 2015. Coupled tectonic evolution of Andean orogeny and global climate. *Earth-Science Reviews*, 143, pp.1-35.
- Gutscher, M.A., Spakman, W., Bijwaard, H. and Engdahl, E.R., 2000. Geodynamics of flat subduction: Seismicity and tomographic constraints from the Andean margin. *Tectonics*, 19(5), pp.814-833.
- Perfettini, H., Avouac, J.P., Tavera, H., Kositsky, A., Nocquet, J.M., Bondoux, F., Chlieh, M., Sladen, A., Audin, L., Farber, D.L. and Soler, P., 2010. Seismic and aseismic slip on the Central Peru megathrust. *Nature*, 465(7294), p.78.
- Villegas-Lanza, J.C., Chlieh, M., Cavalié, O., Tavera, H., Baby, P., Chire-Chira, J. and Nocquet, J.M., 2016. Active tectonics of Peru: Heterogeneous interseismic coupling along the

Nazca megathrust, rigid motion of the Peruvian Sliver, and Subandean shortening accommodation. *Journal of Geophysical Research: Solid Earth*, 121(10), pp.7371-7394.

Mountain Building of the Peruvian Andes and the Altiplano

Kelvin Tian

Introduction

According to Wikipedia, the Andean Mountains are the longest above-sea-level mountain range in the world (figure 1). It spans for ~7000 km from about 10°N to 50°S along the western edge of South America. Geographically, it is subdivided into Northern Andes in Venezuela, Colombia and Ecuador; Central Andes in Peru and Bolivia as well as Southern Andes in Argentina and Chile. Our visit sites cover latitudinally from ~11°S (Lima) to ~17°S (Arequipa) within Central Peruvian Andes. The Andes has a width ranging from 200 km to 700 km (widest at around the Peru-Chile boundary ~19°S).

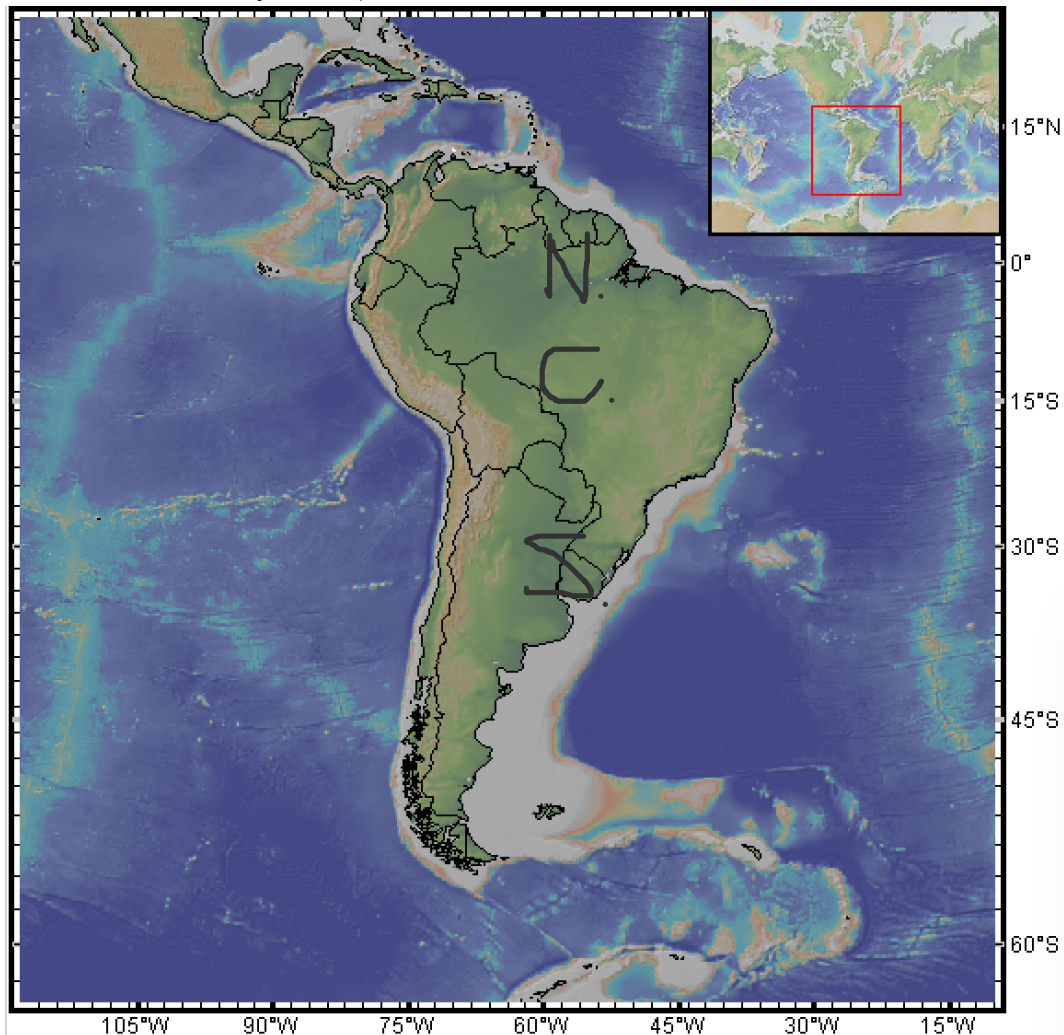


Figure 1. Topography map of South America featuring Andean mountains and country boundaries. From GeoMapApp (Ryan et al., 2009).

The Andean mountains are of great interests to both climate and tectonics studies as they form the only barrier to atmospheric circulation in the S. hemisphere and include the Altiplano plateau, the highest plateau on Earth at a non-collisional plate margin (Gregory-wodzicki, 2000). The Andes are on average 4000 m high similar to the Tibetan Plateau, but form the largest tectonic relief breaking the Earth's surface (13 km vertically) (Armijo et al., 2015). The Argentinean Mt. Aconcagua is the highest mountain outside Asia with an elevation of 6961 m. Due to the centrifugal force from the Earth's rotation, the summit of the stratovolcano Chimborazo from Northern Ecuadorian Andes is the farthest point on the Earth's surface away from the center of the sphere.

Geology

To the first order, the Andean mountains are the results of tectonic processes when oceanic Nazca and Antarctic plates to the West subducting beneath S. American Plate.

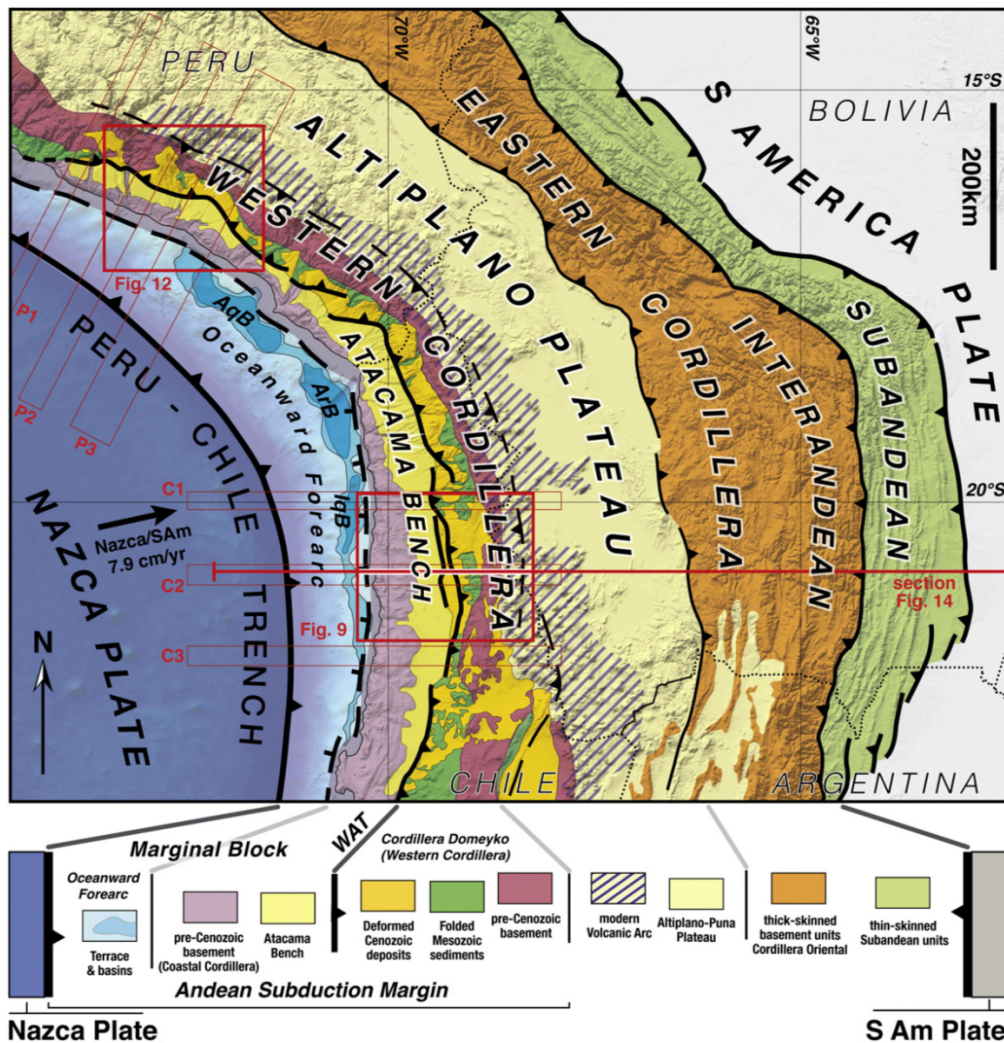


Figure 2. Geological sketch map of Andean orogen. The main morphological-structural units of the bivergent Central Andes (continental region with over-thickened crust constituting the core of the Andean

orogen) are represented within horizontal boundary conditions (converging Nazca and South America plates) (Armijo et al., 2015).

Before the formation of Andes, western rim of S. America has been through several orogenies since late Proterozoic constituting the S. American part of supercontinent Gondwana. Observable Andes have remnants of rifts since Triassic when Pangaea began to breakup. During Cretaceous, modern Andes started to take form by uplifting, faulting and folding. Across the Central Andes, from West to East constitutes several geological units: the Nazca subducting oceanic plate, the Peru-Chile trench, the oceanward forearc, the Coastal Cordillera and the Atacama Bench, Western Cordillera (including Deformed Cenozoic deposits, Folded Mesozoic sediments, pre-Cenozoic basement), modern Volcanic Arc, Altiplano-Puna Plateau, Eastern Cordillera and subandean units (figure 2) (Armijo et al., 2015).

Orogeny

Armijo et al., (2015) reconstruct the orogenic 2D structure of the Andean mountains across 21°S:

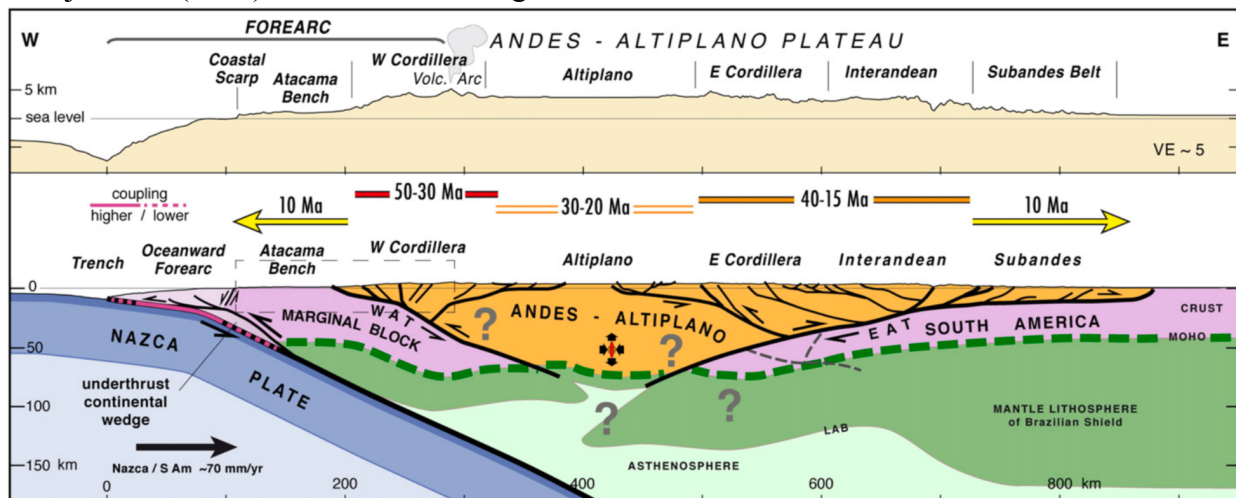


Figure 3. Large-scale 2D structure of Andean orogen. Interpreted section at 21°S, across the southern limb of the Andean orogen. (Armijo et al., 2015)

They further construct the evolution history of the orogeny since 50 Ma with an assumed total shortening of 360 km:

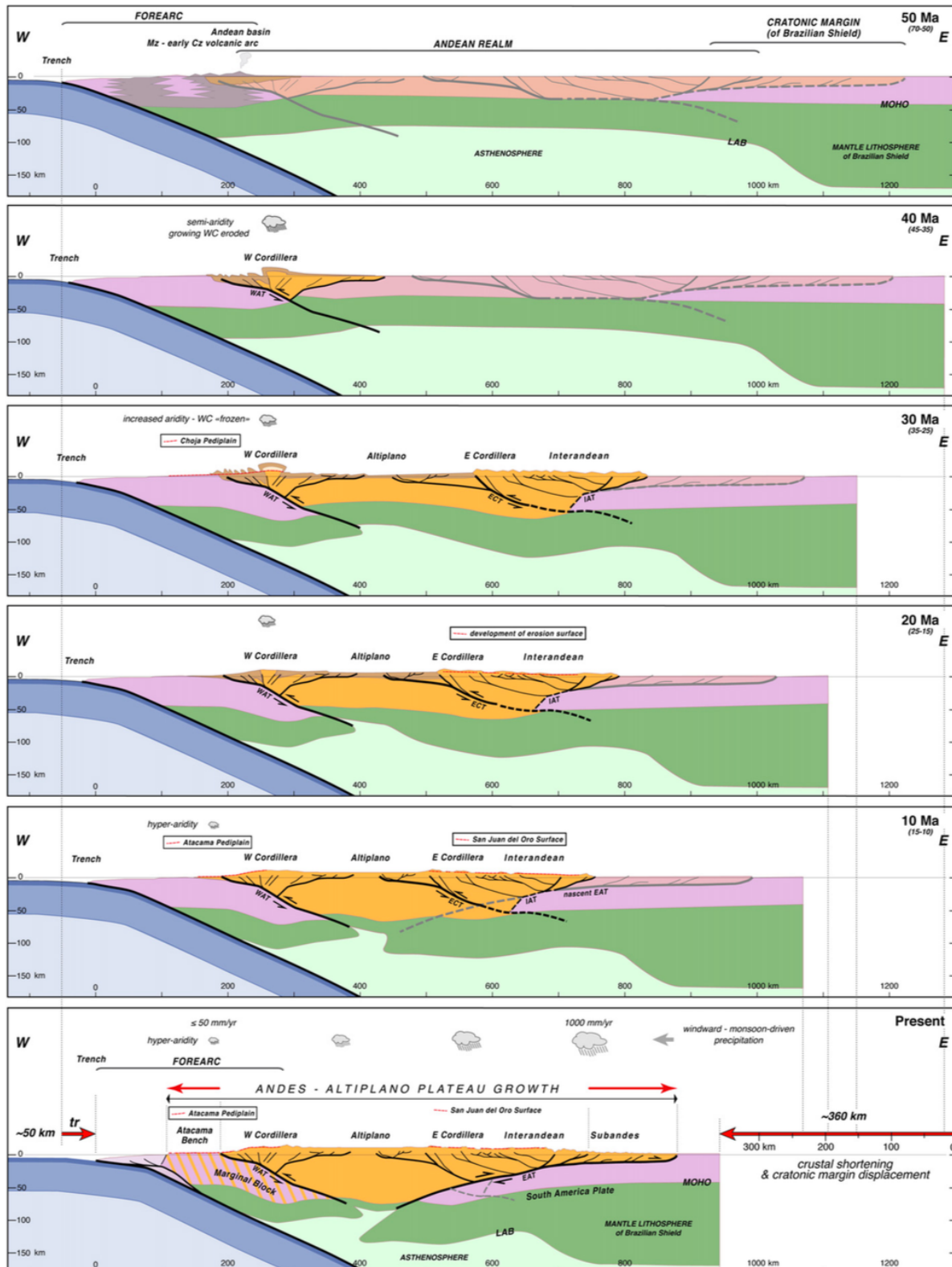


Figure 4. Evolution of Andean orogeny (from 50 Ma to present) (from Armijo et al., 2015). The growth process of the Central Andes is schematically represented for a section at 21°S, across the southern limb of the Andean orogen.

Paleo-elevation

Gregory-wodzicki, (2000) provide a paleo-topography estimates of central Andes by reviewing indicators including upper crustal deformation, marine facies, geochemistry of volcanic rocks, climate from fossil floras, erosion rates, erosion surfaces, fission-track ages, and rates of terrigenous flux:

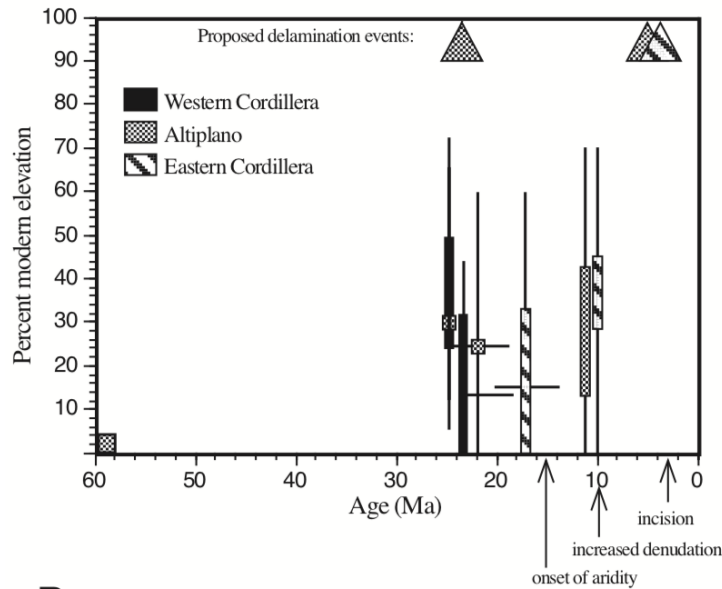


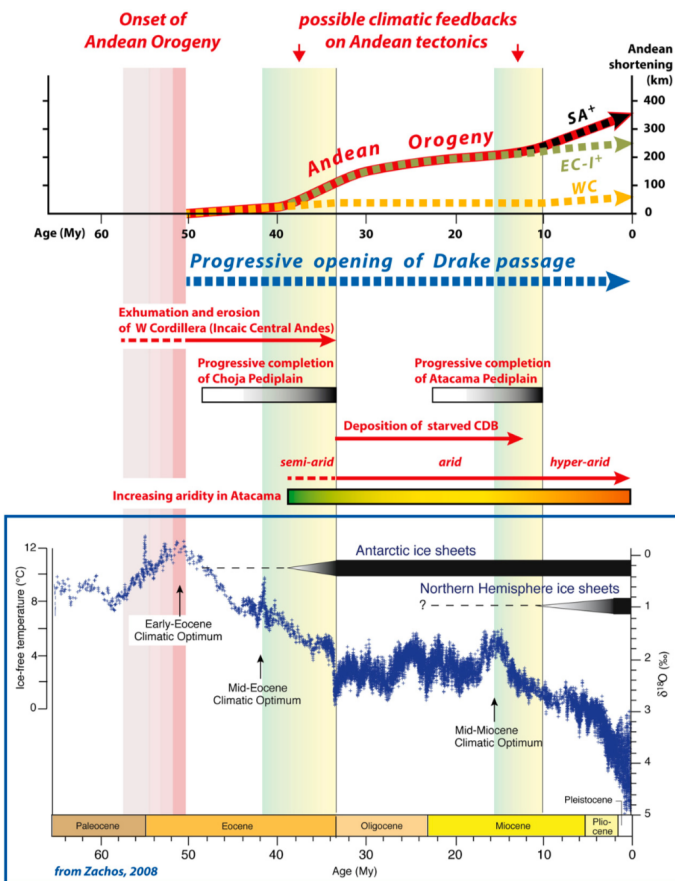
Figure 5. Paleo-elevation estimates for the Altiplano subdomain of the Central Andes.

According to (Gregory-wodzicki, 2000), in the Central Andes, paleobotanical evidence suggests that the Altiplano-Puna had attained no more than a third of its modern elevation of 3700 m by 20 Ma and no more than half its modern elevation by 10.7 Ma. These data imply surface uplift on the order of 2300–3400 m since the late Miocene at uplift rates of 0.2–0.3 mm/yr.

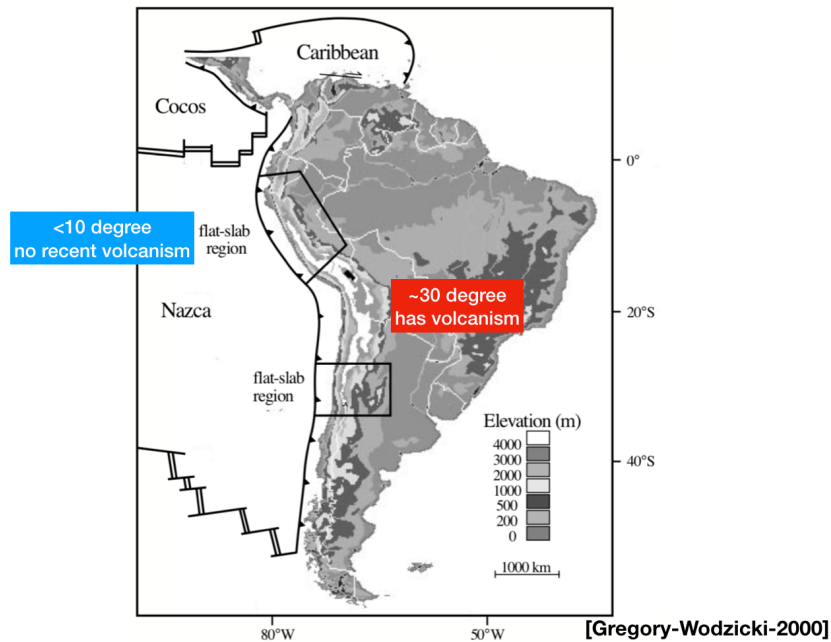
Paleobotanical and geomorphological data suggest a similar uplift history for the Eastern Cordillera—namely no more than half the modern elevation present by 10 Ma. No evidence exists for an exponential increase in uplift rate, as has been interpreted from fission- track data. These uplift rates mostly reflect mean surface uplift rather than rock uplift—that is, uplift of material points—because little dis- section of the western Eastern Cordillera has occurred south of 19°S and of the Altiplano-Puna. Thus, the Central Andean Plateau appears to be young. In the Colombian Andes, paleobotanical data imply rapid uplift of the Eastern Cordillera between 2 and 5 Ma at rates on the or- der of 0.6–3 mm/yr.

Potential Research Topics

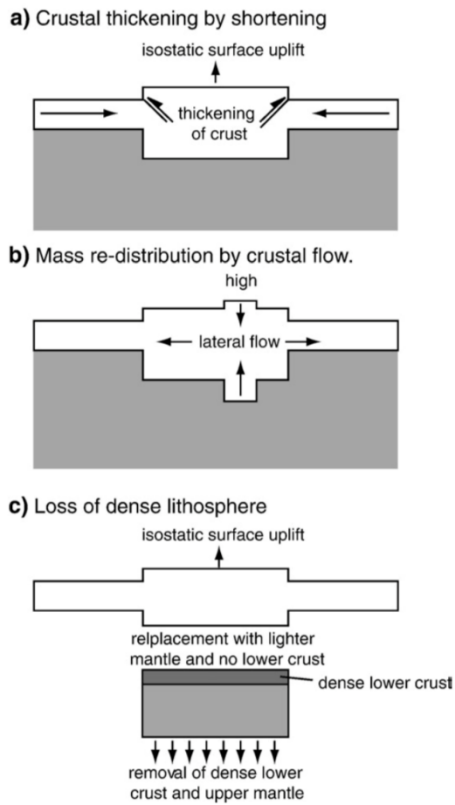
1. The possible climatic feedbacks on Andean tectonics (Armijo et al., 2015):



2. Relationship between subduction slab angle and volcanism:



3. Mechanisms for crustal deformation during late Miocene (Hoke & Garzione, 2008):



Conceptual diagrams showing possible mechanisms for large magnitude surface uplift of the central Andean plateau described in the text. a) Shortening as a means for crustal thickening and b) lower crustal flow would result in isostatically induced surface uplift related to the thickening of the felsic (upper) continental crust. c) Loss of a dense lithospheric root would result in positive (upward) isostatic rebound.

References:

- Armijo, R., Lacassin, R., Coudurier-Curveur, A., & Carrizo, D. (2015). Coupled tectonic evolution of Andean orogeny and global climate. *Earth-Science Reviews*, 143, 1–35. <https://doi.org/10.1016/j.earscirev.2015.01.005>
- Gregory-wodzicki, K. M. (2000). Uplift history of the Central and Northern Andes : A review. *GSA Bulletin*, 112(7), 1091–1105. Retrieved from <https://pubs.geoscienceworld.org/gsa/gsabulletin/article/112/7/1091-1105/183664e>
- Hoke, G. D., & Garzione, C. N. (2008). Paleosurfaces, paleoelevation, and the mechanisms for the late Miocene topographic development of the Altiplano plateau. *Earth and Planetary Science Letters*, 271(1–4), 192–201. <https://doi.org/10.1016/j.epsl.2008.04.008>
- Ryan, W. B. F., Carbotte, S. M., Coplan, J. O., O'Hara, S., Melkonian, A., Arko, R., et al. (2009). Global multi-resolution topography synthesis. *Geochemistry, Geophysics, Geosystems*, 10. <https://doi.org/10.1029/2008GC002332>

Lake Titicaca: Geology, Climate, Culture, History, Ecology, Etc.

Jonathan Lambert

Background

Lake Titicaca is located on the border between southeastern Peru and eastern Bolivia, from 16 to 17.5°S and 68.5 to 70°W. It is the largest lake in South America, with an area of 8,400 square kilometers (3,200 square miles). Some reports claim Lake Maracaibo is the largest on the continent at 13,200 square kilometers, but Maracaibo is a tidal estuary rather than a true lake. Lake Titicaca is also the highest navigable lake in the world, at an elevation of 3,800 meters (12,500 feet) above sea level in the high Altiplano region of the Andes. Its average depth is 107 m (350 ft), with a maximum depth of 281 m (922 ft) in the northern basin. The Lake also contains over 40 natural islands.

Approximately 2 million people live within the drainage basin of Lake Titicaca and it is a vital water and food source for the region. The Lake also creates a unique microclimate that supports agricultural goods such as potatoes and grains not normally available at such high altitudes. In addition to crop production, animal agriculture (alpacas, llamas, bovine) is also an important source of livelihood in the region.

The Peruvian region of the drainage basin is more populated with the largest city being Juliaca and second-largest being Puno (Fig. 1). Both of these cities are larger than the largest Bolivian city of Copacabana in the southern half of the Lake.



Figure 1: Political map of the Lake Titicaca region (Wikipedia)

Hydrology

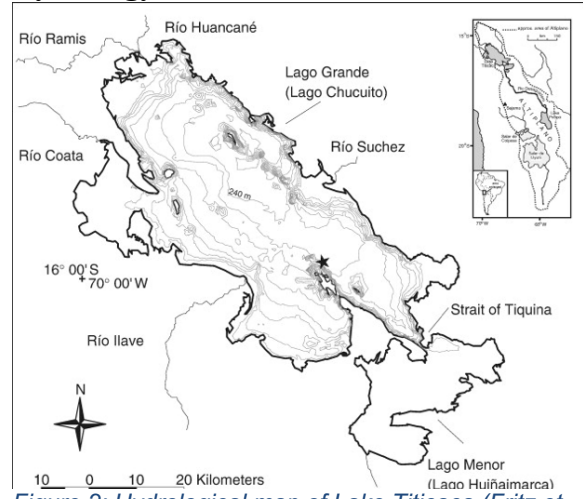


Figure 2: Hydrological map of Lake Titicaca (Fritz et al., 2007)

Lake Titicaca is comprised of two sub-basins (Figure 2): the larger and deeper Lago Grande (a.k.a. Lago Chucuito) and the smaller and much shallower Lago Menor (a.k.a. Lago Huiñaimarca). There are many small and ephemeral streams that run into the Lake but the five major rivers that feed the Lake are: Río Huancané, Río Ramis, Río Coata, Río Llave, and Río Suchez. The sole outlet for Titicaca is Río Desaguadero, which drains approximately 10% of the volume making Lake Titicaca a near closed-basin lake, controlled almost solely by evaporation (90%). Because of this, the residence time of the Lake is particularly

long at ~1300 years. In fact, during periods of low flow for Río Desaguadero, the lake transitions to closed-basin conditions.

Intense evaporation is driven by dry conditions, high solar intensity, and vigorous consistent Altiplano winds.

Due to its great depth and the high winds in the Altiplano, Lake Titicaca never freezes. Because of this, the lake is a monomictic system – only stratifying once per year, as opposed to most mid/high-latitude lakes which stratify twice per year (dimictic)(Figure 3). As ice never

develops, leading to winter stratification, the Lake only stratifies over the summer.

Climate

While Lake Titicaca is located at a tropical latitude (16 to 17.5°S), due to its elevation the climate is subtropical highland/alpine. Average annual precipitation in the largest city on the lake (Juliaca, Peru) is 610 mm (24 in) and this mostly comes during summer storms, with winters being exceptionally dry (5.8 mm/0.2 in precipitation in August)(Figure 4). Juliaca is also on the northern edge of Lake Titicaca and generally receives more annual precipitation than areas in the South. Because of the high elevation and tropical latitude, solar radiation is very intense in around the Lake and there is large daily thermal variation. In August (winter), the average high in Juliaca is 17°C (63°F), but the average low is well below freezing at -5°C (22°F). As previously mentioned, strong winds from the altiplano persist throughout the year and lead to substantial evaporation of the Lake.

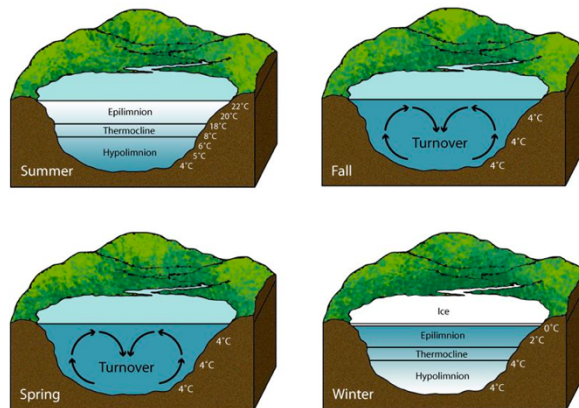


Figure 3: Cartoon illustrating a typical dimictic lake. While Titicaca is monomictic, these processes are similar (National Geographic)

Climatological Information for Juliaca, Peru

Location of weather station : 15.5 S, 70.0 W, altitude : 3825 m

| | Data Period | Jan | Feb | Mar | Apr | May | Jun | Jul | Aug | Sep | Oct | Nov | Dec |
|--|-------------|-------|-------|------|------|------|------|------|------|------|------|------|------|
| Mean Maximum Temperature (deg. C) | 1961-1990 | 16.7 | 16.7 | 16.5 | 16.8 | 16.6 | 16.0 | 16.0 | 17.0 | 17.6 | 18.6 | 18.8 | 17.7 |
| Mean Minimum Temperature (deg. C) | 1961-1990 | 3.6 | 3.5 | 3.2 | 0.6 | -3.8 | -7.0 | -7.5 | -5.4 | -1.4 | 0.3 | 1.5 | 3.0 |
| Rainfall Amount (mm) | 1961-1990 | 133.3 | 108.7 | 98.5 | 43.3 | 9.9 | 3.1 | 2.4 | 5.8 | 22.1 | 41.1 | 55.3 | 85.9 |

Figure 4: Climate Information for Juliaca, Peru. Not August climate info for when we will travel there (weather.gov/hk)

Geology

Lake Titicaca sits in the high Altiplano between Andean mountain ranges (the Eastern and Western Cordilleras). The lake basin originated in the late Oligocene with reactivation of

Andean tectonism and was later abandoned ~7 Ma in the late Miocene (Marocco et al., 1995). However, more in-depth pre-Quaternary history is uncertain due to a lack of sampling/observations in the region. One of the earliest known precursors to Lake Titicaca is mega-lake Mantaro which covered most of the Altiplano (Fritz et al., 2007).. Mantaro is thought to have originated in the late Pliocene and to have subsequently reduced in size due to intense evaporation. Following Lake Mantaro, Lake Cabana is thought to have re-inhabited the basin with the Caluyo glaciations in the mid-Pleistocene – also drying up with later glacial retreats. In the late Pleistocene, Lake Ballivian and Lake Escara were present in the area approximately 100 ka, with the small salt lakes of Coipasa and Uyuni present during Marine Isotope Stages (MIS) 5 and 3, respectively. Lakes Minchin and Tuaca are the high-stand lakes present during the glacial MIS 4 and 2, with Lake Titicaca developing in the early Holocene and persisting until today.

Studies of lake sediments in the Titicaca basin back to 370 ka reveal glacial-interglacial cycles consistent with the global benthic marine isotope record (Figure 5)(Fritz et al., 2012). Deeper and fresher lakes are detected during glacial periods due to positive water balance (associated with more glacial runoff and less evaporation), while shallow closed-basin conditions are detected during interglacials due to negative water balance (associated with less glacial runoff and higher evaporation).

Ecology

There are three major ecosystem types in the Lake Titicaca region: aquatic, puna, and mountain (Figure 6). The aquatic ecosystem includes the rivers, lakes and wetlands (largely in the southern subbasin). Aquatic totora reeds (*Schoenoplectus tatora*), which grow on the edges of the Lake are crucial for the region, as they are used as building materials for houses/roofs, artificial islands, and boats. The puna ecosystem

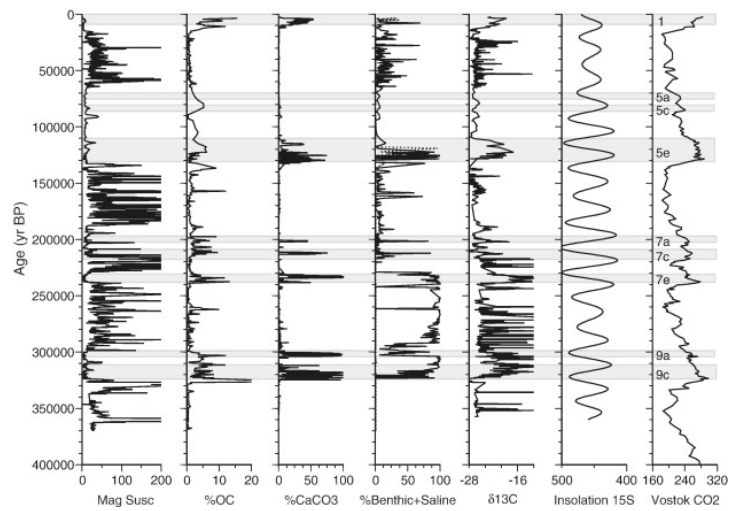


Figure 5: Multiproxy lake sediment record for the Titicaca basin showing glacial-interglacial cycles, with %organic carbon, %calcium carbonate, %Benthic+saline foraminifera, and $\delta^{13}\text{C}$ increasing during interglacial periods (high Vostok CO_2), and magnetic susceptibility increasing during glacials (low Vostok CO_2) (Fritz et al., 2012)

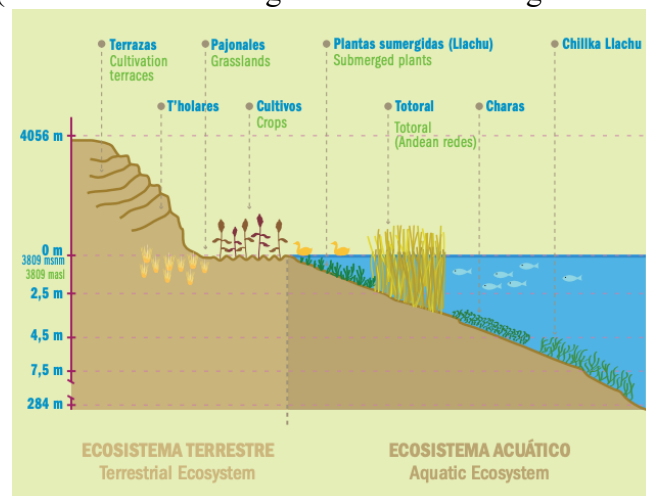


Figure 6: Illustration of aquatic and terrestrial agricultural and ecosystem zones in the Lake Titicaca basin (globalnature.org)

includes the area in close proximity to the shore of the Lake and can be separated into many other sub-ecosystems, but the main classifications are: humid, dry, semi-desert, grassland, prairie, woodland, and micro-foliated forest. Finally, the mountain ecosystem includes the high Andean woodlands that flank the drainage basin.

Focusing specifically on the aquatic ecosystem in the Lake, there are two main native fish groups: killifish (*Orestias*) and catfish (*Trichomycterus*). However, trout were introduced in 1939 and are now outcompeting some of the native fish species. The Titicaca water frog (*Telmatobius coleus*) is a unique deep-dwelling frog native to the lake and the Titicaca grebe (*Rollandia microptera*), which is a flightless aquatic bird, are both critically endangered species in the region. Because of the diversity and importance of the region, the Titicaca wetlands were designated a Ramsar site (wetland of international importance) in 1998.

History & Culture

Due to colonization, Spanish is the primary language in Peru, but there are many indigenous languages unique to certain regions of the country. Near Lake Titicaca, the Aymara and Quechua languages are common, in addition to Spanish. Many geographical names have their origin in these indigenous languages and Lake Titicaca is no exception. In the Aymara language, “titi” refers to a cat or puma, and “Karkha” refers to a stone/rock, giving Titicaca the meaning of “puma rock” or “rock of the puma.” It is rumored that the Lake (when viewed from above) resembles a puma resting on a rock, lending it this name. The Lake is also known to some as Lago Chucuito (from “chuquitivu” meaning lance point).

The region surrounding Lake Titicaca was first settled ~3500 years ago by the Aymara people. However, the Aymara were absorbed by the Incas in the 15th century. The Inca also held Titicaca as important mythologically and associated it with the “Birthplace of the sun” referring to the birthplace of the leader of the Inca. In contrast to the Aymara who were absorbed into the Inca empire, the Uru people developed floating islands (made from totora reeds) to avoid conflict with the Incas. These islands still function today and tourism is a large industry among the Uru people.

Climate Change/Anthropogenic Influences

With increasing development around Lake Titicaca, the anthropogenic influence on the Lake has risen. For many years, untreated sewage has been discharged directly into the lake from residences and industries such as food processing, leathermaking, cement, and timber. For example, only 20% of Puno’s sewage is treated. Pollution such as this is more of a problem on the northern end of the lake due to higher population, creating large duckweed blooms due to elevated nutrients. In addition to sewage, pesticides and fertilizers from agriculture and metals such as zinc and mercury from mining enter the lake. In order to combat this, the Reserva Nacional del Titicaca was founded in 1978 north of Puno to protect a portion of the drainage basin. In Bolivia as well, USAID has been partnering with local communities since 2008 to

reduce pollution, and two new wastewater treatment plants have been built in the city of El Alto since this partnership.

From a climatological standpoint, water levels have been declining in the Lake recently due to increasing water removal from tributaries by irrigation and industrial use combined with a shortening rainy season (from six to three months) induced by drought variability from El Niño Southern Oscillation. Bolivia is working to raise awareness about potential climate change impacts such as this and formed the Bolivian Nature Conservation Organization (TRÓPICO) with this goal.

References

- Fritz, Sherilyn C., et al. "Quaternary glaciation and hydrologic variation in the South American tropics as reconstructed from the Lake Titicaca drilling project." *Quaternary Research* 68.3 (2007): 410-420.
- Fritz, Sherilyn C., et al. "Evolution of the Lake Titicaca basin and its diatom flora over the last ~ 370,000 years." *Palaeogeography, Palaeoclimatology, Palaeoecology* 317 (2012): 93-103.
- Marocco, René, Alain Lavenu, and R. Baudino. "Intermontane late Paleogene-Neogene basins of the Andes of Ecuador and Peru: Sedimentologic and tectonic characteristics." (1995): 597-613.
- Peruperto, S.A. "Titicaca Basin – A Technical Report: The Hydrocarbon Potential of Titicaca Basin." Geological – Geophysical Evaluation Group Exploration Management. (2008). 108 pp.
- TRÓPICO - Asociación Boliviana para la Conservación. 2011. "Libro de Viaje - Lago Titicaca." TRÓPICO - Red Lagos Vivos de América Latina y el Caribe. Banco Interamericano de Desarrollo. (2011): 207 pp.
- <https://www.nationalgeographic.org/media/lake-turnover/>
- <https://www.globalnature.org/35193/Living-Lakes/America/Lake-Titicaca/resindex.aspx>
- http://www.weather.gov.hk/wxinfo/climat/world/eng/s_amERICA/ec_per/juliaca_e.htm
- <https://www.globalnature.org/34783/Themes-Projects/Sustainable-Development-Development-Cooperation/References/Fighting-Climate-Change/resindex.aspx>

Marine Life in Peru

Elise M. Myers

High Production in the Humboldt Current

About 500-1000 km (310-620 miles) from shore, directly adjacent to the coast of Peru flows the powerful Humboldt Current, also known as the Peru Current (Figure 1). This cold, low-salinity ocean current of water flowing northward from the Antarctic region is driven by eastward blowing trade winds that, due to the Coriolis force acting in the opposite direction in the southern hemisphere, pull the water from the western coast of South America. The westward movement of water leads to strong upwelling of colder, nutrient rich water,

which provides the basis for higher phytoplankton biomass and overall increased production throughout the food web. The well-known NASA Ocean Color image of chlorophyll a, as measured by satellites, shows a notable increase in chlorophyll a (a proxy for phytoplankton biomass) along this coast, due to this upwelling effect.

The high production in the Humboldt Current contributes to the largest permanent oxygen minimum zone (OMZ) in the world (Figure 2 - Löscher *et al.* 2015). This OMZ is 2,200,000 km³ large and is generally found between 100 to 600 meters in depth (Löscher *et al.* 2015). Contributing to this OMZ is the decay of the abundant primary production in this region. Additionally, the Humboldt current splits into both an equatorward current and a northward current, which

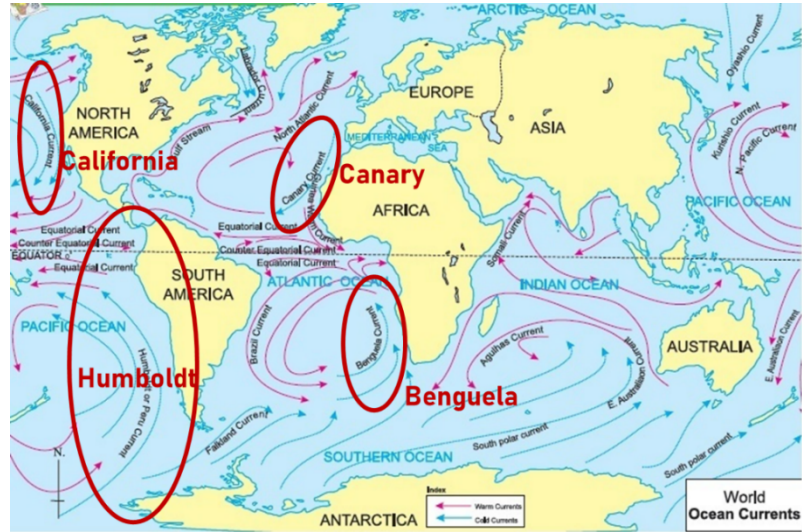


Figure 1 – Global map of major ocean currents with eastern boundary currents circled, adapted from Brainly.in.

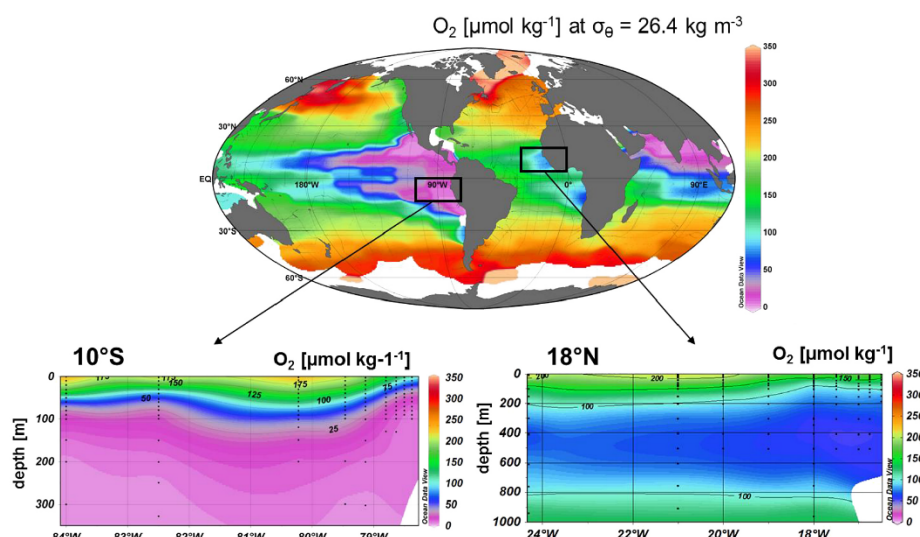


Figure 2 – Oxygen concentrations across the globe and in the oxygen minimum zones off the coast of South America and Northern Africa.
From Löscher *et al.* 2015

then decreases ventilation in the region (Figure 1). A side effect of the low oxygen in the water column is a concentration of marine organisms in the surface waters.

Marine Life in the Humboldt Current

Of the four eastern boundary currents (California, Canary, and Benguela), the Humboldt Current is the most productive system. An eastern boundary current is characterized as a relatively shallow, broad, and slow-flowing current along the eastern side of an oceanic basin (i.e. along the western coast of continents). The western coast of South America accounts for a significant amount of global fish catch (Figure 3 – Stock et al 2017). Marine life that is heavily fished in this region includes sardines, anchovies, jack mackerel, hake, and squid. Marine mammals are also found in abundance in this region, including sea lions, fur seals, cetaceans, and the highly endangered marine otter. In fact, about 1/3 of the world's species of dolphins can be found in the ocean off the Peruvian coast (*).

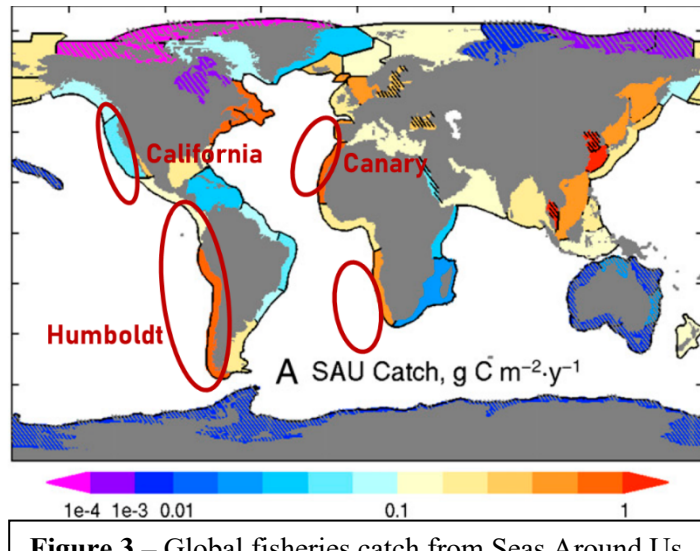


Figure 3 – Global fisheries catch from Seas Around Us database, as analyzed in Stock et al. 2017

Some of the earliest evidence for cetaceans has been found in coastal Peru. In 2019, Lambert et al published a paper detailing a fossil of the mandibles and most of the post cranial skeleton of a quadrupedal whale. The fossil was found in 42.6 myr old marine deposits in Playa Media Luna, which is a 5-minute drive from downtown Paracas. The fossil, named *Peregocetus pacificus*, had a body of up to 4 meters (13 feet), hooves, and caudal vertebrae in the tail that are reminiscent of beavers and otters (Figure *). The quadrupedal whale would have been able to both walk on land and swim, and likely had its tail contribute notably to its swimming ability. Older quadrupedal whale fossils found in Pakistan (57 myr – Gingerich et al 2001) and India (50 myr – Thewissen et al 2007) were appear very similar to this fossil, suggesting a crossing of the South Atlantic by early quadrupedal whales less than 10 million years after their origin. This fossil discovery also suggests that the quadrupedal whales crossed to South America before dispersing northward to North American latitudes.

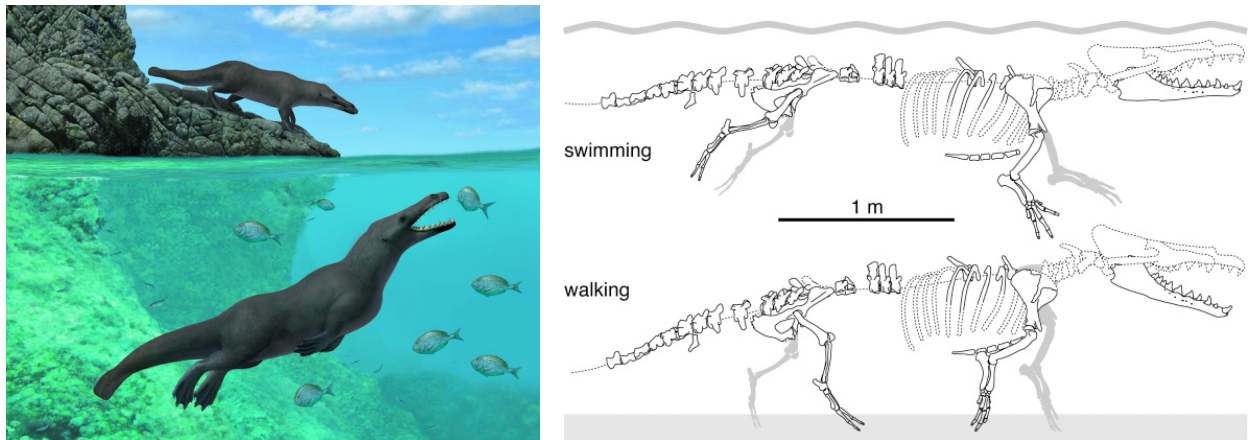


Figure 4 - An artist's representation of *Peregocetus pacificus* (left, A Gennari/Cell Press) and the fossil remains discovered in different locomotive styles (right, Lambert et al 2019).

Historical Fisheries in Peru

Fishing began early along the western coast of South America, with the fishing of various marine vertebrates and invertebrates occurring as early as the Terminal Pleistocene (~ 12 kyr, Sandweiss et al. 2004). During the Early to Middle Holocene (11.7 kyr → _), the primary source of animal protein for humans living in this region derived from fisheries (Reitz et al 2008). In 3500 BCE, fishing nets and hooks were employed by humans during the Preceramic period, where fishing villages also became more common (*). Later, Chimú art depicted fishermen on vessels (Figure *), which suggests that deeper water fishing began occurring at least by 1100 – 1400 CE. In more modern history, the fish meal industry in Peru was nationalized in the 1960s, increasing fishing pressure (Reitz et al 2008). By the 1980s, the waters of the Peruvian coast were considered to be heavily fished (Reitz et al 2008).



Figure 5 – An artifact from the Chimú period depicting a fisherman on a vessel. (Luis García)

Fisheries Management in Peru

A major challenge for fisheries management is to forecast the abundance of exploited stocks (of marine life) to then be able to manage the fishing intensity in the region (Karjalainen & Marjomaki 2005). Without this kind of management, a fishery can tip past a sustainable yield point and enter into an overfished or depleted state. Fisheries ecologists model systems and consider both the ecological parameters (e.g. ecosystem state under fishing pressure) and financial parameters (e.g. the economic incentives in the fishing industry for fish more or less intensively). Fluctuations in fish populations that occur naturally are also important to consider when designing effective management strategies for sustainable fisheries.

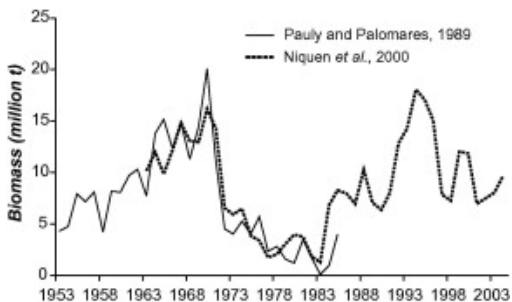


Figure 6 – A plot of anchovy biomass over time, as presented in Fréon et al 2008.

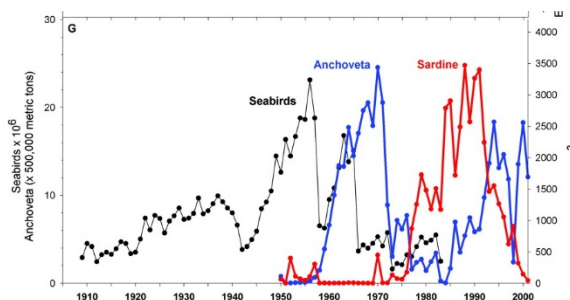


Figure 7 – A plot of anchovy, sardine, and seabird biomass over time, as presented in Chavez et al 2005.

The Peruvian anchovy fishery is the largest single-species fishery in the world and predominantly used for fish oil and fish meal (ground up anchovies) that sustains livestock and agriculture. Since the 1950s, there have been observed interannual and interdecadal variability in populations of anchovies and other pelagic fishes. In a time series of anchovy populations from 1953 to 2003, Fréon et al noted interannual fluctuations of populations, but a large drop of the anchovy biomass around 1970, before a recover to higher numbers by about 1995 (Figure 6 - Fréon et al 2008). A similar time series that also include sardines saw a similar trend, though the population fluctuations of the groups appear to be out of phase (Figures 7 and 8 - Chavez et al 2005 & Sandweiss et al 2004). Environmental variables like sea surface temperature anomalies and accumulation in the Quelccaya Ice Cap mapped during these same periods are impacted notably by changes in El Nino Southern Oscillation (ENSO). During warmer and more frequent El Nino events, noted by decreased accumulation and higher sea surface temperature, the anchovy catches decrease, while the sardine fish catches increase (Figure 8 - Sandweiss et al 2004).

In the paleorecords, the shifts between anchovy and sardine biomass can also be identified and, because of their regularity and magnitude, they can be interpreted as larger regime shifts between

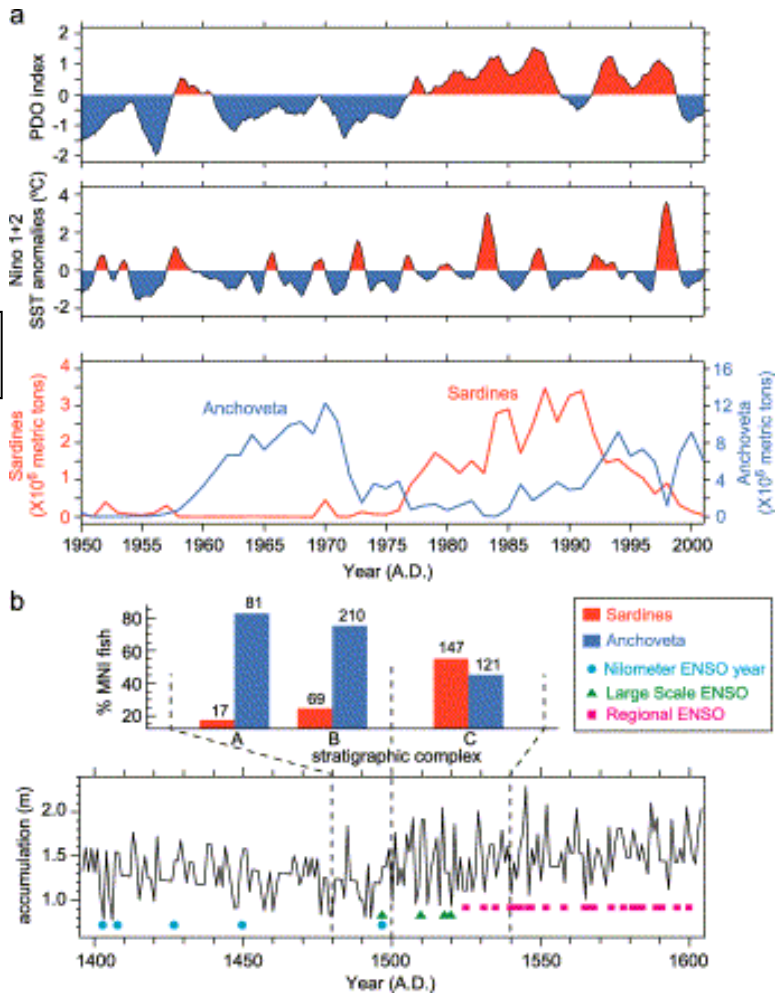


Figure 8 – Two different time series: Biomass of anchovies and sardines from 1950-2000 is paired with Pacific Decadal Oscillation (PDO), Sea surface temperature (SST) fluctuations. Biomass of sardines and anchovies from 1470-1540, interpreted from fish remains, is shown adjacent to a paleorecord of accumulation on the Quelccaya Ice Cap. (Sandweiss et al 2004)

the fish populations (Sandweiss et al 2004). Fish remains have been used to note these shifts; fish remains found at Lo Demás from the Incan period of 1480-1540 indicate a shift of reliance from anchovy to sardine fisheries around 1500 (Sandweiss et al 2004). This regime shift correlates with an increase in ENSO frequency (Figure 8). The correlation with environmental factors and the lower fishing pressure at this earlier shift suggests that fish regime changes can occur due to natural variability (Sandweiss et al 2004), as opposed to only from anthropogenic pressure. The increase in sardine abundance during warmer and more frequent ENSO periods is partially attributed to their long, 25-year lifespan. Sardines then are more likely to shift their range south, but maintain population size with their decreased sensitivity to ENSO changes (Sandweiss et al 2004). Further, sardines generally outnumber anchovies in nearshore, warmer waters with higher phytoplankton concentrations (Sandweiss et al 2004).

Modern technology has also been employed in Peru to combat overfishing and harmful fishing practices. In 2017, Peru decided to allow its Vessel Monitoring System (VMS) data to be incorporated into the Global Fishing Watch (Jordan 2017). GFW uses satellite surveillance to track boat presence and fishing effort across the globe to combat overfishing. It primarily had relied upon the Automatic Identification Systems found on many vessels, but this system was not as common on Peruvian vessels.

Threats to Marine Life

Peru faces many similar threats to marine life as other countries around the world. There are some endangered marine species (*e.g.* Humboldt penguins) and highly endangered species (*e.g.* marine otter), which suffer from pressures including habitat loss, hunting, and climate change. The high fishing pressure in this area in combination with climate change effects exerts significant pressure on the food web. The warmer water temperatures of El Nino overall drive anchovies and sardines into deeper water, which restricts the food for fur seals, sea lions, Humboldt penguins, cormorants, and Peruvian boobies. This can then cause massive die-offs of these higher trophic level organisms, like in the 2013 El Nino event when sea lions stranded themselves in record numbers, about 10 times higher than normal (NOAA Fisheries West Coast 2015) all along the Pacific coast (NOAA Fisheries 2015). Other threats to marine life in Peru include ship ballast water dumping in Peru's coastal waters, plastic pollution, and other anthropogenic pollution.

Paracas: Paracas National Reserve & Islas Ballestas

The Paracas National Reserve was established in 1975 and is home to 216 species of birds, 16 mammals, and 10 reptiles. The national reserve is one of the largest concentrations of birds in the world. Within the region of Paracas, there are archaeological remains of the Paracas culture, which thrived between 800-100 BCE. Two sites related to this ancient culture are the Museo de Sitio Julio Tello and the Paracas Necropolis/Cerro Colorado. There is also an ecology and conservation center for visitors to learn more about the nature in this region. The Centro de Interpretación de la Reserva Nacional de Paracas only offers exhibits/signs in Spanish. Also located in Paracas are stunning examples of coastal geomorphology, like Playa Roja, a red-sand beach that is the result of the erosion of porphyry rocks (large-grained igneous rock of feldspar and quartz).

On the way to Islas Ballestas via boat, visitors can see the Candelabra geoglyph carved on Pisco Bay shore, which was approximately made in 200 BCE (World Atlas). The geoglyph was dug up to 3 meters deep into the stony desert soil and is about 190 meters in length (Gerster). Islas Ballestas are colloquially called the “Poor Man’s Galapagos” for the richness of biodiversity found there. Marine life visible on the islands includes Humboldt penguins, sea lions, marine otters, flamingos, and Peruvian boobies. On the way to the islands, it is possible to view whales and dolphins. Islas Ballestas sea caves and natural arches are further examples of weathering and coastal geomorphology.

References

- Candelabra of the Andes.* (2019). World Atlas.
<https://www.worldatlas.com/webimage/countrys/samerica/attractions/candelabra.htm>
- Chavez, F. P., Ryan, J., Lluch-Cota, S. E., & Ñiquen, M. (2003). From anchovies to sardines and back: multidecadal change in the Pacific Ocean. *science*, 299(5604), 217-221.
- Fréon, P., Bouchon, M., Mullon, C., García, C., & Ñiquen, M. (2008). Interdecadal variability of anchoveta abundance and overcapacity of the fishery in Peru. *Progress in Oceanography*, 79(2-4), 401-412.
- Gerster, G., & Trümpler, C. (2005). *The past from above: Aerial photographs of archaeological sites*. Los Angeles, CA: J. Paul Getty Museum.
- Gingerich, P. D., ul Haq, M., Zalmout, I. S., Khan, I. H., & Malkani, M. S. (2001). Origin of whales from early artiodactyls: hands and feet of Eocene Protocetidae from Pakistan. *Science*, 293(5538), 2239-2242.
<https://earthsky.org/earth/ancient-4-legged-whale-ancestor-fossil>
- Jordan, M. (2017, June 07). Peru Commits to Publish Vessel Tracking Data through Global Fishing Watch.
- Karjalainen, J., & Marjomäki, T. J. 3.1. Sustainability in fisheries management.
- Lambert, O., Bianucci, G., Salas-Gismondi, R., Di Celma, C., Steurbaut, E., Urbina, M., & de Muizon, C. (2019). An amphibious whale from the middle Eocene of Peru reveals early South Pacific dispersal of quadrupedal cetaceans. *Current Biology*, 29(8), 1352-1359.
- Löscher, C., Bange, H. W., Schmitz, R. A., Callbeck, C. M., Engel, A., Hauss, H., ... & Melzner, F. (2016). Water column biogeochemistry of oxygen minimum zones in the eastern tropical North Atlantic and eastern tropical South Pacific oceans. *Biogeosciences (BG)*, 13, 3585-3606.
- NOAA Fisheries (National Oceanic and Atmospheric Administration Fisheries). 2015a. 2013-2015 California sea lion unusual mortality event in California.
<http://www.nmfs.noaa.gov/pr/health/mmume/californiasealions2013.htm>.
- NOAA Fisheries West Coast (National Oceanic and Atmospheric Administration Fisheries West Coast Region). 2015. 2015 elevated California sea lion strandings in California: FAQs.
http://www.westcoast.fisheries.noaa.gov/mediacenter/faq_2015_ca_sea_lion_strandings.pdf.
- Reitz, E. J., Andrus, F. T., Sandweiss, D.H. “Ancient Fisheries and Marine Ecology of Coastal Peru”. Eds. Rick, T. C., & Erlandson, J. (2008). *Human impacts on ancient marine ecosystems: A global perspective*. Berkeley: University of California Press

- Sandweiss, D. H., Maasch, K. A., Chai, F., Andrus, C. F. T., & Reitz, E. J. (2004). Geoarchaeological evidence for multidecadal natural climatic variability and ancient Peruvian fisheries. *Quaternary Research*, 61(3), 330-334.
- Stock, C. A., John, J. G., Rykaczewski, R. R., Asch, R. G., Cheung, W. W., Dunne, J. P., ... & Watson, R. A. (2017). Reconciling fisheries catch and ocean productivity. *Proceedings of the National Academy of Sciences*, 114(8), E1441-E1449.
- Thewissen, J. G., Cooper, L. N., Clementz, M. T., Bajpai, S., & Tiwari, B. N. (2007). Whales originated from aquatic artiodactyls in the Eocene epoch of India. *Nature*, 450(7173), 1190.

Terrestrial Biodiversity of Peru

Joshua B. Russell

Peru Microclimates, Ecosystems, and Biodiversity

A current estimate of the total number of animal species on Earth is $5 +/- 3$ million, only 1.5 million of which have been named (Costello et al., 2013). Global patterns of fauna (and flora) biodiversity are largely correlated with climatic factors such as temperature and precipitation, with hotter and wetter climates sustaining more diverse ecosystems (Bass et al., 2010).

Therefore, latitude is a primary controller with biodiversity generally decreasing from the equator to the poles (Figure 1). This phenomenon is known as the latitudinal biodiversity gradient (LBG) and explains the overall distribution of both terrestrial and marine flora and fauna on Earth (Mannion et al., 2013). In addition, longitudinal and local variations also occur, as shown in Figure 1.

Peru's microclimates and habitats are exceptionally diverse. Coastal regions west of the Andes mountains are arid with warm temperatures and little rainfall associated with the rain shadow. The high elevation of the Andes leads to typically cold climate with wet summers and dry winters. In contrast, the lowlands east of the Andes exhibit wet and hot equatorial climate with rain consistently throughout the year.

Due to its range of climates and proximity to the Amazon rain forest, Peru is one of the most biodiverse places on the planet, hosting ~1,800 species of birds, ~500 mammal, ~300 reptile, >10,000 beetles (Figure 2). Peru is home to ~20% of the world's total known bird species, more than any other country on Earth (1). Generally, the geographic distribution of plant and animal species increases from west to east across the country toward the Amazon. The lowest biodiversity occurs along the coastal and mountain regions with an abrupt increase in the eastern lowlands. For the majority of our field trip, we will be in the coastal and highlands regions but will still have opportunities to view wildlife, particularly at Islas Ballestas, Lago Titicaca, and Machu Picchu.

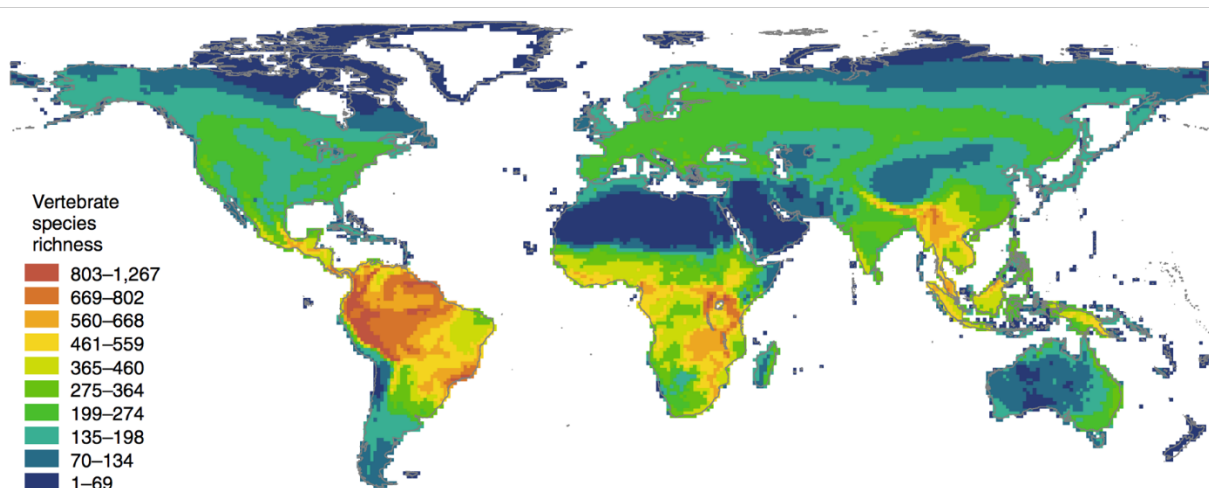


Figure 1. Global biodiversity of vertebrate species (amphibians, birds, and mammals) from a global database at 1° resolution (Antonelli et al., 2018).

Because of its vast biodiversity particularly in the Amazon, Peru has set aside ~13% of its territory as protected areas. The system of 46 protected areas in the Peruvian Amazon, known as SINANPE (El Sistema Nacional de Áreas Naturales Protegidas por el Estado), covers 19.5 million hectares and plays a crucial role in conservation efforts (Figure 3). Outside these protected regions, deforestation rates are estimated to be more than twice that within the protected areas (Finer & Novoa, 2015).

Tectonic influences on Biodiversity

It is clear that the Andes mountains play a significant role in shaping the ecosystems and in turn the biodiversity of Peru. Only recently have studies begun to evaluate the influence of orogeny and subsequent erosion on global biodiversity. Antonelli et al. (2018) considered climatic variables including annual precipitation, mean annual temperature, temperature range, and seasonal precipitation together with geological variables such as topographic relief, long-term erosion rates, and soil type to evaluate their individual impacts on global biodiversity. They found that topographic relief is a strong indicator of biodiversity, with higher local elevation range (max-min elevation) correlating with higher species richness (Figure 4). Furthermore, the role of topographic relief on species richness is shown to be comparable to or even more important than precipitation and temperature.

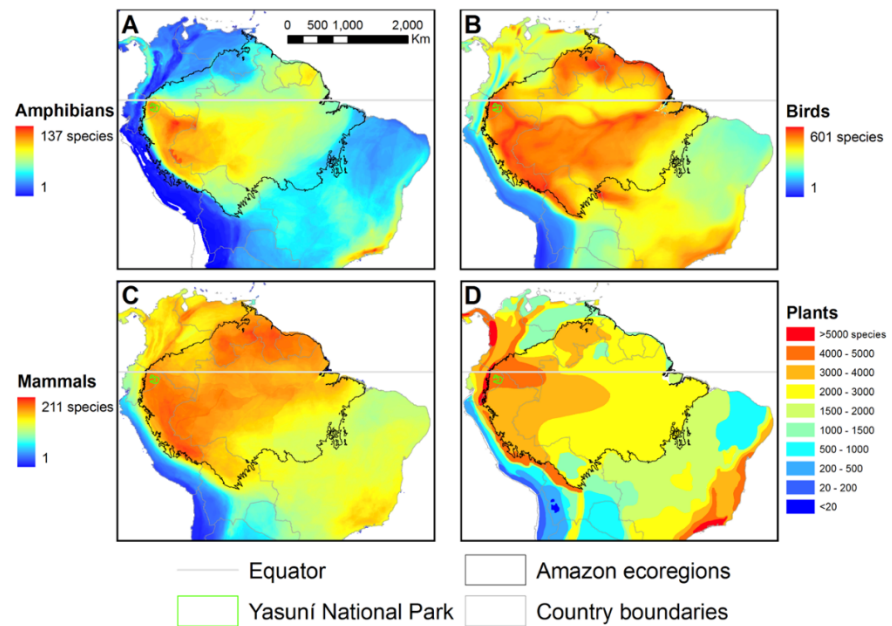


Figure 2. Zoom in of amphibian, bird, mammal, and plant biodiversity in Peru and the surrounding Amazon (Bass et al., 2010).

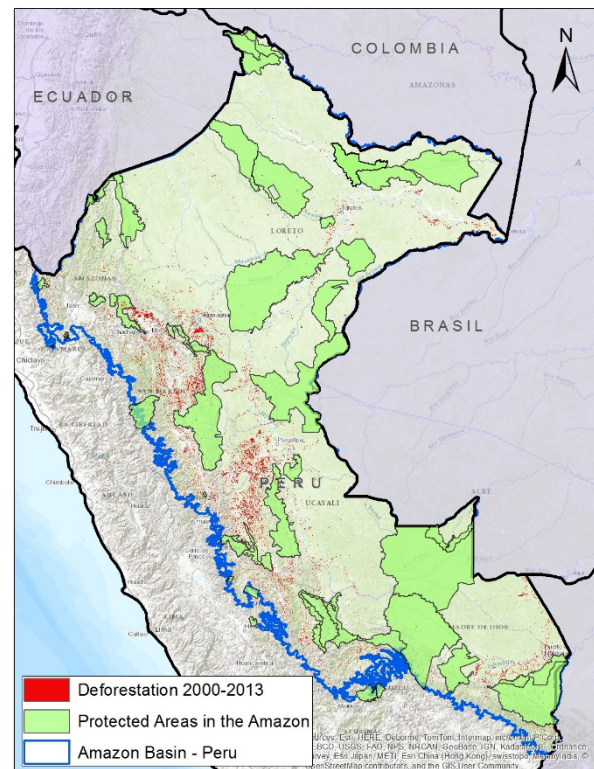


Figure 3. Map of protected areas within the Amazon basin of Peru and deforestation from 2000-2013 (Finer & Novoa, 2015).

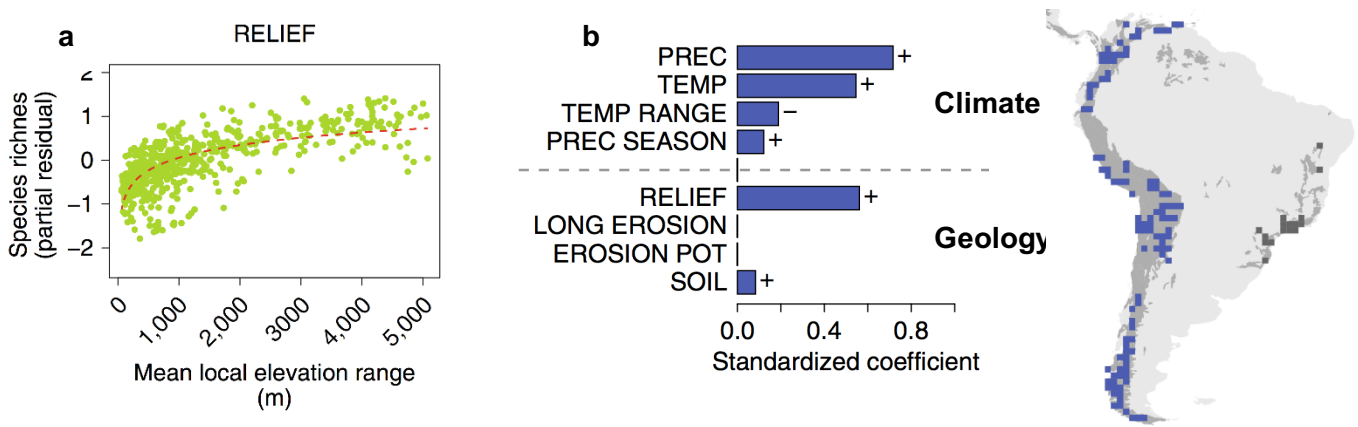


Figure 4. a) Global species richness variation with mean local elevation range (max-min elevation) showing a general increase with elevation range. b) Similar analysis for the Andes showing relief importance relative to climate parameters (Antonelli et al., 2018).

Although there is certainly a link between mountains and biodiversity, it is still unclear what exactly that link is. Orogenic processes alter the previously homogeneous landscape consisting of mature, often nutrient poor soils characterized by low erosion rates and low speciation rates. Mountain building processes lead to uplift that outpaces previous erosion rates through tectonic and volcanic processes, causing increased relief. This produces a rain shadow, which further diversifies the local habitat and vegetation.

Microhabitats begin to form at different elevations and increased landmass allows outside species to migrate in. Eventually, these processes lead to enhanced speciation across low-to-mid elevations. As uplift rates cease and fall below erosion rates, the local elevation range begins to decrease and the environment begins to homogenize, lowering local biodiversity to background levels.

Avian Biodiversity in Peru

Peru is one of the most avian diverse regions on the planet, home to ~1847 species, more than North America and Europe combined. This includes more than 50 species of parakeets, and ~120 species of hummingbirds as well as many others and some that also occur in North America. Of these species, 120 are endemic and only 143 (~7.8%) are migratory. Of the migratory species, 79 are northern migrants traveling northward to Central America, the United States, and Canada during April to September; 42 are southern migrants (austral migrants) relocating within South

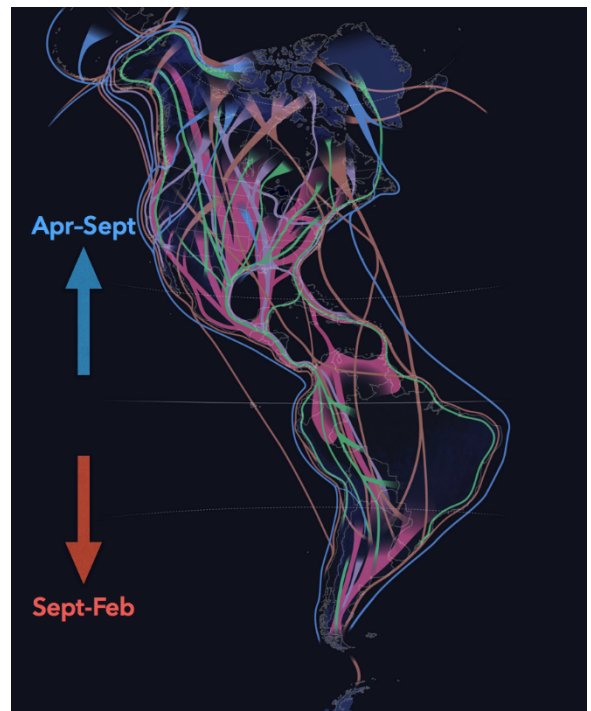


Figure 5. Schematic showing a range of avian flyways between North and South America (3).

America from September through February; 20 species come from the southern ocean and tropical islands; and 4 migrate to the Galapagos (2). Figure 5 shows a schematic of typical flight pathways between North, Central, and South America for various species.

Macaw Clay Licks

Hundreds of Macaws and other species of parrots flock to the clay banks along the western edge of the Amazon basin to feed on the clay (Figure 6). These so-called “clay licks” have become a large tourist attraction, with sighting opportunities at Tambopata Research Center, Manu Wildlife Center, Heath River Wildlife Center, Refugio Amazonas Lodge, Posada Amazonas Lodge, and others. However, there are still questions regarding why Macaws are attracted to these clay licks. The Tambopata Macaw Project established in 1989 is a multidisciplinary team of scientists that study Macaw behavior, including at clay licks, to aid conservation efforts and protect their habitats. Prior to recent work, the prevailing theory was that the clay detoxifies the birds (5). However, it has been pointed out that parrots in other parts of the world that ingest toxins do not consume clay. Current theories now link clay ingestion with the lack of sodium in the western Amazon, as was demonstrated by Kaspari et al. (2008). They also found that clay lick populations peak during breeding season presumably as mature Macaws feed clay to their young. Overall, use of clay licks depends on daily weather, seasonal climate, food supply, and breeding season (6).

Guano Islands

Islands offshore Peru containing hundreds to thousands of seabirds are affectionately known as the guano islands (Figure 7). They are home to four main species of guano-producing seabirds: the Peruvian pelican, the white-breasted cormorant, the guanay cormorant, and the Peruvian booby (Figure 8). Bird guano is very high in nitrogen and phosphorous and therefore makes an excellent fertilizer (7). Peruvians have been harvesting guano from these islands for



Figure 6. Scarlet red-and-blue, and blue-and-yellow macaws at Chuncho Clay Lick, Tambopata National Reserve, Madre de Dios, Peru (4).



Figure 7. 22 of the largest Guano islands in Peru.

the past 150 years, making Peru the world's leading producer of guano at more than 21,000 tons from the Chincha islands alone per year.

The guano islands have an important historical significance to Peru. During 1845-1866, the export of guano generated economic stability for the country and is now known as the "Guano Era". However, as synthetic fertilizers became more popular in years following the market crashed. Recently, the demand for guano has climbed with increased interest in organic options and rising prices of synthetic fertilizer. During our trip, we will be visiting one of the largest guano islands, Isla Ballestas, where we are likely to see many species of seabirds, in addition to the endangered Humboldt Penguin and other marine wildlife.



Peruvian pelican **White-breasted cormorant** **Guanay cormorant** **Peruvian booby**

Figure 8. The four most common guano-producing seabirds

References

- Antonelli, A., Kissling, W.D., Flantua, S.G.A., Bermudez, M.A., Mulch, A., Muellner-Riehl, A.N., Kreft, H., Linder, H. P., Badgley, C., Fjeldsa, J., Fritz, S.A., Rahbek, C., Herman, F., Hooghiemstra, H., Hoorn, C. (2018). Geological and climatic influences on mountain biodiversity. *Nature Geoscience*. 11, 718-725.
- Bass MS, Finer M, Jenkins CN, Kreft H, Cisneros-Heredia DF, et al. (2010). Global Conservation Significance of Ecuador's Yasuní National Park. *PLoS ONE*. 5(1): e8767. doi:10.1371/journal.pone.0008767.
- Costello, M.J., May, R.M., Stork, N.E. (2013). Can We Name Earth's Species Before They Go Extinct? *Science*. 339(6118). 413-416.
- Finer M, Novoa, S. (2015). Importance of Protected Areas in the Peruvian Amazon. MAAP: Image #11. Link: <https://maaproject.org/2015/image-11-importance-of-protected-areas-in-the-peruvian-amazon/>
- Kaspari, M., Yanoviak, S.P., Dudley, R. (2008). On the biogeography of salt limitation: A study of ant communities. *Proceedings of the National Academy of Sciences*. 105(46). 17848-17851.
- Mannion, P.D., Upchurch, P., Benson, R.B.J., Goswami, A. (2013). The latitudinal biodiversity gradient through deep time. *Trends in Ecology & Evolution*. 29(1). 42-50.

Websites (last accessed 8/3/2019)

- (1) https://www.go2peru.com/peru_bird_watching.htm
- (2) <https://www.peruaves.org/migration/>
- (3) <https://www.nationalgeographic.com/magazine/2018/03/bird-migration-interactive-maps/>
- (4) http://www.petercavanagh.us/wp-content/uploads/2016/07/Clay_lick_0143.jpg
- (5) <https://www.smithsonianmag.com/travel/why-do-hundreds-macaws-gather-these-peruvian-clay-banks-180955719/>
- (6) <https://www.perunature.com/about-rainforest/macaw-project/>
- (7) <https://www.audubon.org/news/holy-crap-trip-worlds-largest-guano-producing-islands>

El Niño-Southern Oscillation and Peru

By Thomas Weiss

What is ENSO?

Despite being focused in the Pacific Ocean, El Niño-Southern Oscillation (ENSO) is the strongest control on global interannual climate variability (Wallace et al., 1998). The Pacific Ocean oscillates between three main phases: a neutral phase, El Niño, and La Niña (Figure 1). During the neutral phase, low-latitude trade winds blowing from east to west (called easterlies) push warm Pacific surface water to the western side of the basin (Philander et al., 1989). As a result, the West Pacific Warm Pool has the warmest sea surface temperatures (SST) in the world with temperatures $>30^{\circ}\text{ C}$ (NOAA, 2013). In the eastern Pacific, colder water upwells to fill the void left by warm surface water that was pushed to the west. This creates the so-called “cold tongue” in the eastern Pacific where surface water can reach temperatures $>20^{\circ}\text{ C}$, more than 10° C cooler than in the western Pacific (NOAA, 2013). Buildup of warm surface water in the west and upwelling of cold water in the east tilts the Pacific Ocean thermocline, the $\sim 1000\text{ m}$ transition from warm surface waters to cold bottom waters, so that it is significantly shallower in the east than in the west. It also results $\sim 0.5\text{ m}$ higher sea level in the western Pacific than the eastern Pacific in order to maintain pressure gradients (Philander, 1989). Warm water in the western Pacific causes air to rise generating low sea level atmospheric pressure, while cold water in the eastern Pacific causes air to sink generating high sea level pressure. Ascending air in the west Pacific results in high amounts of precipitation, while descending air in the east Pacific greatly reduces precipitation and results in desert conditions. Atmospheric pressure gradients across the

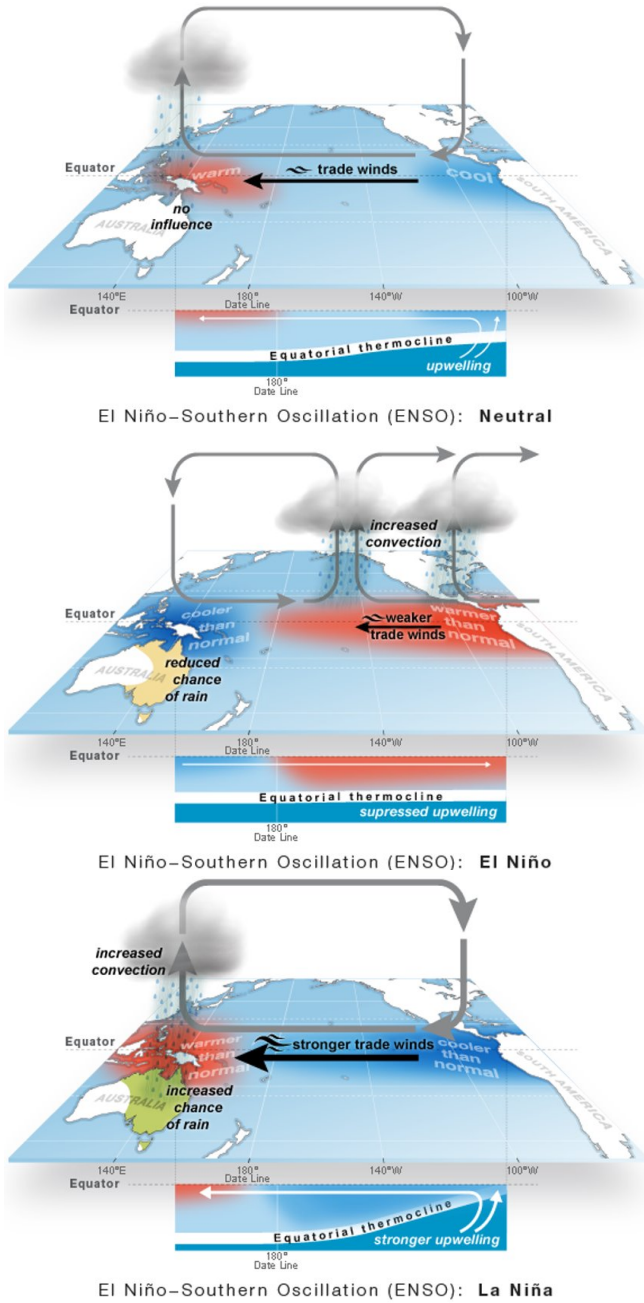


Figure 1—The three phases of ENSO (Bureau of Meteorology, 2008).

© Commonwealth of Australia 2013.

Pacific drive low altitude east to west winds and high altitude west to east winds. This creates a giant, Pacific-wide convection cell called the Walker Circulation with an ascending limb in the west, a descending limb in the east, low-altitude easterlies, and high-altitude westerlies which enhances the east-west SST, thermocline, and sea level gradient in the Pacific Ocean as part of the Bjerknes Feedback (Philander, 1989).

An El Niño event can be thought of as a reduction of the east-west imbalance that exists across the Pacific or a leveling of a metaphorical see-saw. Every 2-7 years during an El Niño Event during Northern Hemisphere winter, warm water in the west Pacific sloshes into the east Pacific, resulting in warm temperature anomalies in the east of $>0.5^{\circ}\text{C}$, cold temperature anomalies in the west, and a reduced east-west Pacific temperature gradient (Philander, 1989). Reduced temperatures in the west Pacific lead to an increase in sea level atmospheric pressure in that region, while increased SST in the east Pacific reduces sea level atmospheric pressure. The term Southern Oscillation derives from this oscillation of atmospheric pressure between El Niño and neutral conditions, and the difference in sea level atmospheric pressure between Darwin Australia and Tahiti is now used as one of the indices for the ENSO system. The reduction in the east-west SST gradient across the Pacific causes the thermocline to shoal in the west Pacific and deepen in the east Pacific and sea level to fall in the west Pacific and rise in the east Pacific, while the reduction in the atmospheric pressure gradient causes the trade winds to slacken as well as a reduction in precipitation in the west Pacific and an increase in precipitation in the east Pacific (Philander, 1989). The strongest El Niño events during the instrumental era occurred in 1982-83, 1997-98, and 2015-16 (Trenberth et al., 2019) (Figure 2). Similar to El Niño events, La Niña occurs every 2-7 years, typically following an El Niño, and results in the increase in the east-west imbalance across the Pacific or the steepening of a metaphorical see-saw. In the west Pacific during a La Niña event, SST warms, the thermocline deepens, sea level increases, atmospheric pressure decreases, and precipitation increases. In the east Pacific, SST cools, the thermocline shoals even more, atmospheric pressure decreases, and precipitation becomes even more sparse. As a result of La Niña events, the walker circulation intensifies and trade winds are strengthened (Philander, 1989).

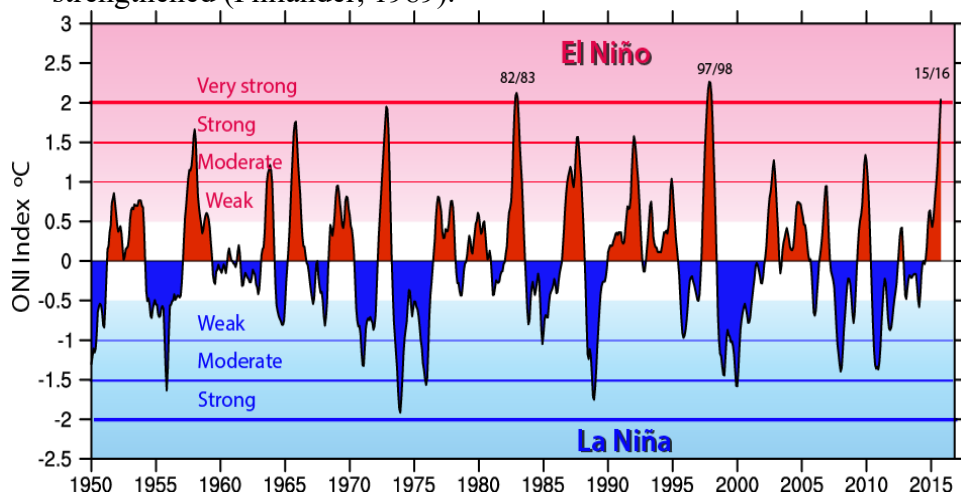


Figure 2—SST from Nino 3.4 region in the east Pacific where ENSO is monitored. An El Niño is classified as any three or more consecutive three-month periods (called the ONI index) when SST anomalies in the Nino 3.4 region exceed 0.5°C (Trenberth et al., 2019)

Effects on Peru

Because Peru is adjacent to the cold tongue, it is one of the countries hit hardest by ENSO events. The 1997-98 El Niño resulted in 374 deaths, 412 injuries, and affected 600,000 people total. Flooding ruined the crop from 114,000 hectares of land. 40,500 homes, dozens of schools, 3,100 km of roads and 370 bridges were destroyed which delayed emergency response and led tons of emergency food to rot because it could not be transported. Peru saw a 6% reduction in its sea food catch due to a reduction in upwelling (see marine life and upwelling sections). Ultimately, Peru lost ~US\$ 3.5 million or 6.2% of its GDP and spent US\$686 million to fix roads and bridges as a result of the 1997-98 El Niño event (McEntire and Fuller, 2002; French and Mechler, 2017).

The most notable impact of El Niño events on Peru is their influence on precipitation. During the average El Niño event, coastal northern Peru and inland southern Peru receive 50 mm more rain than average, while coastal southern Peru and inland northern Peru receive up to 50 mm less precipitation than average (Figure 3) (Dai and Wigley, 2000). Extreme El Niño events can see even larger precipitation anomalies. For example, northern Peru saw an increase of >2.5 m during the 1997-98 El Niño (Figure 4) (French and Mechler, 2017). Peruvian architecture often uses adobe, woven material, cane and stucco, and other cheap building materials and as such, it is particularly vulnerable to such intense rain events. It is estimated that ~51% of homes in urban areas were susceptible to harsh weather prior to the 1997-98 El Niño event. In the town of Ica (a town we drive through on day three) alone, intense rain during the 1997-1998 El Niño event caused 14,000 adobe homes to collapse from waterlogging (French and Mechler, 2017).

As a mountainous desert nation, Peru's watersheds react poorly to such dramatic increases in rain. Huaicos refer to flooding or mudslides that occur in the mountains as a result of torrential rainfall that is usually related to El Niño events. The Peruvian government classifies most of the country as a hazard zones for such risks (Figure 5)

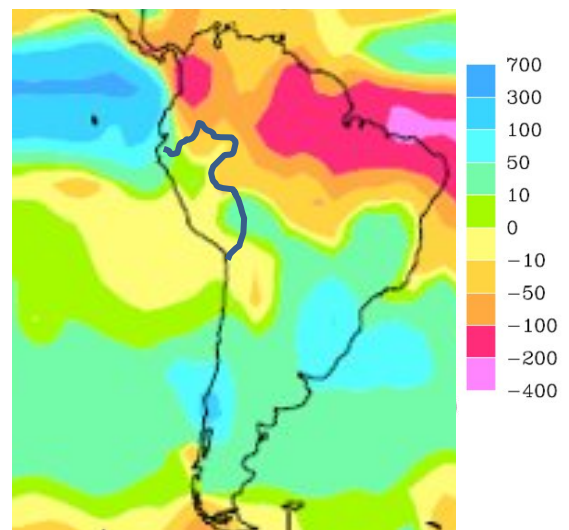


Figure 3—Precipitation anomaly (mm) during the average El Niño event (Dai and Wigley, 2000)

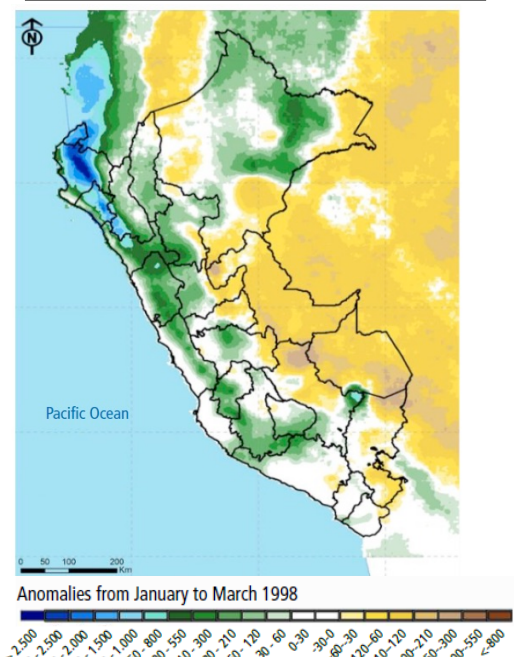


Figure 4—Precipitation anomaly (mm) during the 197-98 El Niño event (French and Mechler, 2017)

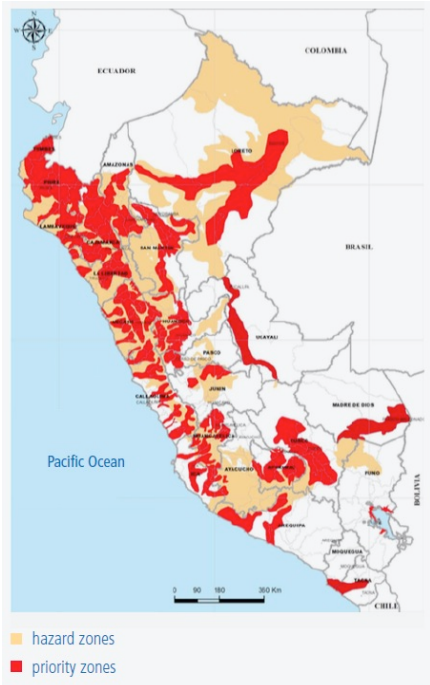


Figure 5—Hazard and Priority zones for moderate El Niño Events (French and Mechler, 2017)

(French and Mechler, 2017). Santa Teresa in a Mountain Valley outside the Area de Conservacion Regional Choququirao and near Humantay Glacier is particularly vulnerable to Huaicos and was decimated during the 1982-83 and 1997-98 El Niño Events. On January 13th 1998, maximum intensity flooding in Santa Teresa as a result of El Niño lasted 12 hours, killing 21 and leaving 430 homeless (see photos after references) (McEntire and Fuller, 2002). Peru's vulnerability to Huaicos increased significantly with the development of modern agriculture and reduction of *minifundistas* (independent small farms) following World War II. This led to mass migration to cities, with cities seeing an annual growth rate of 2.3% from 1990-1996 and Lima's population growing from 6.7 to 8.3 people between 1995 and 2000 (McEntire and Fuller, 2002). Such rapid population growth led to poor city planning allowing for construction in vulnerable areas such as on hillsides and next to rivers, a problem that was exacerbated by coastal Peruvians' desire to live near water due to the dryness of the region. Ultimately, poor city planning significantly increased the damage caused by the 1997-98 El Niño event (McEntire and Fuller, 2002).

Increased precipitation during El Niño events also increases Peruvian vulnerability to disease by putting pressure on

their lacking healthcare system. The 1997-98 El Niño destroyed sewage systems, contaminating cooking and bathing water and leading to skin irritation and intestinal disease (McEntire and Fuller, 2002). Warm humid conditions that accompany El Niño events also support the growth of malaria. The 1997-98 event created a 90 x 20 mile 10 ft deep lake in the Sechura desert in northern Peru that resulted in 30,000 diagnoses of malaria in the surrounding Piura region (Suplee, 2015). El Niño has also been cited as one of the causes of the spread of Cholera in Peru in 1991. Prior to 1991, Cholera was rare in Peru, but high SST and increased runoff associated with the 1991-92 El Niño are thought to have driven algal blooms that incubated the disease and led to the infection of 400,000 Peruvians in 1991. Aided by poor sanitation due to El Niño, the disease spread to neighboring countries and by the end of the decade, 1.2 million people in the region, 703,000 in Peru had been infected by the disease. During the 1997-98 El Niño, Peru saw a 1,000% increase in confirmed cases (Ramirez et al., 2013).

La Niña events receive less press than El Niño events likely because El Niño is more catastrophic and La Niña typically results in an intensification of conditions that already exist (i.e. the desert gets drier). Cold weather typically accompanies La Niña events. During the 2010 La Niña event, temperatures in Lima reached as low as 8.8° C for the first time in 40 years, while the Amazon region of Peru saw temperatures 10-20° C colder than typical. Cold temperatures

during that La Niña event contributed to the death of 250 children total, 64 of those in the Puno region where temperatures can reach as low as -20° C (Barbier, 2010).

History of Peruvian Adaptations to ENSO

There is geologic evidence of ENSO variability as far back as the late Miocene and geologic evidence for ENSO events in 13 kyr old Incan settlement remains (Suplee, 2015; Weiss et al., 2017). The largest known human and camelid (the camel family) sacrifice in the Americas was found in Las Llamas where the bodies of over 140 children and 200 young llamas sacrificed 550 years ago by the Inca were uncovered (Prieto et al., 2019). Based on an associated mud layer, archaeologists think the sacrifice was in response to the failure of adult sacrifices to lessen effects of an El Niño event (Prieto et al., 2019). Incan civilization mitigated the effects of El Niño events by living in the mountains and avoiding river valleys at risk of flooding (Suplee, 2015). They also actively managed erosion using terracing, drainage channels, crop rotation, contour planting and forest management (McEntire and Fuller, 2002). To prepare for food shortages as a result of El Niño, the Incans also stored food in the mountains (Suplee, 2015). Spanish colonization in the 1500s brought Spanish settlement conventions including living next to rivers and building homes out of adobe, significantly increasing Peruvian vulnerability to El Niño (McEntire and Fuller, 2002).

Scientific advances mean that ENSO events can now be predicted months to over a year in advance. After the 1982-83 El Niño event caused massive damages and the loss of ~11.6% of their GDP, Peru spent US\$300 million on 271 projects including the construction of canals, dikes, and retention walls, the expansion of drainage systems, and the reinforcing of bridges in order to prepare for the forecasted 1997-98 event (The Economist, 1998; French and Mechler, 2017). As has already been discussed, this El Niño event still had a devastating impact. This is because not all El Niño events are the same. While canonical El Niño events focus warm water in the east Pacific on the Peruvian coast, central Pacific events, also called El Niño Modoki, focus warm water in the central Pacific and produce a different temporal and spatial rainfall pattern (Figures 6 and 7) (Sanabria et al., 2018). Because the mitigation efforts for the east Pacific 1997-98 event were based on the 1982-83 central Pacific event, they largely failed, an

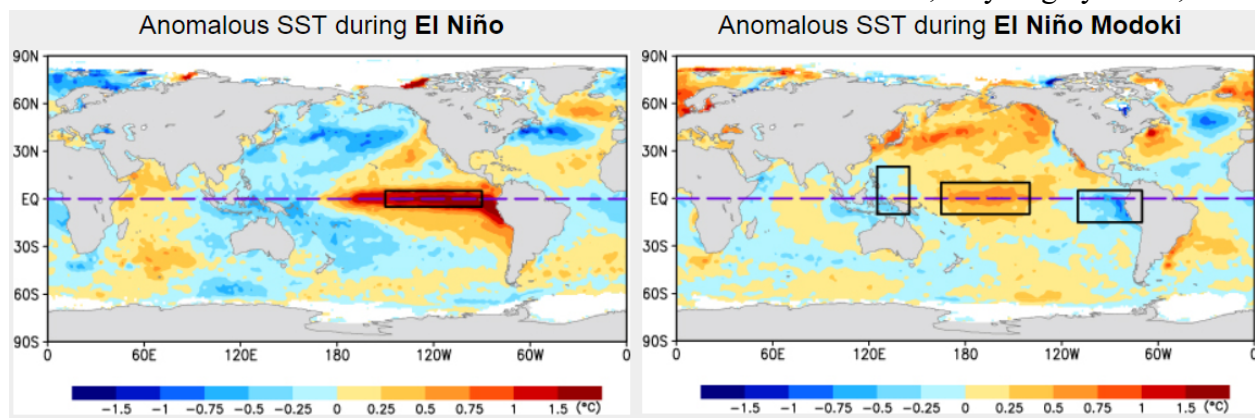


Figure 6—SST anomalies of eastern and central Pacific El Niño events (JAMSTEC)

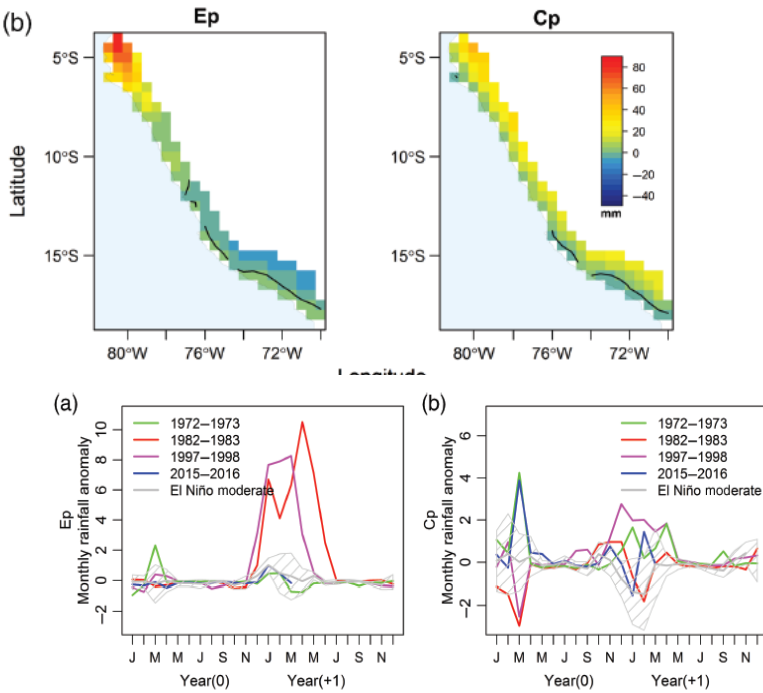
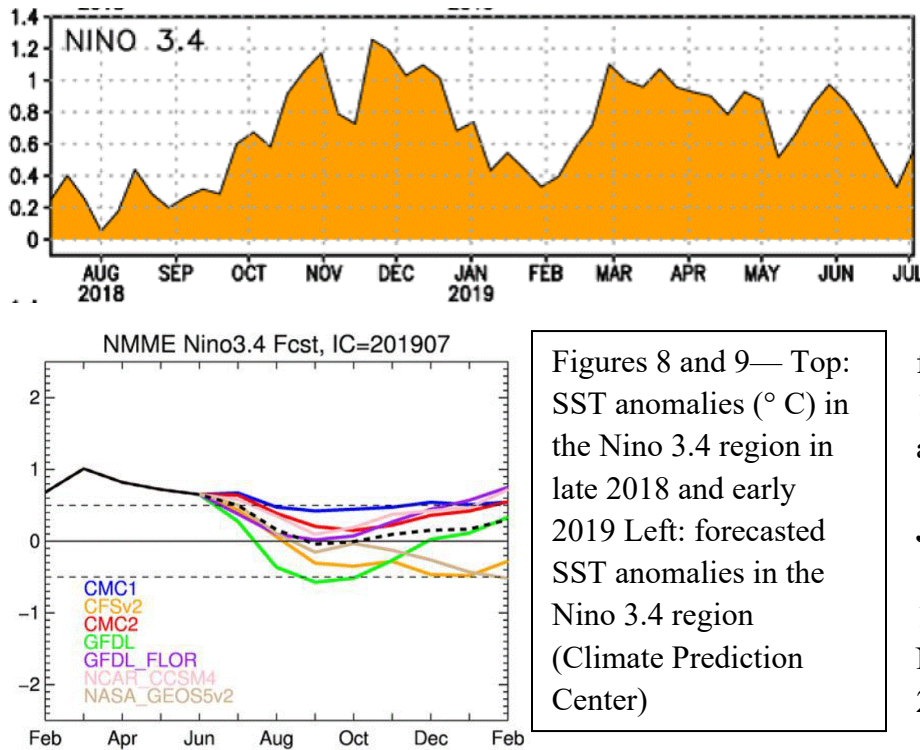


Figure 7—Top: Difference in spatial rainfall pattern during eastern Pacific (Ep) and central Pacific El Niño events. Bottom: Difference in temporal signature of eastern and central Pacific El Niño events (Sanabria et al., 2018)



Figures 8 and 9—Top: SST anomalies ($^{\circ}$ C) in the Nino 3.4 region in late 2018 and early 2019 Left: forecasted SST anomalies in the Nino 3.4 region (Climate Prediction Center)

issue made worse by the centralization of Peruvian government that slowed the response process (French and Mechler, 2017).

In 2011, the Peruvian government passed a law to form the National System for Disaster Risk Management (Si-NAGERD) to provide a structure for preparing for and

responding to natural disasters that puts an emphasis on sub-national response (French and Mechler, 2017). Under this system, Peru spent ~US\$1.5 billion to prepare watersheds for the 2015-16 El Niño which was forecasted to be on par with the 1982-83 and 1997-98 El Niño events. Despite the SST anomalies being on par with those events, the climate impacts of the 2015-16 event were muted and the preparations were not needed.

However, in 2017 a weaker coastal

El Niño occurred and though Peruvians were somewhat prepared because of the 2015-2016 event, damages from the 2017 event are considered as devastating as those from the 1982-83 and 1997-98 events (French and Mechler, 2017).

July 2019 ENSO

In winter of 2018-19, there was a weak El Niño event. As of July 19, 2019, the NOAA Climate

Prediction Center in conjunction with the International Research Institute for Climate and Society (IRI) declared a continuing El Niño Advisory, meaning there were still El Niño conditions with a +0.6° C SST anomaly in the Niño-3.4 region and a weakened Walker Circulation (Figure 8). They predict the Pacific to return to ENSO neutral conditions within the next few months and remain in neutral conditions through the coming winter (Figure 9).

References

- Australian Bureau of Meteorology. (2008). El Niño Southern Oscillation (ENSO). Retrieved August 6, 2019, from <http://www.bom.gov.au/climate/about/australian-climate-influences.shtml?bookmark=enso>
- Barbier, C. (2010). Extreme La Niña brings illness and misery to Peru. Retrieved August 6, 2019, from The Guardian website: <https://www.theguardian.com/world/2010/aug/24/peru-cold-weather-temperature-el-ninia>
- Climate Prediction Center/NCEP/NWS, & International Research Institute for Climate and Society (IRI). (2019, July). El Niño/Southern Oscillation (ENSO) Diagnostic Discussion. Retrieved August 6, 2019, from National Weather Service website: https://www.cpc.ncep.noaa.gov/products/analysis_monitoring/enso_advisory/ensodisc.shtml
- Dai, A., & Wigley, T. M. L. (2000). Global patterns of ENSO-induced precipitation. *Geophysical Research Letters*, 27(9), 1283–1286. <https://doi.org/10.1029/1999GL011140>
- French, A., & Mechler, R. (2017). *Managing El Niño Risks under uncertainty in Peru: Learning from the Past for a More Disaster-Resilient Future*. International Institute for Applied Systems Analysis.
- JAMSTEC. (2012). El Niño Modoki. Retrieved from http://www.jamstec.go.jp/aplinfo/sintexf/e/elnmodoki/about_elnm.html
- McEntire, D. A., & Fuller, C. (2002). The need for a holistic theoretical approach: An examination from the El Niño disasters in Peru. *Disaster Prevention and Management: An International Journal*, 11(2), 128–140. <https://doi.org/10.1108/09653560210426812>
- NOAA. (2013). Sea Surface Temperature (SST) Contour Charts. Retrieved August 6, 2019, from NOAA Office of Satellite and Product Operations website: <http://www.ospo.noaa.gov/Products/ocean/sst/contour/index.html>
- Philander, G. (1989). El Niño and La Niña. *American Scientist*, 77, 451–459.
- Prieto, G., Verano, J. W., Goepfert, N., Kennett, D., Quilter, J., LeBlanc, S., ... Tschinkel, K. (2019). A mass sacrifice of children and camelids at the Huanchaquito-Las Llamas site, Moche Valley, Peru. *PLOS ONE*, 14(3), e0211691. <https://doi.org/10.1371/journal.pone.0211691>
- Ramírez, I. J., Grady, S. C., & Glantz, M. H. (2013). Reexamining El Niño and Cholera in Peru: A Climate Affairs Approach. *Weather, Climate, and Society*, 5(2), 148–161. <https://doi.org/10.1175/WCAS-D-12-00032.1>
- Sanabria, J., Bourrel, L., Dewitte, B., Frappart, F., Rau, P., Solis, O., & Labat, D. (2018). Rainfall along the coast of Peru during strong El Niño events: RAINFALL ALONG THE COAST OF PERU DURING STRONG EL NIÑO EVENTS. *International Journal of Climatology*, 38(4), 1737–1747. <https://doi.org/10.1002/joc.5292>

- Supplee, C. (2015). El Nino/La Nina: Nature's Vicious Cycle. *National Geographic Magazine*. Retrieved from <https://web.archive.org/web/20150818152353/http://www.nationalgeographic.com/features/99/elnino/mainpage.html>
- The season of El Nino. (1998). Retrieved August 6, 2019, from The Economist website: <https://www.economist.com/the-americas/1998/05/07/the-season-of-el-nino>
- Trenberth, K., & National Center for Atmospheric Research Staff. (2019). The Climate Data Guide: Nino SST Indices (Nino 1+2, 3, 3.4, 4; ONI and TNI). Retrieved August 6, 2019, from <https://climatedataguide.ucar.edu/climate-data/nino-sst-indices-nino-12-3-34-4-oni-and-tni>
- Wallace, J. M., Rasmusson, E. M., Mitchell, T. P., Kousky, V. E., Sarachik, E. S., & von Storch, H. (1998). On the structure and evolution of ENSO-related climate variability in the tropical Pacific: Lessons from TOGA. *Journal of Geophysical Research: Oceans*, 103(C7), 14241–14259. <https://doi.org/10.1029/97JC02905>
- Weiss, T. L., Denniston, R. F., Wanamaker, A. D., Villarini, G., & von der Heydt, A. S. (2017). El Niño–Southern Oscillation–like variability in a late Miocene Caribbean coral. *Geology*, 45(7), 643–646. <https://doi.org/10.1130/G38796.1>

Santa Teresa Photos (From: Americo Rivas <https://tiempo26.com/la-corriente-del-nino-en-1998-borro-del-mapa-a-santa-teresa-la-convencion-cusco/#>)



Coastal Productivity & Upwelling

N. A. O'Mara

Upwelling basics: drivers and physics

Winds on Earth and other planetary bodies are primarily driven by gradients in atmospheric pressure flowing from areas of high to low pressure due to what is known as the pressure gradient force (PGF). As a result of the rotation of the Earth and the law of conservation of angular momentum, winds in the Northern Hemisphere are deflected to the right of the PGF and winds in the Southern Hemisphere are deflected to the left of the PGF in a process known as the Coriolis Effect.

When wind blows over water, a secondary deflection occurs. Water travels more slowly than the wind above it because of its higher viscosity and thus feels the Coriolis Effect to a greater degree resulting in a net motion 45° to the primary wind direction. This apparent deflection is carried down vertically in the water column as each layer (in reality of infinitesimal thickness) is dragged by the layer above it, moves more slowly and is further deflected from the original direction of movement. The friction between each subsequent layer results in a decreasing magnitude of velocity with depth bottoming out at zero around 100-150 m depending on the initial wind speed. This phenomenon is known as the Ekman spiral (fig. 1a).

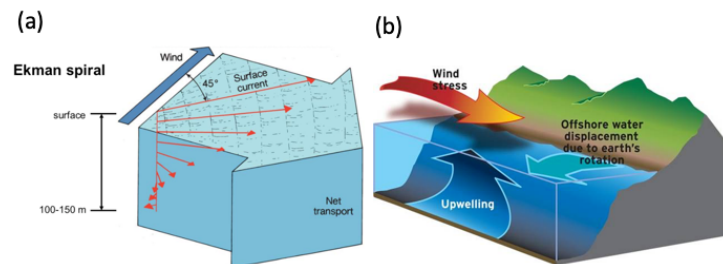


Figure 1. (a) Ekman spiral, (b) source: NOAA Fisheries

The depth integral of the water motion associated with the Ekman spiral solves to a net motion of water in the upper few hundred meters of 90° to the right (left) of the wind in the Northern (Southern) Hemisphere. When this vector of net water motion is away from a coastline or opposite in sense to an adjacent vector of water motion (e.g. fig 1b) conservation of mass dictates that water from depth must migrate toward the surface, or *upwell*, to replace the missing water in a process also known as Ekman pumping.

Where does upwelling occur?

There are seven major upwelling zones in the world's oceans: in the California Current in the North Pacific, the Canary Current in the North Atlantic, the Humboldt (or Peru) Current in the South Pacific, The Benguela Current in the South Atlantic, the West Australian Current in the Indian Ocean, along the equator (especially in the Pacific and Atlantic Oceans), and in the Antarctic Circumpolar Current (fig. 2). The common thread among the first five of these areas is their location along the eastern boundaries of the major ocean gyres where prevailing wind and ocean current directions favor offshore Ekman transport driving coastal upwelling. The

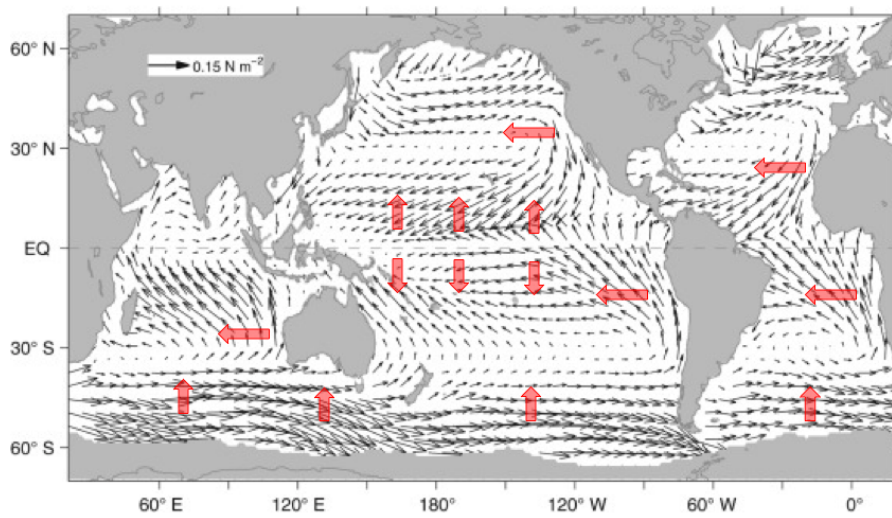


Figure 2. Vector field of global surface winds from the Encyclopedia of Atm. Sciences (2015), red arrows show major regions of surface current divergence leading to upwelling

where the strong westerly winds that circumscribe Antarctica drive intense upwelling of waters from depths of 100s-1000s of meters, providing the only connection in the world where deep waters (North Atlantic Deep Water) upwells to the surface and exchange with the atmosphere before cooling, becoming more saline and re-subducting to form Antarctic Bottom Water.

The signature of upwelling: biological productivity and the carbon cycle

Upwelling brings cooler waters rich in nutrients like nitrate (NO_3^-) and phosphate (PO_4^{3-}) into the surface ocean where light is plentiful (the photic zone) which fosters the development of phytoplankton primary producers (fig. 3a). This can be seen in satellite measurements of Chlorophyll-a (Chl-a), the primary photosynthetic pigment in most marine algae (fig. 3b). These phytoplankton serve as the base of the foodweb, ultimately providing the energy needed to support diverse and plentiful fisheries. The injection of nutrients from deeper sub-

equatorial upwelling zones result from the divergence of surface waters to the north and south of the equator as the waters of the westward moving Pacific and Atlantic equatorial currents are diverted by Ekman transport. Perhaps the most important for controlling the Earth's climate is the Southern Ocean Upwelling Zone in the Antarctic Circumpolar Current,

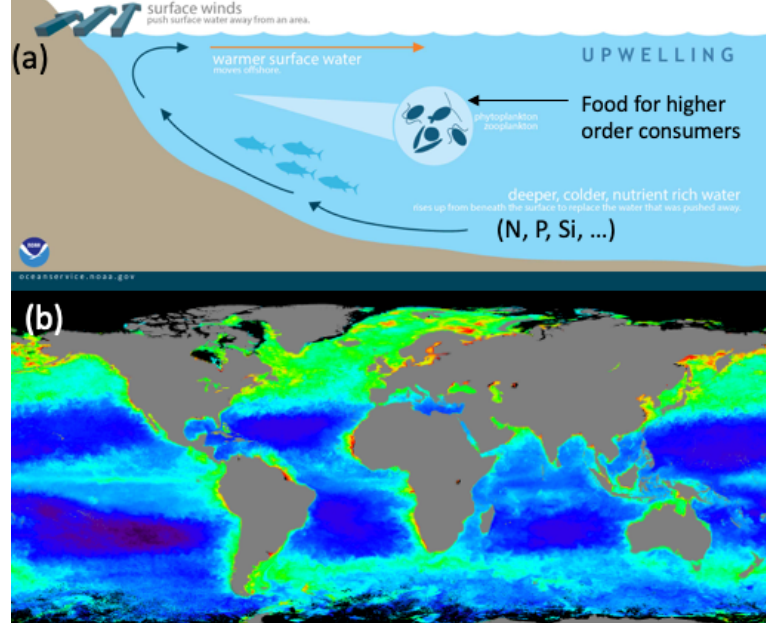


Figure 3. (a) Schematic diagram of the biological impact of upwelling from NOAA National Ocean Service, (b) satellite image of Chl-a concentration from the NASA Earth Observatory.

thermocline waters in the Humboldt Upwelling Zone supports a plethora of phytoplankton primary producers including 168 species of diatoms, 209 species of radiolarians and various other species of nano and pico-plankton (Caldwell et al., 2000).

Biological productivity also plays an important role in the ocean carbon cycle. The ocean stores ~50 times the amount of carbon as the atmosphere, and so the apportionment of carbon between the surface ocean, which readily exchanges with the atmosphere, and in the deep ocean, where it is sequestered from exchange with the atmosphere on timescales less than 1000s of years and as long as tens of millions of years if buried in marine sediment, is a critical lever on the Earth's climate. High productivity leads to enhanced export of carbon from the surface to the deep ocean serving as a major conveyor of carbon from the atmosphere to the deep ocean. Understanding this process is an incredibly important and relevant avenue of research in attempting to explain glacial/interglacial cycles and will have a profound impact on predicting the ultimate fate of anthropogenic carbon.

The Humboldt (Peru) Current Upwelling Zone

The Humboldt, or Peru, Current Upwelling Zone extends along the coast of Peru and Chile from approximately 4-40°S and is the most productive region in the world's oceans. Despite representing only 0.02% of the Earth's surface area and only 10% of the surface area of all marine upwelling zones, the Humboldt Upwelling Zone supports 15-20% of the global marine catch of the 50-58% encompassed by all upwelling zones combined. In this region the easterly Tradewinds result in year-round upwelling with enhanced upwelling during austral summer (Tarazona & Arntz, 2001).

Upwelling and ocean chemistry

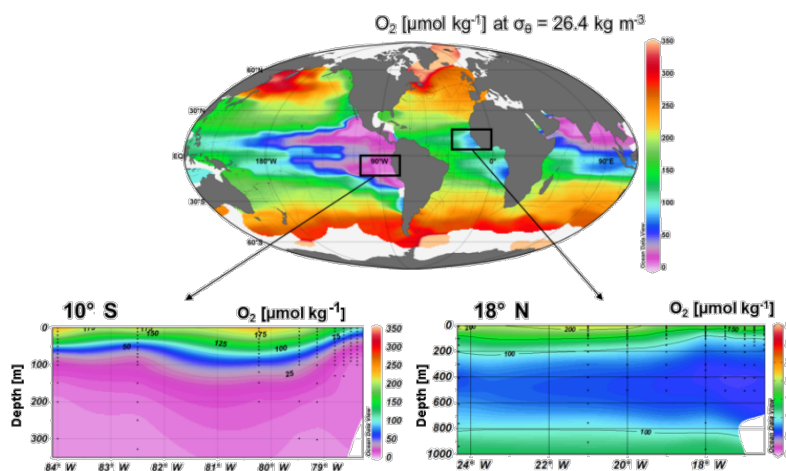


Figure 4. Map of global surface ocean dissolved oxygen concentrations, with subpanels of cross sections with depth across the Humboldt and Canary Upwelling Zones. From Löscher et al., (2016).

Phytoplankton convert atmospheric CO_2 which diffuses into the surface ocean into organic carbon (carbon fixation) to build their tissue via photosynthesis. Much of this carbon is respired or remineralized (eaten) by higher organisms and microbes back into CO_2 , however the portion that is not respired sinks to the deep ocean and is stored in marine sediment. The process of respiration (when oxygen is present) consumes oxygen in

order to convert organic carbon into energy for an organism's metabolism. Beneath the Humboldt Current exists the ocean's largest oxygen minimum zone (OMZ) where so much oxygen has been used for respiration of organic matter that dissolved oxygen (DO) concentrations in the sea water fall to zero at shallow depths. The OMZ in the eastern tropical Pacific is the largest in the world at $26.3 \cdot 10^6$ km² (Paulmier & Ruiz-Pino, 2008) with concentrations of dissolved oxygen falling to zero at depths of ~100m (Löscher et al., 2016) (fig. 4). Low DO can be detrimental to marine life, especially sessile coastal organisms like shellfish and poses a threat to coastal marine food resources in Peru and around the world. Increased anthropogenic use of nitrogen and phosphorous fertilizers is leading to eutrophication (excessive nutrients) of coastal regions and is expected to exacerbate this problem via expansion of the OMZs in the future (Sherman & Hempel, 2008).

The impact of oscillatory climate variability and upwelling

On interannual and interdecadal timescales respectively, the El Niño Southern Oscillation (ENSO) and the Pacific Decadal Oscillation (PDO), two oscillatory climate modes, are important drivers of sea surface temperature (SST) and climate variability on the planet. These two phenomena result from complex interactions between atmospheric circulation and ocean SSTs. ENSO is characterized by changes in the Walker Circulation where a slackening of the Tradewinds allows for the migration of warm waters from the western tropical Pacific towards the eastern tropical Pacific to occur. During this scenario termed an El Niño by Peruvian fisherman in as early as 1892 (Ros-Tonen & Van Boxel, 1999) the warm water increases stratification in the east and deepens the thermocline resulting in a decrease in upwelling occurring about every ~5-7 years. The PDO on the other hand oscillates on timescales of 20-50 years with positive phases being characterized by a strong Aleutian Low pressure system which similarly results in enhanced westerly winds in the Pacific bringing more warm water towards the east (Mantua & Hare, 2002). Both of these phenomena have detrimental impacts on productivity in the eastern tropical Pacific (Correa-Ramirez et al., 2012; Huyer et al., 1987).

During positive phases of the ENSO and PDO, primary productivity is reduced and SSTs are warmer in the eastern tropical Pacific but these conditions do not universally impact all fisheries in the same way. Observations show that during negative phases of ENSO/PDO anchovy catches are elevated off the coast of Peru, but during positive phases sardine catches are much higher (Sandweiss et al., 2004). An acoustic stock survey conducted by Swartzman et al., (2008) found that anchovies (Peru's current largest fishery and the largest overall fishery in the world (Schreiber et al., 2011)) prefer a specialized habitat of cooler waters and to prey on large zooplankton, while sardines, a more generalist filter-feeding species, can consume smaller prey and often reside in warmer waters. Positive phases of the ENSO and PDO have been shown to decrease size of phytoplankton in addition to increasing SST (Iriarte, José Luis; González, 2004). In recent decades, changes in fish stocks resulting from these oscillatory climate modes has become a problem for Peruvian fisheries; since the expansion of the fishmeal and fish oil

industries in the 1950's anchovies have become the preferred catch. Much of the infrastructure of the fishing industry in Peru is geared for catching the more profitable anchovies, so the industry today is vulnerable to these swings.

Climate change and upwelling: future outlook

Since the middle of the 19th century SSTs off the coast of Peru have been decreasing, organic carbon flux to depth has been increasing, and Chl-a concentrations have been increasing, all suggestive of an increasing trend in upwelling over the last 150 years, however it remains an open question of whether this trend will continue. Over the last few decades there has been fierce debate over the future of coastal upwelling in a warming world resulting from anthropogenic

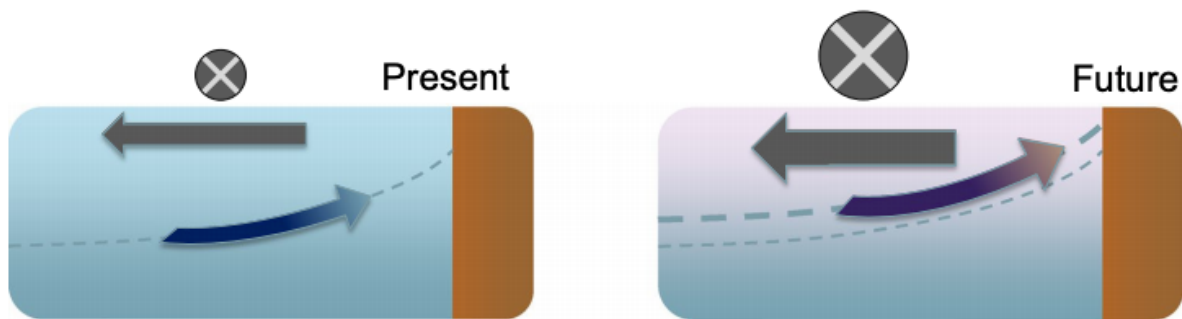


Figure 5. Schematic diagram depicting the relative projected change in wind strength (X), ocean temperature (colors), and location and magnitude of upwelling waters between the present (left panel) and future (right panel) as predicted by Oyarzún and Brierley et al., (2019)

climate change. Two primary arguments are at odds: (1) increased ocean temperatures will result in increased stratification of the ocean resulting in buoyancy barrier, or in other words a physical "cap," that will reduce the amount of cool deep water from upwelling to the surface, while the second argument (2) posits that increases pole-to-equator temperature gradients which result from disproportionate warming of polar regions compared to the tropics will lead to higher global wind stress and thus increase coastal upwelling (Bakun et al., 2010). A recent study comparing the output of 13 different ocean-atmosphere coupled general circulation models (GCMs) all from the Coupled Model Intercomparison Project (CMIP5) found that perhaps both scenarios are true (Oyarzún & Brierley, 2019). This model ensemble comparison found that increased wind stress globally is likely to increase the amount of upwelling, while increased ocean stratification changes the source depth of these upwelling waters. The predictions of these models suggest that while upwelling will increase, more water will be sourced from shallow thermocline waters that are warmer and far less rich in nutrients which will likely have troublesome effects on primary productivity and fisheries as well as reduce the uptake of heat from the atmosphere by the ocean.

References

- Arias Schreiber, M., Ñiquen, M., Bouchon, M., Arias Schreiber, M., Ñiquen, M., & Bouchon, M. (2011). Coping Strategies to Deal with Environmental Variability and Extreme Climatic Events in the Peruvian Anchovy Fishery. *Sustainability*, 3(6), 823–846.
<https://doi.org/10.3390/su3060823>
- Bakun, A., Field, D. B., Redondo-Rodriguez, A., & Weeks, S. J. (2010). Greenhouse gas, upwelling-favorable winds, and the future of coastal ocean upwelling ecosystems. *Global Change Biology*, 16(4), 1213–1228. <https://doi.org/10.1111/j.1365-2486.2009.02094.x>
- Caldwell, M., Heldmaier, U. G., Mooney, H., & E-D Schulze, U. (2000). *Coastal Marine Ecosystems of Latin America. Ecological Studies* (Vol. 144). Retrieved from <https://link.springer.com/content/pdf/10.1007%2F978-3-662-04482-7.pdf>
- Correa-Ramirez, M. A., Hormazabal, S. E., & Morales, C. E. (2012). Spatial patterns of annual and interannual surface chlorophyll-a variability in the Peru–Chile Current System. *Progress in Oceanography*, 92–95, 8–17. <https://doi.org/10.1016/J.POCEAN.2011.07.008>
- Huyer, A., Smith, R. L., & Palusziewicz, T. (1987). *Coastal upwelling off Peru during normal and El Niño times, 1981–1984. JOURNAL OF GEOPHYSICAL RESEARCH* (Vol. 92). <https://doi.org/10.1029/JC092iC13p14297>
- Iriarte, José Luis; González, H. E. (2004). *Phytoplankton size structure during and after the 1997/98 El Niño in a coastal upwelling area of the northern Humboldt Current System.* Retrieved from www.int-res.com
- Löscher, C. R., Bange, H. W., Schmitz, R. A., Callbeck, C. M., Engel, A., Hauss, H., et al. (2016). Water column biogeochemistry of oxygen minimum zones in the eastern tropical North Atlantic and eastern tropical South Pacific oceans. *Biogeosciences*, 13, 3585–3606. <https://doi.org/10.5194/bg-13-3585-2016>
- Mantua, N. J., & Hare, S. R. (2002). The Pacific Decadal Oscillation. *Journal of Oceanography*. <https://doi.org/10.1023/A:1015820616384>
- Oyarzún, D., & Brierley, C. M. (2019). The future of coastal upwelling in the Humboldt current from model projections. *Climate Dynamics*, 52(1–2), 599–615. <https://doi.org/10.1007/s00382-018-4158-7>
- Paulmier, A., & Ruiz-Pino, D. (2008). Oxygen minimum zones (OMZs) in the modern ocean. <https://doi.org/10.1016/j.pocean.2008.08.001>
- Ros-Tonen, M. A. F., & Van Boxel, J. H. (1999). *El Niño in Latin America: The Case of Peruvian Fishermen and North-East Brazilian. Estudios Latinoamericanos y del Caribe.* Retrieved from <https://www.jstor.org/stable/pdf/25675842.pdf?refreqid=excelsior%3A3d52cc27341afb178e52f3863636512f>
- Sandweiss, D. H., Maasch, K. A., Chai, F., Fred, C., Andrus, T., & Reitz, E. J. (2004). Geoarchaeological evidence for multidecadal natural climatic variability and ancient Peruvian fisheries. <https://doi.org/10.1016/j.yqres.2004.02.008>

- Sherman, K. (ed. ., & Hempel, G. (ed. . (2008). The UNEP Large Marine Ecosystem Report: a perspective on changing conditions in LMEs of the world's Regional Seas. np npub. Retrieved from <http://agris.fao.org/agris-search/search.do?recordID=XF2015036057>
- Swartzman, G., Bertrand, A., Gutiérrez, M., Bertrand, S., & Vasquez, L. (2008). The relationship of anchovy and sardine to water masses in the Peruvian Humboldt Current System from 1983 to 2005. *Progress in Oceanography*, 79(2–4), 228–237.
<https://doi.org/10.1016/j.pocean.2008.10.021>
- Tarazona, J., & Arntz, W. (2001). The Peruvian Coastal Upwelling System (pp. 229–244). Springer, Berlin, Heidelberg. https://doi.org/10.1007/978-3-662-04482-7_17

Arc Volcanism in Peru
Henry Towbin

(Awaiting Submission to Group Leaders)

Rainbow Mountain (Vinicunca) Mineralogy

Jonathan Lambert

Background

Rainbow Mountain is located approximately 80 km southeast of Cusco in Peru (Figure 1). It is accessible by an approximately three-hour drive followed by a 5 km hike to the mountain ridge, which is 5,200 meters (17,100 ft) above sea level. Rainbow Mountain (a.k.a. Vinicunca or “Cerro Colorado”) is within Vilcanota Range of the Cordillera Oriental in the Andes Mountains. One of the highest mountains in Peru (Mount Ausangate), at 6,400 m, is snowcapped throughout the entire year and is located in the same Vilcanota Range as Vinicunca.

Rainbow Mountain is a relatively new tourist destination, only greatly increasing in numbers of visitors since the early 2000s. Therefore, trails and infrastructure on the Mountain are not pristine. Additionally, few detailed reports or scientific studies on the Mountain have been prepared, especially in English.

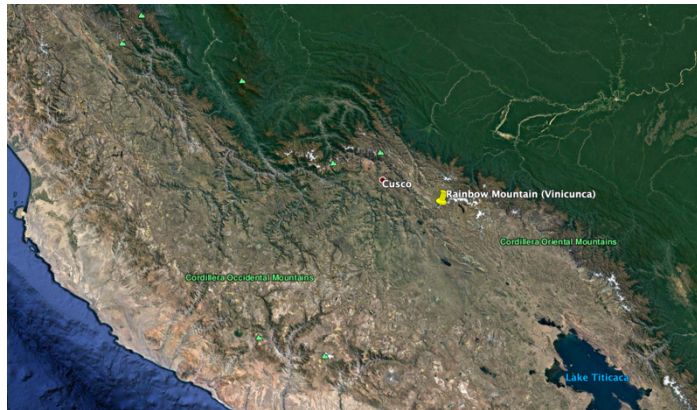


Figure 7: Satellite image of southern Peru showing the location of Rainbow Mountain (yellow pin) (Google Earth)

Regional Geology

Rainbow Mountain is located in the Andes. As has been discussed previously in this course, the Andes formed by subduction of the Nazca Plate underneath the South American Plate, initiating mountain building and uplift. Around Rainbow Mountain, pre-Cambrian metamorphic schists and quartzites dominate, overlain by Ordovician slates as well as upper Paleozoic brown-red shales and sandstones (Oppenheim, 1946). The coloration of Rainbow Mountain in particular is due to environmental conditions and mineralogy when the sediments were deposited, as well as subsequent diagenetic alteration.



Figure 8: Digitally enhanced photograph showing the vivid colors of Rainbow Mountain (travelandleisure.com)

Mineralogy

Rainbow Mountain has seven different distinct colors that can be seen (Figure 2) and their mineralogy has been briefly described in a report by the *Cultural Landscape Office of the*

Decentralization of the City of Cusco. The colors are: pink, white, purple/lavender, red, green, yellow/gold/mustard, and brown. Below, further detail is given on the mineral composition that leads to these colors.

The **pink** color at Rainbow mountain is due to a combination of red clay (ultisols)(Figure 4) and sandstone. Ultisols are formed in very humid regions (Figure 3) due to intense weathering and leaching, resulting in a clay-enriched soil layer dominated by minerals such as quartz, kaolinite, and iron oxides. They contain no calcareous material and are formed over hundreds of thousands of years, so are not present in formerly glaciated regions, as typical interglacial periods are shorter than 100 kyr.

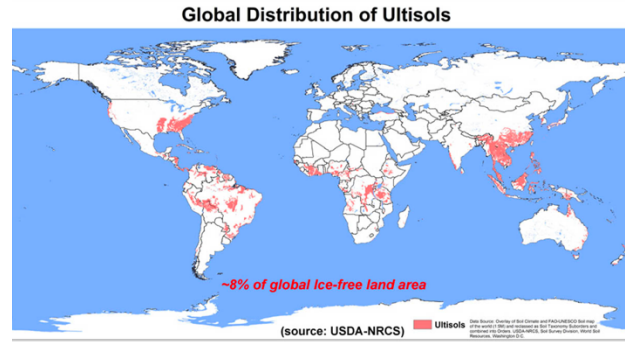


Figure 9: Map of global distribution of ultisols showing high prevalence in tropics/subtropics (USDA NRCS)



Figure 10: Photo of ultisol horizon within the soil column (USDA NRCS, Georgia)



Figure 11: Quartz sandstone (csmgeo.csm.jmu.edu)



Figure 12: Fossiliferous limestone (Wikipedia)

The **white** color of the Mountain is due to a combination of quartz sandstone (Figure 5) and limestone (Figure 6). Quartz sandstones are formed after extreme weathering and sorting of sediments. Complete chemical weathering occurs, with final removal of clay in high energy environments such as beaches. Quartz sandstones are not very common due to the extremely energetic conditions needed leading to their formation. Limestone is usually composed of skeletal calcite/aragonite from marine organisms such as corals, foraminifera, mollusks, etc. However, limestone can also be formed through chemical precipitation in warm, shallow marine waters.

The **purple/lavender** color is from a combination of marlstone (Figure 7) and silicates (opal)(Figure 8). Marlstones are a calcium carbonate rich mudstone with variable amounts of clay and silt. They are typically found in lacustrine environments. Edrett et al. (2015) observed cyclic limestone/marlstone formation within lakes associated with basin-level hydrological changes due to Milankovitch orbital variability. These processes may have been in play in the formation region of Rainbow Mountain. Opal can be formed multiple ways, but on land it is formed as water passing through the earth leaches silica from sandstones into natural cracks and voids, leaving silica deposits. Opal is also formed from diatom oozes, as diatoms make their tests from silica. As the opal in Rainbow Mountain is purple in color, it was likely formed terrestrially rather than by diatoms, as diatomaceous opal is white in color.



Figure 13: Marlstone (mindat.org)



Figure 14: Peruvian opal ([Wikipedia](https://en.wikipedia.org))



Figure 15: Argillite ([Smithsonian](https://www.smithsonianmag.com))
shale.



The **red** color is from argillites (Figure 9) and Neogene claystones (~23 – 2.6 Ma) high in iron oxides (Figure 10). Argillites are a more highly indurated mudstone (compacted without the introduction of heat) and contain variable amounts of silt and clay-sized particles. Argillites are less laminated than shale and lack the cleavage distinctive of slate. Claystones are defined as greater than 50% hardened clay (< 1/256 mm particles) and contain no laminations such as in



Figure 16:
Claystone veins
(red)(Karim et al.,
2017)



Figure 17: Phyllite (geology.com)

The **green** color is from metamorphic phyllites (Figure 11), which are foliated (comprised of thin sheets) due to low levels of heat, pressure and chemical activity. Phyllites are composed of flake-shaped mica minerals (sheet silicates) in parallel alignment, giving them a reflective sheen which distinguishes phyllites from shale. They are usually gray, black or greenish in color and weather to tan/brown. This type of rock is formed from fine-grained sedimentary rocks (shale or mudstone) in convergent plate boundary environments involving continental lithosphere. Directed pressure moves the clay mineral grains to parallel alignment, and heat and chemical activity transforms the grains into chlorite or a mica mineral. Continued heat and pressure enlarge the grains and further aligns them.

The **yellow/gold/mustard** color is a product of limonites (Figure 12). Limonites are not true minerals, but rather a “mineraloid” composed of hydrous iron oxides in association with iron minerals such as goethite and hematite. They occur as a secondary material formed from the weathering of hematite, magnetite, pyrite and other iron and iron-sulfide materials, and are often not crystalline by amorphous. Limonites are sometimes found in paleo-swamps, lakes, and marine environments where hydrous iron oxides form as precipitated sediments. They can also be seen at springs and mine openings where acidic, iron-rich waters emerge and are subsequently oxidized. Often, limonites provide the major iron/color component to laterite (“brick”) soils, which are formed in tropical areas under extreme weathering and high concentrations of iron and aluminum.



Figure 18: Limonite (Wikipedia)



Figure 19: Conglomerate (Wikipedia)

The **brown** color is due to Quaternary conglomerates (2.6 Ma to present)(Figure 13) containing goethite or oxidized limonite. Conglomerates are coarse-grained clastic sedimentary rocks containing rounded grains larger than 2 mm. The space between these large grains in conglomerates is filled by smaller particles such as sand, silt, and/or clay, with calcite or quartz binding the rock together. These large rounded grains are delivered to sites during extreme flow or

wave action or during events such as shoreline transgressions. The smaller grains infill pores spaces from above and compaction and deposition of chemical cement binds the sediments to form rock.

Mining Interests

Because of the wealth of mineral deposits in the Rainbow Mountain region, there has been recent interest in mining copper and iron ore. In March 2018, Camino Minerals Corp (a Canadian company) was given a mining concession after showing interest in March 2015. However, subsequent local outcry led to an alleged voluntary withdrawal of mining rights by the company in June 2018. Soon after, in November 2018, the president of Peru banned all mining activity in the area for 12 months in hopes that this would provide enough time for the classification of the Rainbow Mountain as a regional conservation area.

References

- Eldrett, James S., et al. "Origin of limestone–marlstone cycles: astronomic forcing of organic-rich sedimentary rocks from the Cenomanian to early Coniacian of the Cretaceous Western Interior Seaway, USA." *Earth and Planetary Science Letters* 423 (2015): 98-113.
- Karim, Kamal H., Hyam S. Daoud, and Abdulla RH Kuradawy. "Record of Khurmala Formation (Late Paleocene–Early Eocene) in the Sulaimaniah governorate, Kurdistan region, northeast Iraq." *The Iraqi Geological Journal* (2018): 34-55.
- Oppenheim, Victor. "Geological reconnaissance in southeastern Peru." *AAPG Bulletin* 30.2 (1946): 254-264.
- <https://www.travelpulse.com/news/destinations/peru-protects-famed-rainbow-mountain-from-mining-interests.html>
- <https://busquedas.elperuano.pe/normaslegales/suspenden-admision-de-petitorios-mineros-en-el-area-de-la-mo-decreto-supremo-n-032-2018-em-1716342-4/>
- <https://csmgeo.csm.jmu.edu/geollab/Fichter/SedRx/Rocks/SSquartz.html>
- https://www.nrcs.usda.gov/wps/portal/nrcs/detail/soils/survey/class/maps/?cid=nrcs142p2_053609
- <https://collections.si.edu/search/gallery.htm?og=national-museum-of-natural-history>
- https://www.geocaching.com/geocache/GC6ZF9W_colored-mountains-of-vinicunca
- <https://www.gob.pe/cultura/>
- Mineralogy/Sedimentology basics from mindat.org and geology.com
- Some images from Wikipedia.org
- Google Earth Pro

Tropical glaciers, mass balance and Peruvian glacial change

Jonathan Kingslake

Tropical glaciers make up a small proportion of global ice mass, but provide vital water resources to communities and ecosystems in the high-elevation environments in which they are found. Peru's glaciers are retreating rapidly due to rising air temperatures (Bradley et al., 2009). Between 1970 and 1997 Peru's glaciated area reduced by 22% (Bury et al., 2011) and the Vilcanota-Urubamba basin (around Cusco) lost 37.3% of its ice (by volume) between 1988 and 2016 (Drenkhan et al., 2018). As ice is lost, decadal changes (initial increases and subsequent decreases) in water resources are being observed. On a centennial timescale, Peruvian glaciers, similar to European glaciers, have retreated since the end of the Little Ice Age, LIA. We will be visiting some incredibly-well preserved LIA moraines in the Salcantay region, which were dated by Licciardi et al. (2009). The way to understand all changes in ice mass is through the simple concept of mass balance. This is introduced below, followed by the energy balance, which controls parts of the mass balance. Decadal and centennial changes in ice mass in Peru are discussed and then the Salcantay and Licciardi et al.'s work are described.

Mass balance

Mass balance controls the growth and retreat of ice masses. It is the difference between the total mass entering the glacier or ice sheet per unit time and the total mass leaving the system per unit time. Mass balance is sometimes expressed as a mass per unit time, but you can also divide this value by the surface area of the glacier and by the density of either water or ice (917 kg m^{-3}) and express mass balance in distance per time (e.g., m yr^{-1}).

Mass entering the system is called accumulation and the primary source of accumulation is snow fall. Other sources of accumulation include freezing of rain or other water that flows on to the ice, direct deposition from the atmosphere, and freezing on to the base of the ice, but snow fall is the primary source in most glaciers and ice sheets. Snowfall is nonlinearly controlled by air temperature. The simplest temperature dependence comes from the fact that above 0°C precipitation falls as rain. A secondary temperature dependence arises from the increased capacity of warmer air to hold moisture.

Mass leaving the system is called ablation. Sources of ablation include scouring (mechanical removal of snow or ice by the wind), calving (when portions of a glacier or ice shelf fracture and detach from the margin of the ice), sublimation (transformation of snow/ice into water vapor), and melting. Melting is dominant in mountain glaciers. Sublimation is also potentially significant in tropical glaciers (Vuille et al., 2008) and dry parts of Antarctica (Bintanja et al., 1999). Just like accumulation from snow fall, ablation from sublimation and melting are sensitive to air

temperatures. This can be understood in detail by examining the *surface energy balance* (next section).

Because accumulation and ablation are weather dependent, different parts of glaciers contribute positively and negatively to mass balance at different times of year. Glaciers in non-tropical climates (where there is significant seasonality in weather conditions) generally experience distinct ablation and accumulation seasons (aligning broadly with Summer and Winter, respectively). Furthermore, lower temperatures at higher elevations generally lead to a high-elevation region called the accumulation zone, which averaged over the whole year experiences *net* accumulation, i.e. total Winter accumulation is higher than total Summer ablation. Vice versa, high temperatures at low elevations lead to an ablation zone which averaged over the whole year experiences *net* ablation.

Glaciers in tropical climates also have ablation zones and accumulation zones dictated primarily by elevation, but they do not always have clear ablation and accumulation seasons. In some cases, tropical glaciers experience higher ablation in the dry season (e.g., Bradley et al., 2006), but in others (Sicart et al., 2011) coupling between snowfall, humidity, albedo and melting create complex seasonality through the surface energy balance.

Surface energy balance

The surface energy balance dictates sublimation and melting rates. It is the balance between incoming and outgoing energy fluxes. Incoming fluxes include shortwave solar radiation, which depends on cloudiness, time-of-day, season, latitude, and altitude, and longwave radiation from the atmosphere, which depends on atmospheric temperature and cloudiness. Outgoing fluxes include the reflected shortwave radiation, which is dictated by the incoming shortwave radiation and the albedo, and the longwave radiation from the surface, which depends on the surface temperature. Fluxes that can either be positive (by convention a flux that supplies energy to the ice surface) or negative (one that removes energy from ice surface) are sensible heat exchange with the air, which depends on near-surface air temperature and wind speed, and latent heat exchange (the energy used during sublimation or liberated during deposition), which depends on air temperature, wind speed, and humidity.

The energy left over after these energy fluxes are summed is used to either change the temperature of the surface if it is colder than the melting point, or to melt snow and ice if the surface is at the melting point.

Returning to the seasonality of mass balance, the surface energy balance dictates ablation and can lead to complexity seasonality in tropical-glacier mass balance. Sicart et al. (2011) instrumented Zongo Glacier, Bolivia, 200 km east-south-east of Puno, and modelled the glacier's

mass balance and surface energy balance over one year. Due to its low latitude air temperatures varied little seasonally. However, melt rates did vary on this timescale. They found that low melt rates during the dry season were due to low cloudiness that provided limited incoming longwave radiation. Melt rates increased as the incoming solar radiation increased from September to December, due simply to the solar zenith angle increasing. In the wet season, snowfall increased the albedo, increasing the outgoing shortwave radiation, and reducing melting. In summary, melting is strongly dictated by temperature in all glaciers and ice sheets, but even though in tropical glaciers air temperatures do not significantly vary seasonally, other surface-energy-balance components can lead to complex seasonality in melting.

Debris or sediments accumulated on the surface of glaciers has a profound effect on the surface energy balance and therefore the mass balance of glaciers. Debris comes from the valley walls or the bed of the glacier, and is carried through or along the surface of the ice by ice flow. Surface debris lowers albedo, decreasing outgoing shortwave radiation and increasing melting. However, when debris accumulates in a surface mantle of a few centimeters or more in thickness it tends to insulate the ice from warm air temperatures and increasing debris thickness leads to lower melt rates (Nicholson and Benn, 2006). Recent modelling has tackled complexities arising when the debris layer is porous and wind flow at the ice surface is a strongly decreasing function of debris thickness (Evatt et al., 2015). According to the theory, this decreases the energy used in sublimation, leaving more energy available for melting. When debris layers get very thick, ice can remain for centuries even when the glacier has retreated far up-valley (Östrem, 1959). It is possible that the area inside the moraines we will see at Salcantay contains ice-cored moraines left over from the LIA (see below).

Ice flow, glacier equilibrium and mass changes

In a stationary climate, glaciers and ice sheets reach an equilibrium whereby the total mass in is equal to the mass out – the mass balance is zero. How do they do this? Through ice flow. Ice flows viscously under its own weight and moves mass from high-elevation accumulation areas to lower elevation ablation areas. The rate of ice flow depends on many things, but the most important one is ice thickness. Essentially, a thicker glacier weighs more than a thinner glacier, so a thicker glacier flows faster than a thinning one. This provides the mechanism by which the glacier can reach equilibrium with its climate. If a thin glacier is receiving lots of accumulation and it is flowing too slowly to move mass quickly enough down to the ablation zone, then the ice will remain at high elevations where it's cold and it will not be removed by ablation. The result of this positive mass balance will be that the glacier gets thicker. The ice will consequently flow faster and ice will be moved to lower elevations more rapidly, increasing ablation until it balances accumulation and the glacier reaches a dynamic equilibrium.

In most glaciers worldwide today the reverse is true; glaciers are larger than the climate-dictated equilibrium size. Ablation is increasing, so ice is thinning and flowing more slowly. Under

moderate warming, glaciers can find a new equilibrium where the ice is thinner, flow is slower, and ablation remains the same as it was before warming because the ice doesn't reach such low elevations. But, it is also possible that air temperatures rise so far that the glaciers disappear completely. This is the situation predicted for most Peruvian glaciers (Drenkham et al., 2018).

This is a very simplified way of looking at this as it ignores, among other things, the fact glaciers have lateral extents and that a larger glacier receives more accumulation purely by virtue of its larger surface area. But the simple argument captures the essence of interactions between climate and glaciers.

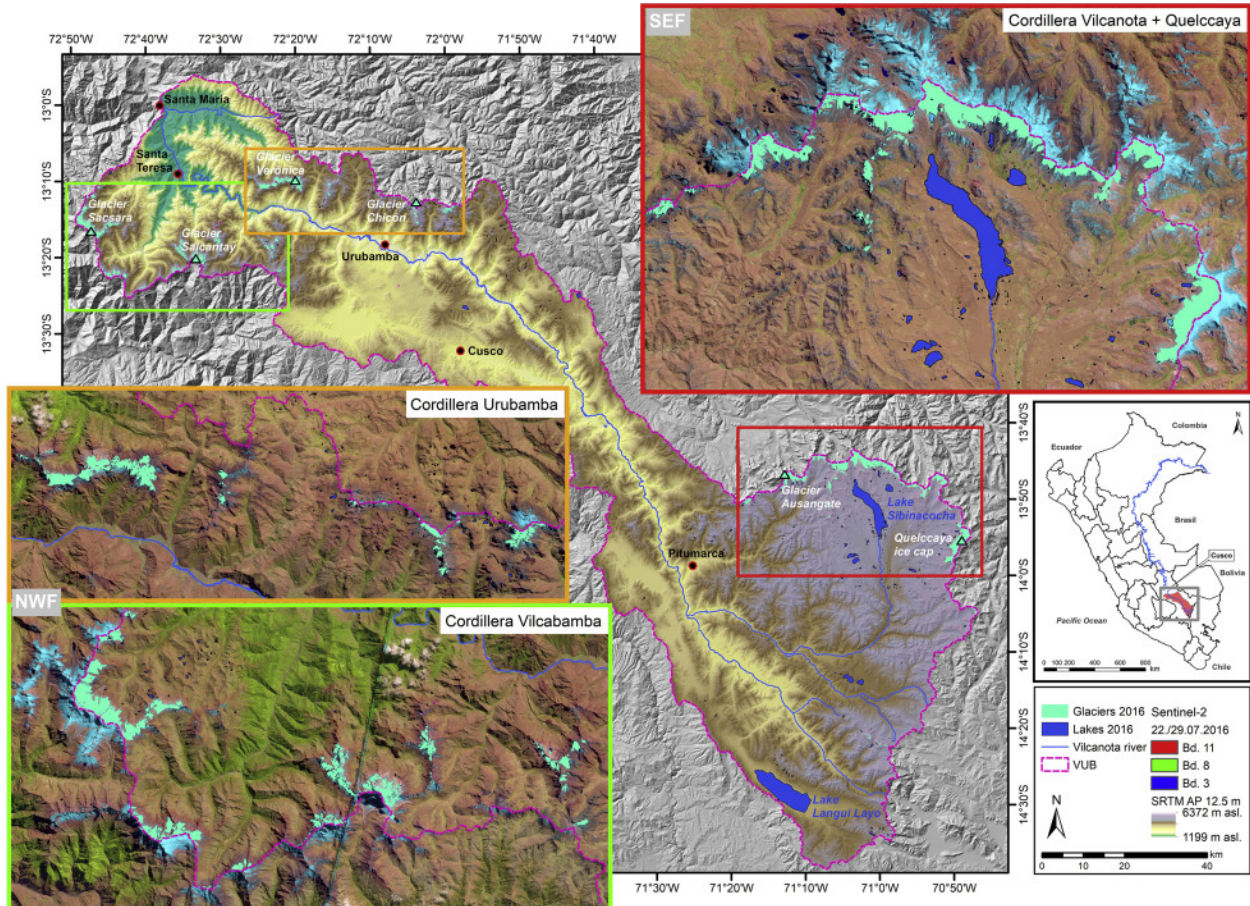


Figure 20: Overview of the Vilcanota-Urubamba-Vilcabamba basin (VUB) situated in Peru (rectangle in the small overview map) with main cities (red circles), prominent glaciers (turquoise triangles) and two principal reservoirs (Sibinacocha and Langui Loy). Glaciers belonging to the VUB (dashed pink delimitation) are highlighted as turquoise area. NWF=northwestern glacier fragment, SEF=southeastern glacier fragment. Reproduced from Drenkham et al., 2018.

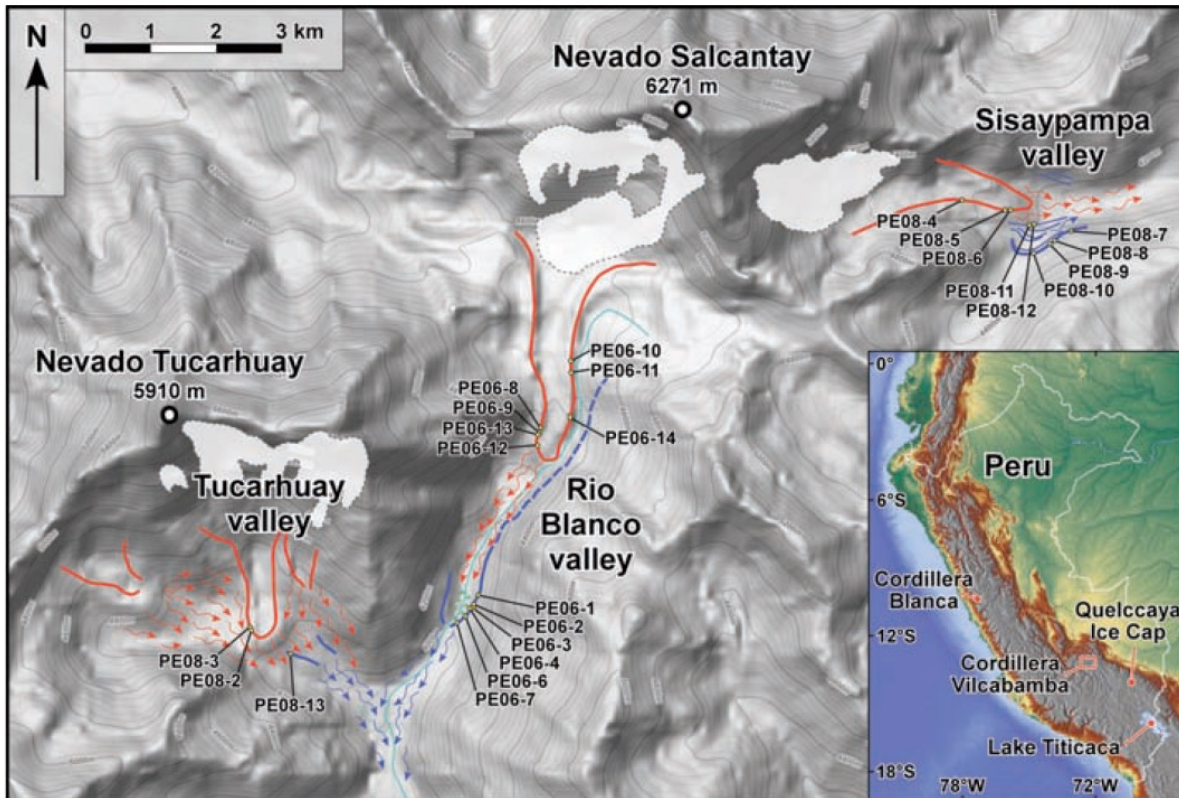


Figure 2: Geomorphic map of the area studied by Licciardi *et al.* (2009). Solid lines show inner (red) and outer (blue) moraines, and arrows show associated outwash; dashed lines indicate inferred locations. White areas represent approximate locations of present-day glaciers in mapped drainages. Base maps from Google Maps. Reproduced from Licciardi *et al.* (2006).

Impacts on water supplies

Much of Peru's population (70%) lives along the arid coast and have access to <2% of the country's water resources. Glaciers currently provide a significant proportion of the water used in households, industry and agriculture high in mountain catchments. Glaciers also reduce the seasonality of water supplies, by generating melt in the dry season, when other sources of water (e.g., rain at lower elevations) is reduced (Bury *et al.*, 2009).

A focus of research into the decadal-to-centennial impacts of glacier recession on water resources in Peru has been the Cordillera Blanca, to the north of Lima. Baraer *et al.* (2012) studied trends in hydrographs from sub-basins within an important watershed in this region, and interpreted the trends with the aid of a hydrological model of glacier runoff. The modelling results (in agreement with previous work; e.g., Huss *et al.*, 2008) suggest that as mass balance decreases, runoff initially increases, as the glaciers lose mass, then decreases as the glacier provides less runoff. This initially increased runoff lasts decades or perhaps a century, depending on the imposed glacier retreat scenario. Hydrograph analysis showed that most of the catchments studied have already past the stage of peak runoff and total runoff will likely decrease 2-30% as the glaciers continue to retreat.

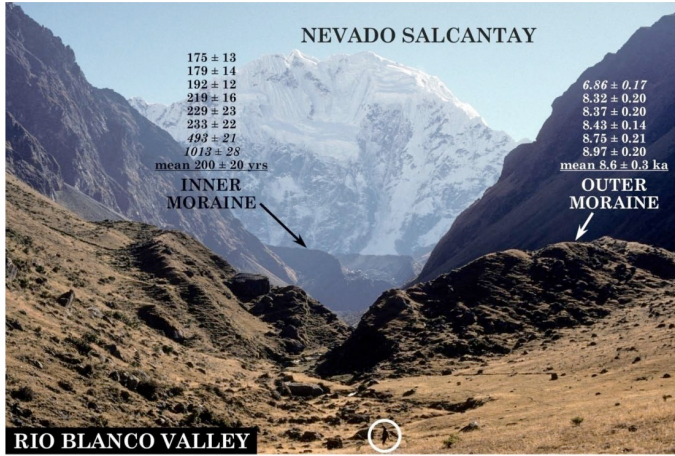


Figure 3: The view north towards Nevado Salcantay, showing the inner and outer moraines dated by Licciardi et al. (2008)

glacier recession also creates significant hazards in the form of glacier lakes (Drenkan et al., 2018). Between 1988 and 2018 in the VUB, lakes adjacent to glaciers have grown by 15.5%, 18.3%, and 9.7% in area, number, and volume respectively. These lakes pose hazards, as their moraine dams can suddenly failed generating destructive floods (Glacial-lake outburst floods; GLOFs).

Salcantay region

On a centennial timescale, glaciers in many places around the globe have been retreating since the Little Ice Age (LIA), a period of relatively cold conditions between 1300 and 1860 C.E. (Common Era). Past glacial maxima are recorded in the position of moraines – piles of sediment deposited at the margins or terminus of the glacier tongue. Licciardi et al. (2008) used exposure dating of material recovered from multiple sets of moraines in the vicinity of Humantay Lake and Nevado Salcantay (Figure 2; immediately to the south of Machu Picchu), to show that the glaciers in this region last retreated from a temporary maximum position around 1800 C.E.

We will visit the Humantay Lake, Tucarhuay Valley (Figure 2). The lake has formed in a basin created by the LIA moraines of one of the three glaciers studies by Licciardi et al. (2008). Further north along the Rio Blancho Valley from Humantay Lake is a larger set of well-preserved moraines generated by glaciers that flow down from Nevado Salcantay (Figure 2). Figure 3 shows the view northwards along the valley towards the Nevado Salcantay.

In one region we will visit, the Vilcanota-Urubamba basin (VUB; Figure 1; the basin containing Cusco), Drenkham et al. (2018) predict under RCP 8.5 (the business-as-usual emissions scenario) that 5.5 km³ of potable water will be lost from glaciers. These authors highlight the significance of this by estimating that if Cusco city's population (currently ~450,000) increases at 1% per year, this volume represents 58 years of the city's water supply.

Along with decreasing water resources,

Figure 4 shows two time-separated Google Earth satellite images. Clear changes in the area inside the moraines suggests that this is ice-cored moraine that has survived since the LIA despite being at a relatively low elevation, through the insulating effect of the debris.



Figure 4: Two Google Earth images showing changes in the surface of the debris field between the LIA moraines in the Rio Blancho Valley south of Nevado Salcantay.

References

- Bintanja, R., 1999. On the glaciological, meteorological, and climatological significance of Antarctic blue ice areas. *Reviews of Geophysics*, 37(3), pp.337-359.
- Bradley, R.S., Vuille, M., Diaz, H.F. and Vergara, W., 2006. Threats to water supplies in the tropical Andes. *Science*, 312(5781), pp.1755-1756.
- Baraer, M., Mark, B.G., McKenzie, J.M., Condom, T., Bury, J., Huh, K.I., Portocarrero, C., Gómez, J. and Rathay, S., 2012. Glacier recession and water resources in Peru's Cordillera Blanca. *Journal of Glaciology*, 58(207), pp.134-150.
- Bury, J.T., Mark, B.G., McKenzie, J.M., French, A., Baraer, M., Huh, K.I., Luyo, M.A.Z. and López, R.J.G., 2011. Glacier recession and human vulnerability in the Yanamarey watershed of the Cordillera Blanca, Peru. *Climatic Change*, 105(1-2), pp.179-206.
- Drenkhan, F., Guardamino, L., Huggel, C. and Frey, H., 2018. Current and future glacier and lake assessment in the deglaciating Vilcanota-Urubamba basin, Peruvian Andes. *Global and planetary change*, 169, pp.105-118.
- Evatt, G.W., Abrahams, D., Heil, M., Mayer, C., Kingslake, J., Mitchell, S.L., Fowler, A.C. and Clark, C.D., 2015. Glacial melt under a porous debris layer. *Journal of Glaciology*, 61(229), pp.825-836.
- Huss, M., Farinotti, D., Bauder, A. and Funk, M., 2008. Modelling runoff from highly glacierized alpine drainage basins in a changing climate. *Hydrological processes*, 22(19), pp.3888-3902.
- Licciardi, J.M., Schaefer, J.M., Taggart, J.R. and Lund, D.C., 2009. Holocene glacier fluctuations in the Peruvian Andes indicate northern climate linkages. *Science*, 325(5948), pp.1677-1679.

- Nicholson, L. and Benn, D.I., 2006. Calculating ice melt beneath a debris layer using meteorological data. *Journal of Glaciology*, 52(178), pp.463-470.
- Östrem, G., 1959. Ice melting under a thin layer of moraine and the existence of ice cores in moraine ridge. *Geografiska Annaler*, 41, pp.228-230.
- Sicart, J.E., Hock, R., Ribstein, P., Litt, M. and Ramirez, E., 2011. Analysis of seasonal variations in mass balance and meltwater discharge of the tropical Zongo Glacier by application of a distributed energy balance model. *Journal of Geophysical Research: Atmospheres*, 116(D13).
- Vuille, M., Francou, B., Wagnon, P., Juen, I., Kaser, G., Mark, B.G. and Bradley, R.S., 2008. Climate change and tropical Andean glaciers: Past, present and future. *Earth-science reviews*, 89(3-4), pp.79-96.

Peru's Deserts and Sand dunes

Bar Oryan

The western coast of South America is home to one of the longest and driest deserts on Earth. This arid piece of land stretches for about 3600km from northern Peru down to Santiago, Chile. This part of the field guide will cover the basic principles leading to the formation of aridity along the pacific coast of South America. It will also briefly describe the general phenomena leading to the formation of sand dunes formation and the dunes we will visit during our trip.

Generally, deserts are divide into a few major types (1)Subtropical deserts (2) Deserts formed in rain shadows (3) Costal deserts formed along cold ocean currents (4) Desert formed in the interiors of continents (5) Deserts of polar region (Marshak, 2015).

Deserts formed in subtropical latitudes are often the result of the high evaporation rates at tropical latitudes. High solar radiation at low latitudes causes hot air with high water content to raise. As it rises, it expands, cools and loses its water content in the form of precipitation. As these parcels of dry air reaches subtropical latitudes they have already lost most of their water content and sinks as dry air. Deserts form in rain shadows are formed due to somewhat similar phenomena. As air with high moisture content is raising above a mountain range it loses most of its water as it cools. By the time it reaches the other side of the mountain rage it has lost most of its water content and does not participate anymore(Figure 21).

Costal deserts are often formed due to cold ocean currents. Cold ocean currents carry cold water relative to the ambit air temperature. The ocean water brings the temperature of the air down and decreases its capacity to hold humidity. This air evidently will absorbs the water content from the adjacent costal land (Marshak, 2015;Figure 22). The Namib desert is an example of such a desert.

There is some uncertainty in the literature regarding the prominent reason for the formation of the desert along the western coast of South America. It has been suggested that the prominent cause for the hyper aridity along the western coast is the closing of the American seaway around 3Ma and the enhanced Humboldt current(Figure 23) it caused (HARTLEY, 2007). It has been also argued that the onset of hyperaridity coincide with the uplift of the Andes (Figure 24) which suggests that the prominent reason is the rain shadow (Rech et al., 2010). It is worth nothing that the prevailing surface winds in the region are the southerly trade winds bringing moisture from the Amazon region. We can conclude with a general statement claiming that the Humboldt current, the prevailing surface winds, and the Andes all conspire to deliver cold, dry air to the western shores of the mid and southern coasts of South America. As a result the coasts of Peru receive little rain (Figure 25). In fact the Atacama desert (Figure 25), south of Peru is the driest place on Earth and with some portions of it received no rain between 1570 and 1971.

Sand dunes can be expected to form when three ingredients exist: (1) Aridity (2) Sand (3)Winds. Aridity is a key factor in the formation of sand dunes as they prevent the growth of vegetation that keeps dunes stable. Once all these three condition exists sand can be moved around by surface winds until encountering obstacles. The obstacle could block the movement of the sand so it will grow around the obstacle. Eventually the obstacle will be buried by the sand and a new

dune will be formed (Figure 26). A few major types of sand dunes exists. The difference between them is usually define by the amount of sand available and the strength of winds (Marshak, 2015). Longitude sand for examples dunes are formed in regions in with strong winds and plenty of sand. Other types of sand dunes are shown in *Figure 27*.

Peru has all the conditions to allow for the formation of sand dunes. As was described above aridity is a prominent feature of the coasts of Peru. Moreover, it can be expected that the erosion of the Andes will generate sand. Lastly as shown by Gay (2005) surface winds is also a feature of costal Peru.

As described in great detail by Haney and Grolier (1991) there are many sand dunes along the coasts of Peru. We will be visiting the sand dunes in Huacachina oasis, nearby Ica. The sand dunes there consist of a mixture of quartz sand that was formed in the Holocene and Pleistocene. Sand dunes in the region include a few type types such barchan, parabolic and star and (Haney and Grolier, 1991). Surrounded by the Huacachina sand dunes is the Huacachina lake. It is a small lagoon that is being feed by the Ica-Villacurí aquifer. The Ica-Villacurí is the biggest aquifer in Peru holding 40% of the national available groundwater resources (Schwarz and Mathijs, 2017).

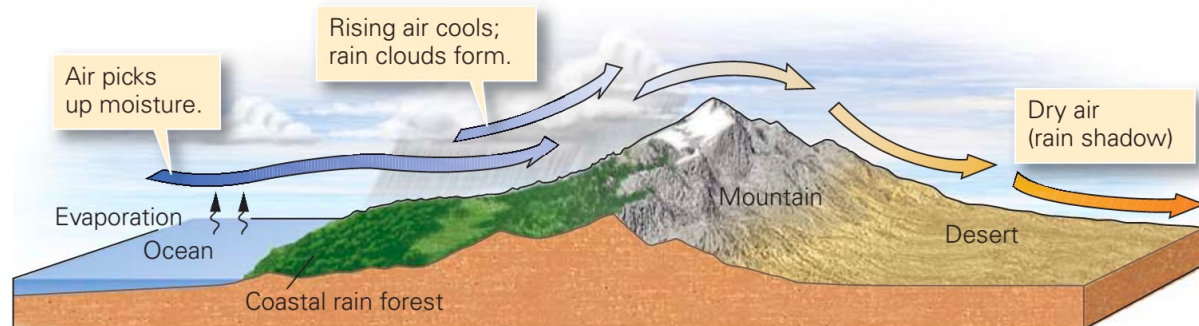


Figure 21 – Carton illustrating the formation of rain shadows deserts. From Marshak, 2015.

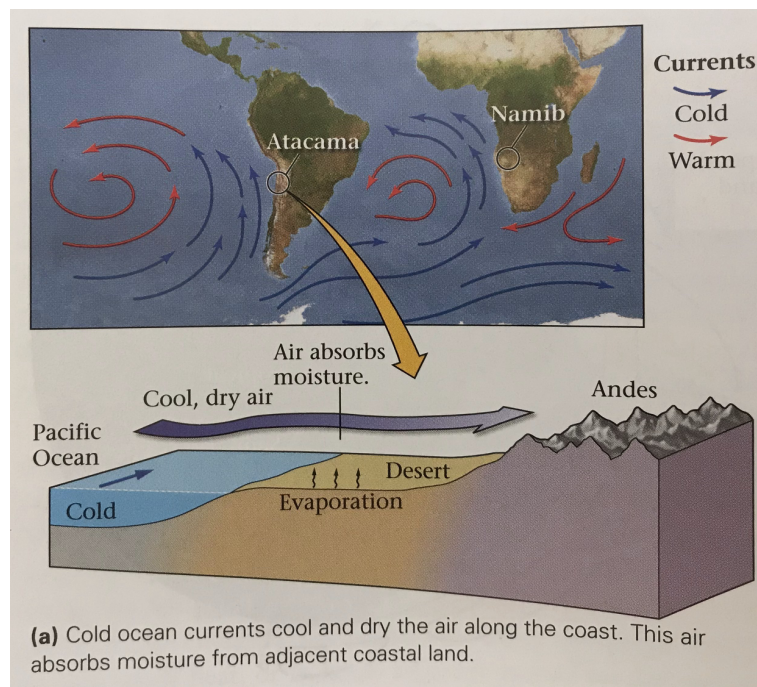


Figure 22 – Carton illustrating the formation of deserts along cold currents. From Marshak, 2015.

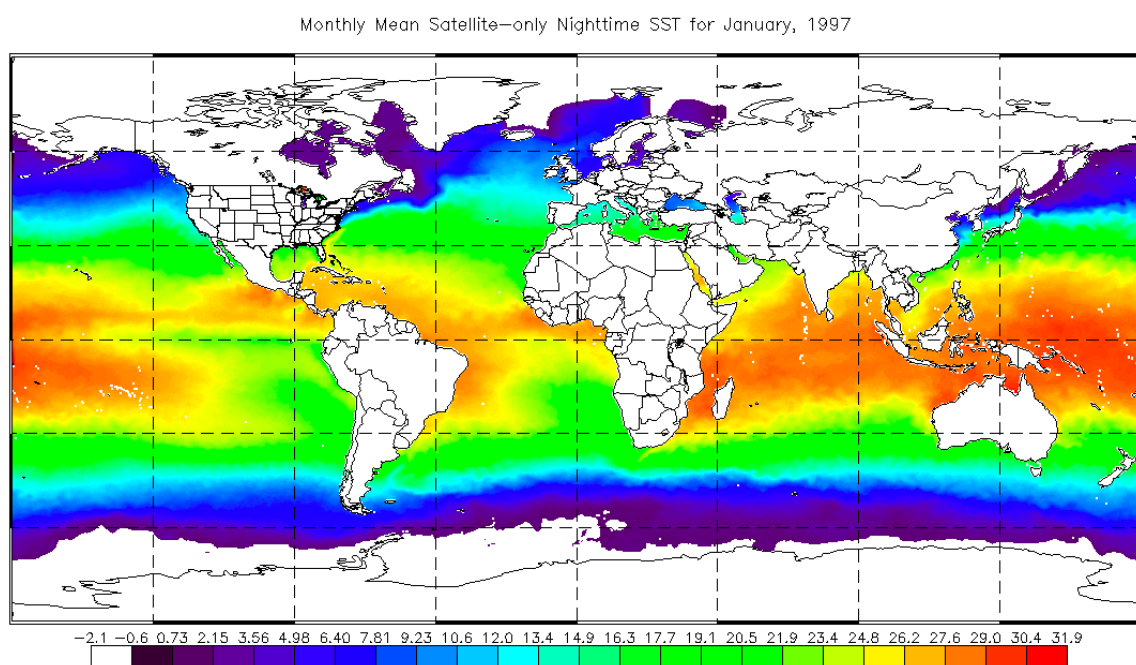
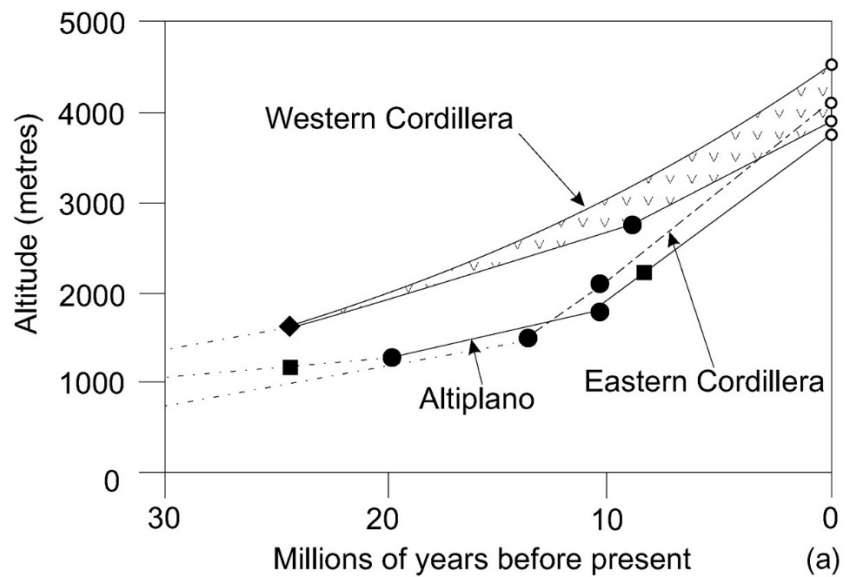
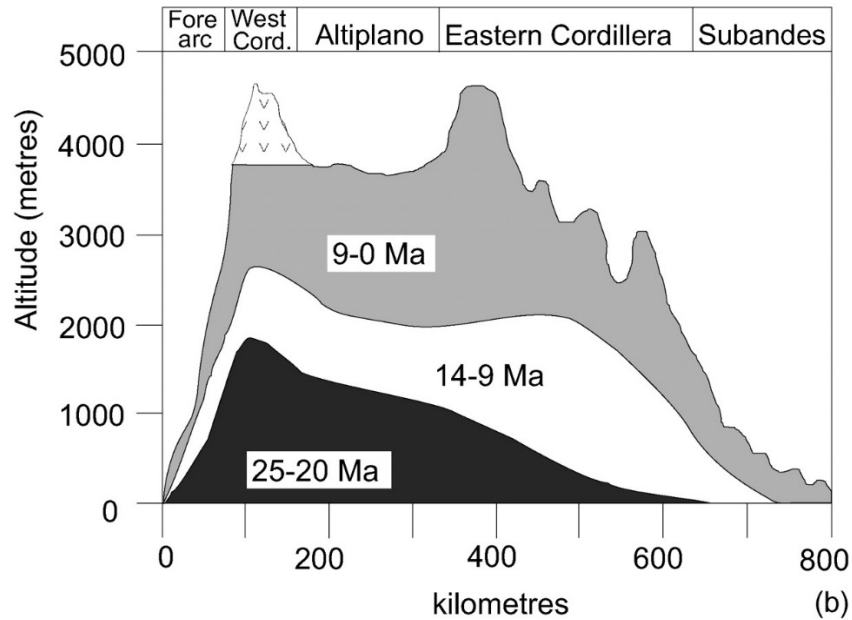


Figure 23 – Surface temperature of the oceans in January 1997 showing the cold Humboldt current.



(a)



(b)

Figure 24 – Upper section: Estimated elevation through time for the Western Cordillera, Altiplano and Eastern Cordillera. Circles, diamonds and squares show data points from different sources. Lower section: Schematic west–east cross-section showing elevation at 18°S. From HARTLEY, 2007.

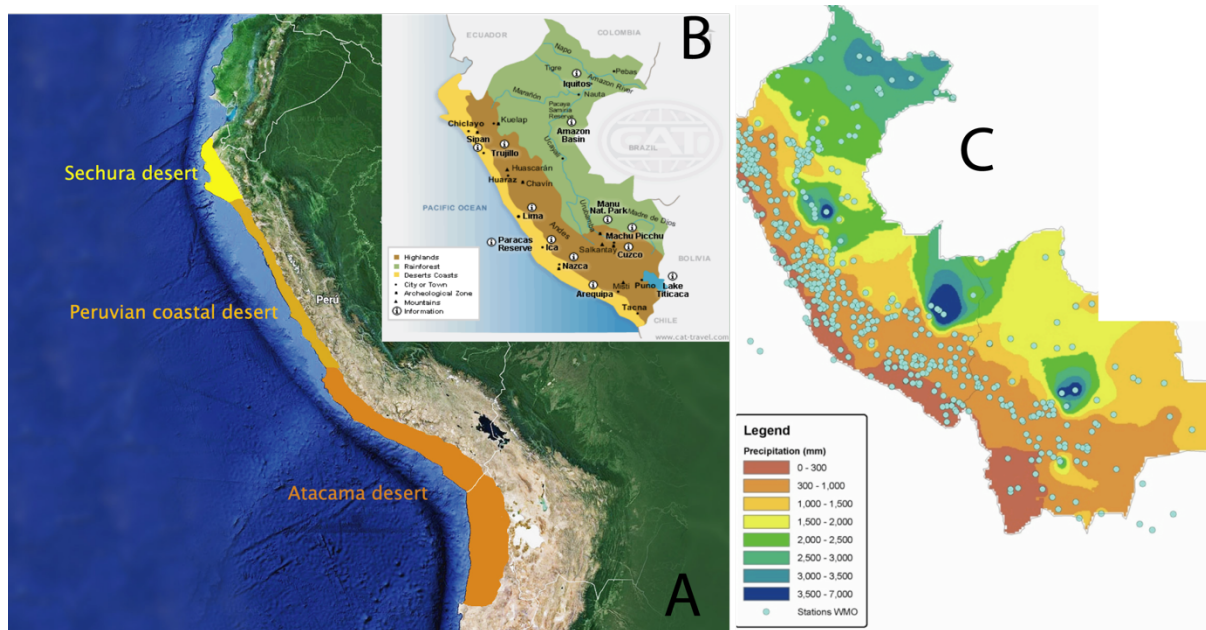


Figure 25 (A) Different deserts along the pacific coast of South America. (B) Different climate regions in Peru. Green, brown and yellow indicate rainforests, high lands and deserts coasts respectively. (C) Precipitation in Peru as indicated by the color bar.

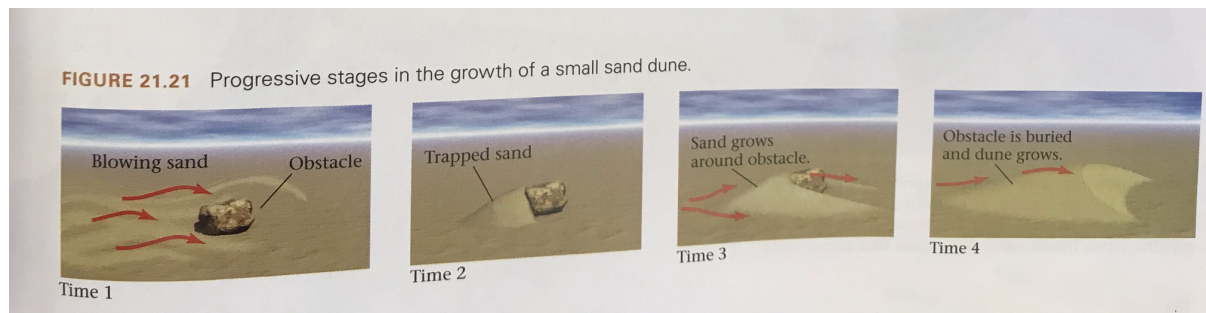


Figure 26 – A cartoon showing the formation of sand dunes.

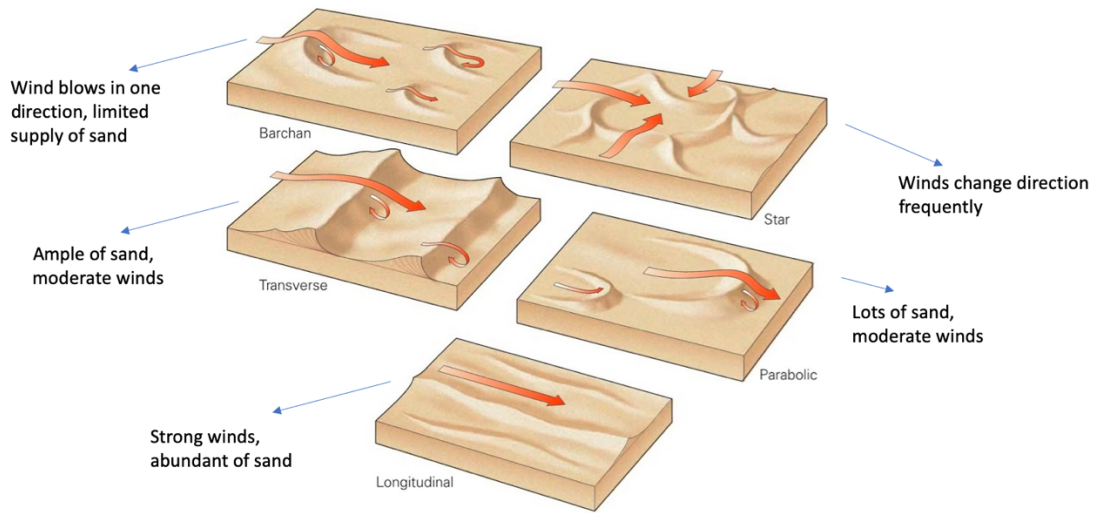


Figure 27 – An illustration showing different types of sand dunes and the conditions leading to their formation.

References

- Haney, E.M., Grolier, M.J., 1991. Geologic map of major quaternary eolian features, northern and central coastal Peru.
- HARTLEY, A., 2007. Andean uplift and climate change. *J. Geol. Soc. London.*
<https://doi.org/10.1144/0016-764902-083>
- Marshak, S., 2015. Earth: Portrait of a Planet: Fourth International Student Edition. WW Norton & Company.
- Rech, J.A., Currie, B.S., Shullenberger, E.D., Dunagan, S.P., Jordan, T.E., Blanco, N., Tomlinson, A.J., Rowe, H.D., Houston, J., 2010. Evidence for the development of the Andean rain shadow from a Neogene isotopic record in the Atacama Desert, Chile. *Earth Planet. Sci. Lett.* <https://doi.org/10.1016/j.epsl.2010.02.004>
- Schwarz, J., Mathijs, E., 2017. Globalization and the sustainable exploitation of scarce groundwater in coastal Peru. *J. Clean. Prod.* <https://doi.org/10.1016/j.jclepro.2017.01.067>

Coastal Geomorphology in Peru

Lloyd Anderson

Background

The coast of Peru is located on the active convergent margin of western South America, where the eastward-moving Nazca plate subducts beneath the South American plate. Because sediments eroded from the continent are lost in the associated subduction trench, the continental shelf off the Peruvian coast is narrow relative to the global average and especially narrow compared to the continental shelf off the passive margin of eastern South America, as visualized in the bathymetric map in Image 1.

Geomorphology along the Peruvian coast can give insights into processes that give the coastal region its structures, both large and small in scale. The constant action of surface forces (wind, waves) sculpt island arches and coastal dunes and gradually build beaches, whereas drastic events (earthquakes) initiate tsunamis which can suddenly overprint coastal formations. Over thousands of years, the interplay between crustal uplift and sea level change form marine terraces that stand as relicts of ancient shorelines.



Image 28: Bathymetric map of ocean surrounding South America.

Island Arches: Islas Ballestas

Known affectionately as the “poor man’s Galapagos”, this small archipelago offshore the town of Paracas contains rich biodiversity. These guano-covered, rocky islands also exhibit beautiful rock arches (seen in Image 2). Over thousands to millions of years, the pounding waves along the coastline gradually eroded the island edges. Due potentially to the heterogeneity of bedrock types in these islands, the strength of this erosion was selective, steadily carving these arched openings through “softer” substrates that are less resistant to erosion.



Image 29: Pictures of Islas Ballestas

Beaches in Paracas: Playa Roja (Red Beach)

Much of the Peruvian forearc consists of plutonic rocks, formed deep underground from crystallizing magma. Included in this underlying geology is pink granodiorite, an intrusive igneous rock that has orthoclase feldspar (a type of potassium feldspar) as a primary mineral component. Orthoclase feldspar, sometimes a pinkish mineral, gives pink granodiorite its color (Image 3). Repeated wave-sourced erosion of plutonic cliffs near Paracas results in the disintegration of pink granodiorite, and the physical sorting of sand grains by waves leaves larger, pinkish grains behind. Therefore, the



Image 30: Pink granodiorite

reddish hue of Playa Roja (Image 4) comes from the erosion of pink orthoclase feldspar minerals contained in the coastal bedrock.



Image 31: Playa Roja (Red Beach) in Paracas

Coastal Dunes in Paracas

One of the most prominent features along the coast in Paracas is a combination beach/foredune topography (Figure 1). The dominance of this topography along the inner arc of the Bahia De Paracas is a result of prevalent and strong diurnal winds in this region (Psuty, 2005). In the afternoon and into the evening, a strong land breeze commonly springs up as the land surface cools more slowly than the ocean, setting up a strong convection cell with a low pressure system over the ocean surface and surface winds blowing offshore. Observing surface winds as high as 50 kmph, the authors attributed the typical foredune profiles along the Bahia De Paracas (Image 5) to offshore sediment transport (Psuty, 2005). In their schematic, sand grains carried offshore by these strong diurnal winds both build up these dunes and contribute to beach

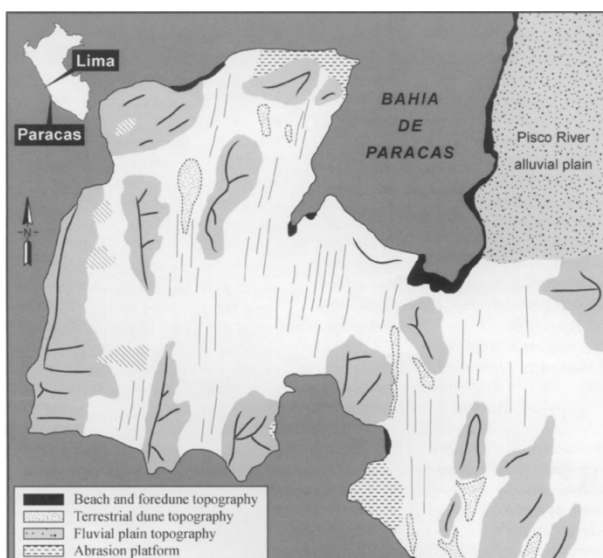


Figure 1: Geomorphology of Paracas Peninsula (Figure 2 in Psuty, 2005)



Image 5: Foredune crest on Paracas Peninsula (Figure 5 in Psuty, 2005)

progradation (positive sediment mass balance), leading to beach growth over time. These observations and hypothesis for the direction

of sediment transport is supported by the observations of north-south “yardangs” on the Paracas Peninsula, grooved formations that have been etched into the land surface by eolian erosion (Figure 1).

Preservation of Tsunami Deposits

In 2007, an earthquake of moment magnitude 8.0 emanating from the interface of the South American and subducting Nazca Plates initiated a tsunami off the coast of central Peru. The highest “runup height” of the tsunami (maximum 10 meters) occurred on the southern edge of the Paracas Peninsula, with weaker propagation of tsunami runup curving around the peninsula and into locations on the northern Bahia De Paracas (Fritz et al., 2008; Figure 2). Because of the tsunami location and direction of wave propagation, the potential of tsunami deposits to be preserved is quite different depending on location on the Paracas Peninsula. A study looking at the remnants of these tsunami deposits a year after the event noted that locations such as Playa Yumaque on the southern coast of the peninsula exhibited clear large-grained tsunami sand layers along the coast, as well as observable ripples created by the tsunami runup that happened a year prior (Spiske et al., 2013; Figure 3). On the northern coast of the peninsula near the Paracas park entrance, the only observable tsunami deposits were eroded backwash channels (Spiske et al., 2013; Figure 4). The authors attributed these differences to the differences of tsunami deposits carried to each location as well as the preservation potential of sedimentary deposits at each site. For example, deposits were less likely to be preserved on the northern coastline of Paracas because only smaller-grained tsunami deposits had been carried that far, and the high wind energy at that location accelerated erosion

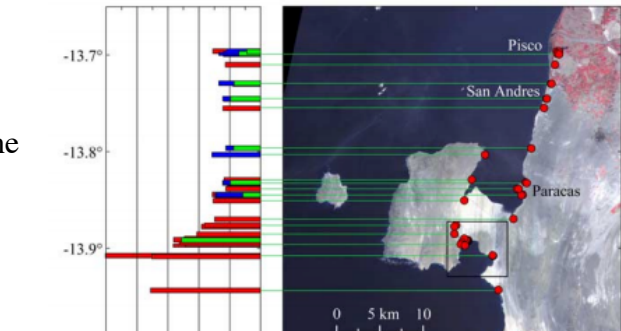


Figure 2: Measured tsunami heights and runup on a) Paracas Peninsula, from 2007 tsunami. Red bars indicate runup height. (Figure 2A in Fritz et al., 2008).

and eradication of the fine-grained tsunami and erosional structures of the Pisco-Paracas tsunami. a) Scouring at Lagunillas (ca. 40 m from shoreline). b) Erosional backwash channel close to the Paracas National Park

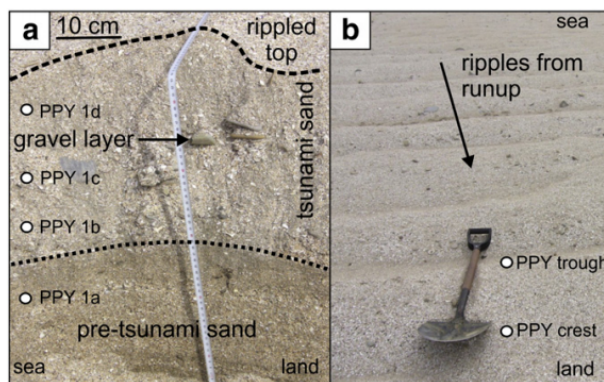


Fig. 8. Tsunami deposits (ca. 90 m from shoreline) and related grain size analysis at Playa Yumaque. a) Shelly tsunami sand with gravel layer and rippled top. b) Run-up ripples on Figure 3: Tsunami deposit evidence from the southern shore of the Paracas Peninsula (Figure 8 in Spiske et al., 2013)

deposits over time (Spiske et al., 2013).



Fig. 10. Erosional structures of the Pisco-Paracas tsunami. a) Scouring at Lagunillas (ca. 40 m from shoreline). b) Erosional backwash channel close to the Paracas National Park

Figure 4: Tsunami deposit erosion on the northern shore of the Paracas Peninsula (Figure 10 in Spiske et al., 2013)

Marine Terraces at San Juan de Marcona and Chala

The coastline between Paracas and Camana contains beautiful examples of marine terraces, specifically at San Juan de Marcona and Chala. Marine terraces, or paleo-shorelines, are created when the combined forces of crustal uplift and wave-cut erosion create “abrasion platforms”: Persistent ocean waves cut into a rocky shoreline and over thousands of years the resulting shallow rocky platform is uplifted beyond the reach of the eroding sea. Globally, these marine terraces commonly correspond to past sea level “highstands” (for example, interglacial periods during the Quaternary when climate was warm and continental ice volume was low).

At San Juan de Marcona, four uplifted marine terraces are observed, running parallel to the present-day shoreline and ranging from 150 to 220 meters above sea level (Saillard et al., 2011; Figure 5). Using the ^{10}Be exposure age dating method (which has also been used to assess ice sheet fluctuations in the past, e.g. Schaefer et al., 2016), the authors determined ages for each of these uplifted terraces. They found that terrace ages (e.g. how long ago the underwater abrasion platforms were first exposed to the atmosphere) largely coincided with interglacial periods as defined in the marine oxygen isotope record (Saillard et al., 2011; Figure 6). In addition, since the oldest terrace at this site was around 400 ka, the authors concluded that the region around San Juan de Marcona has been experiencing increasing uplift in the late Quaternary since 400 ka.



Figure 5: Panorama of the Cerro el Huevo marine terrace sequence in San Juan de Marcona (Figure 3A in Saillard et al., 2011)

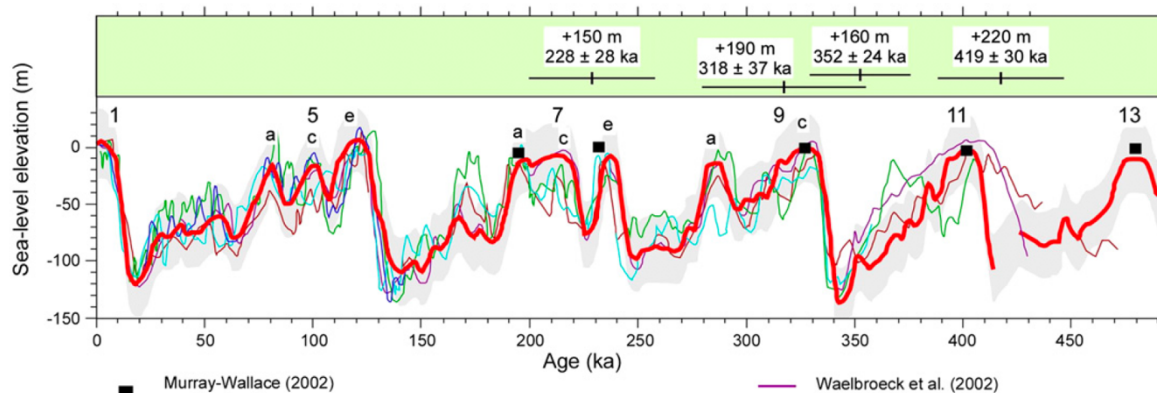


Figure 6: Correlation of marine terrace ages to marine isotopic stages (MIS) from the eustatic curve of Siddall et al. (2006 and references therein). +150, +160, +190, +220 m are names of the dated marine terraces of the San Juan de Marcona area and their respective age. (Figure 5 in Saillard et al., 2011)

At Chala exist slightly different landforms called “rasa”, essentially gentle sloping platforms spreading from a cliff foot out to the shoreline (Regard et al., 2010; Figure 7). This particular rasa extends along 1500 km of coastline in this region. Using the radioactive U/Th

decay series to absolute-date carbonate shells found at this cliff base, the authors discovered that the ages estimated for the cliff base clustered around 400 ka (Regard et al., 2010; Figure 8). Since this cliff base age was consistent throughout the samples collected along the entire 1500 km length of coastline, they argue that this provides evidence for late Quaternary uplift since 400

ka along this Central Andes Forearc region.

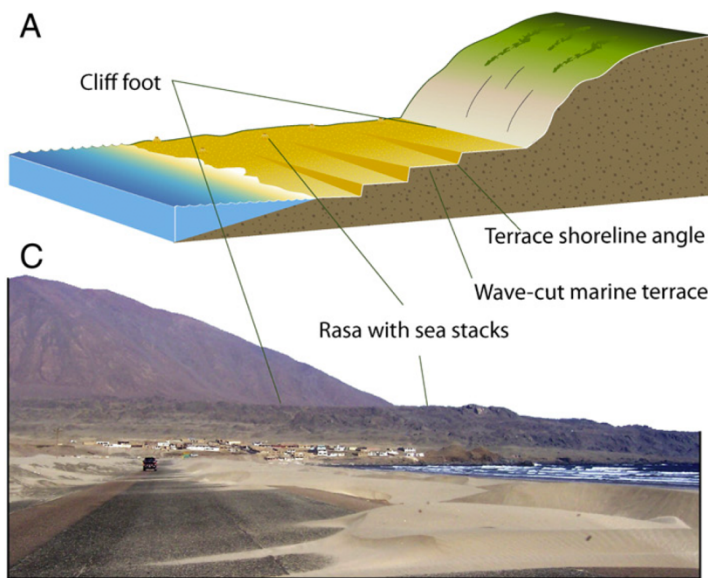


Figure 7: General sketch of a rasa, and a photo of the rasa with cliff and cliff base near Chala (Figure 2A and 2C in Regard et al., 2010)

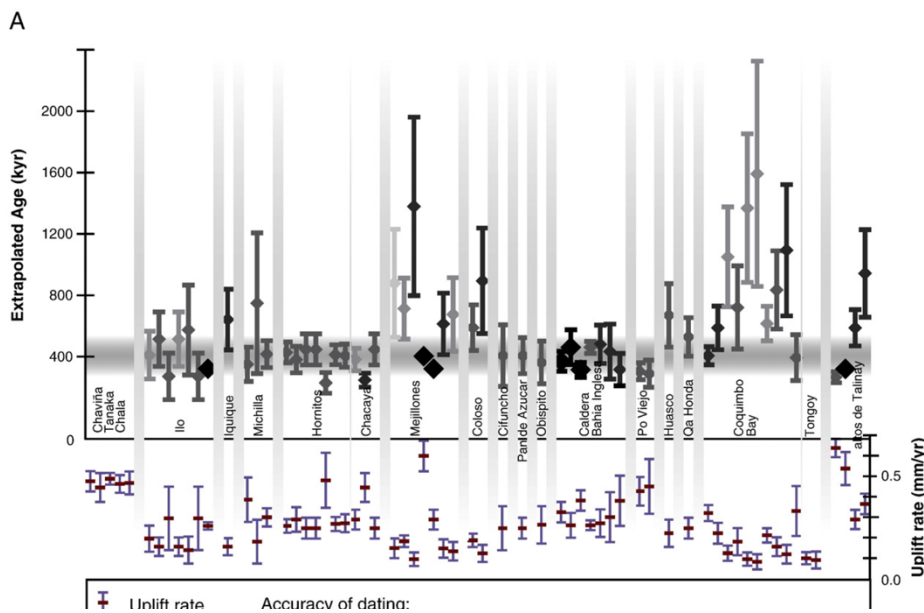


Figure 8: Extrapolation of terrace ages to cliff foot for the main cliff base near Chala. The calculated uplift rates are reported at the bottom. For each site (from north to south), the different evaluations are shown (see Table 1). Extrapolations that seem more reliable than others are highlighted in larger and bolder symbols (see text for why they are more reliable). Most of the extrapolated ages fall in the range, 400 ± 100 ka. (Figure 5A in Regard et al., 2010)

References

- Fritz, H. et al., 2008. "The 15 August 2007 Peru tsunami runup observations and modeling." *Geophysical Research Letters* (35), L10604.
- Psuty, N., 2005. "Coastal Foredune Development under a Diurnal Wind Regime, Paracas, Peru." *Journal of Coastal Research* (42), 68-73.
- Regard, V. et al., 2010. "Renewed uplift of the Central Andes Forearc revealed by coastal evolution during the Quaternary." *Earth and Planetary Science Letters* (297), 199-210.
- Saillard, M. et al., 2011. "Andean coastal uplift and active tectonics in southern Peru: ^{10}Be surface exposure dating of differentially uplifted marine terrace sequences (San Juan de Marcona, $\sim 15.4^{\circ}\text{S}$)."*Geomorphology* (128), 178-190.
- Schaefer, J. et al., 2016.. "Greenland was nearly ice-free for extended periods during the Pleistocene." *Nature* (540), 252-255.
- Siddall, M. et al., 2006. "Eustatic sea-level during past interglacials." In: Sirocko, F., Litt, T., Claussen, M., Sanchez-Goni, M.-F. (Eds.), *The Climate of Past Interglacials*. Elsevier, Amsterdam, pp. 75–92.
- Spiske, M. et al., 2013. "Preservation potential of tsunami deposits on arid siliciclastic coasts." *Earth-Science Reviews* (126), 58-73.

https://www.worldmapsonline.com/np_geo/sa_bathymetric.htm

[https://es.wikipedia.org/wiki/Islas_Ballestas#/media/Archivo:Ballestas_Islands_P%C3%A9rou_2011_\(2\).jpg](https://es.wikipedia.org/wiki/Islas_Ballestas#/media/Archivo:Ballestas_Islands_P%C3%A9rou_2011_(2).jpg)

<https://www.alcademics.com/2015/01/peru-bird-poop-and-the-birth-of-the-agro-industrial-complex.html>

<https://en.wikipedia.org/wiki/Orthoclase>

<https://www.alamy.com/stock-photo-pink-granodiorite-norway-igneousplutonic-rock-containing-quartz-plagioclase-85058833.html>

<https://epod.usra.edu/blog/2014/06/red-beach-peru.html>

Hydrological Happenings: Peruvian Thermal Springs and Salt Mining

Chris Carchedi

Groundwater circulation manifests in a menagerie of geological features across Peru, from gushing geysers heated by deep faults to the mythical “Boiling River” of the Peruvian Amazon to the hypersaline streams in Maras harnessed for salt production since the Incans. This field trip includes trips to a geothermal bath or two as well as a pit stop at the Salterns of Maras, though the following delves into some of Peru’s premier hydrological happenings.

Background: Crustal Heat Flow

Radiogenic heat production is the most prevalent contributor to heat flow in the continental crust and accounts for roughly 25% of total heat flow (Turcotte and Schubert, 2002). Radioactive elements occur preferentially in the crust due to core-mantle differentiation and the continued refinement of crustal material by tectonic recycling. As modeled by Hazma and Silva Dias (2003), regional surface heat flow increases southward within Peru, increasing from 35 to 95 mW/m² with proximity to Peru’s active volcanic features (Figure 1). The lower heat flow measurements in coastal northern Peru are attributed to flat slab subduction. Across South America, lower surface heat flow contours outline the boundaries between tectonically inactive, cold cratons and the warmer Andean subduction system. Note that this model is limited by sparse measurement coverage.

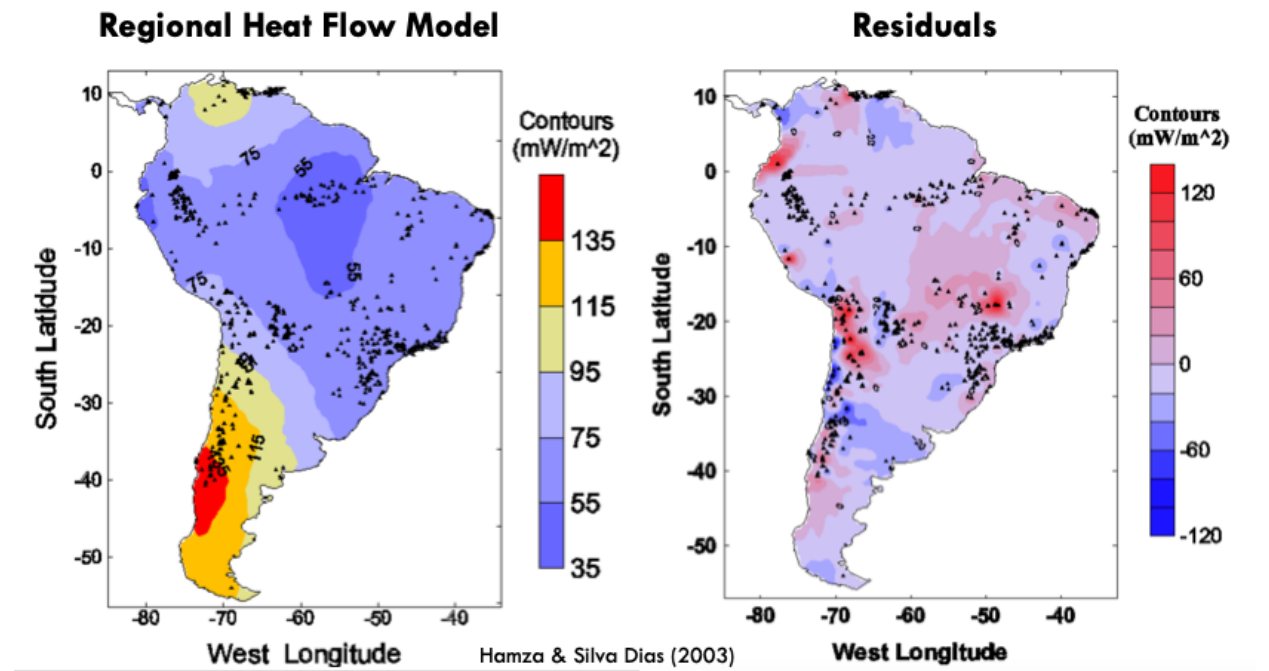


Figure 1: A sixth-degree polynomial fit to regional heat flow data in South America (left) with respective residuals (right). Locations of heat flow measurements marked with black triangles. After Hazma and Silva Dias (2003).

Geothermal Systems in Peru

Today, the Peruvian Geological Survey (INGEMMET) investigates the development of geothermal energy as an environmentally friendly alternative for electric power generation and other direct uses. Since 2010, six geothermal regions have been identified across Peru (Figure 2). From north to south, they are distinguished as (1) Cajamarca-La Libertad, (2) Callejón de Huaylas, (3) Churín, (4) Central, (5) Eje Volcánico Sur, and (6) Cuzco-Puno (Vargas and Cruz, 2010).

The four northernmost regions contain roughly 130 individual geothermal sites with sampled waters reaching up to 65°C. Today, several of these sites are utilized as thermal baths, such as the Baños del Inca with its H₂S and CO₂ steam, La Grama hot springs with more than 100 L/s maximum flow rates, and the acidic sauna Tauripampa in Huanuco. Far from active volcanism, thermal springs in northern Peru warm by deep groundwater cycling, facilitated by fractured and faulted bedrock.

Most of Peru's geothermal sites (> 400 locations) reside near Peru's southern volcanoes in the Eje Volcánico Sur and Cuzco-Puno regions. Waters at these sites can reach temperatures of 90°C at moderate flow rates, making them the most viable for geothermal energy harvesting. Natural features include a number of fumaroles, hot springs, and the Pinchollo geyser in Colca Canyon.

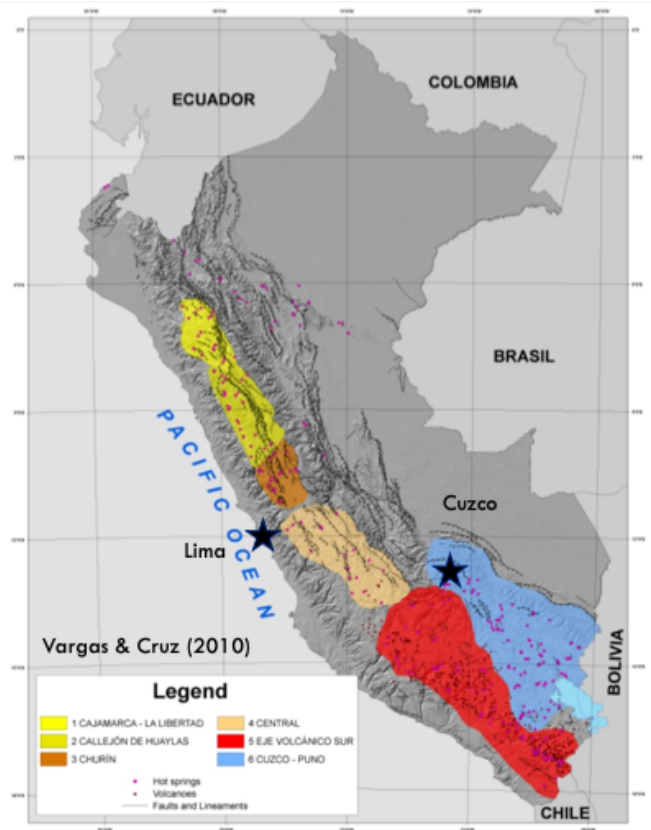


Figure 2: A map of Peru's six geothermal regions, with individual sites marked as pink dots. Eje Volcánico Sur (red) contains the most viable sites for geothermal energy harvesting. Modified after Vargas and Cruz (2010).

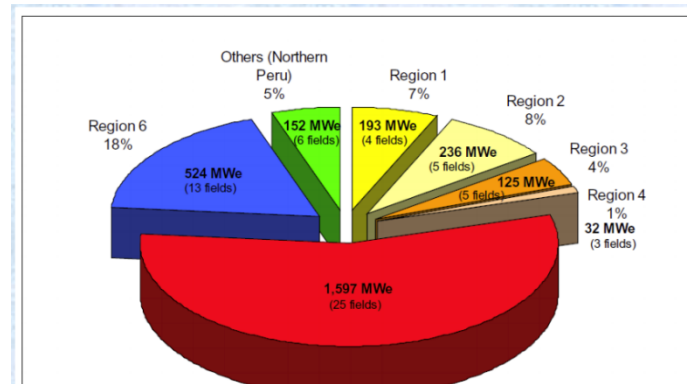
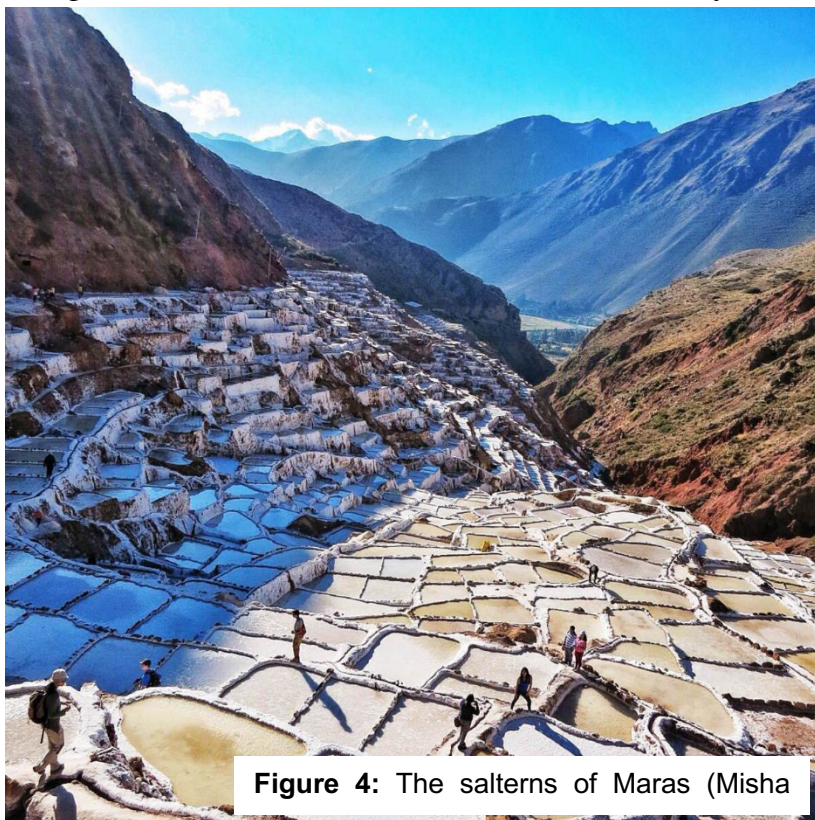


Figure 3: An estimate of potential energy output from geothermal harvesting. After Vargas and Cruz (2010).

The pie chart in Figure 3 estimates the utmost potential for electrical output from Peruvian geothermal regions at

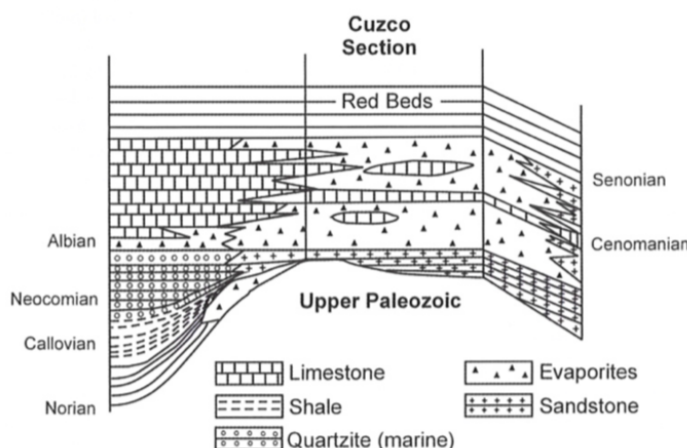
2,860 MWe. As of 2018, only 2.7% of Peru's energy budget originates from renewable sources. In response, the United Nations organized the Peru Initiative for Sustainable Development Goals, with plans to raise the renewable contribution to 25% by 2025 (Richter, 2018).



pool water evaporates, the remaining hypersaline fluid eventually saturates and begins to precipitate salt on the walls of the pool. At 5-10 cm thickness, the salty crust is broken, washed, and stockpiled to dry before sale.

Maras salt is often advertised as “ecological salt” for two reasons. First, without redirection, the hypersaline spring water would flow downhill and contaminate the Urubamba River below. Second, as the inlet spring flows out from the top of the terrace, pool filling does not

require any pumping. However, this simplistic and ecological design of outdoor pools comes with some complications. Precipitation dilutes the open evaporating pools, slowing precipitation. Additionally, contamination from soil runoff and sidewall ruptures can lower the quality of the resulting product.



Interactions between local sediments and groundwater flow produce the hypersaline spring feeding the Maras salterns (Aral et al., 2011). The Maras salt terraces reside within the Yuncaypata Group, as represented in the generalized stratigraphic section provided in Figure 5.

Maras salt terraces reside near the contact between two geological units: the southeast-trending Altiplano and the northwest-trending Eastern Cordillera. Within the Eastern Cordillera, the Yuncaypata Group is a 2000-m thick layer rich in evaporitic, calcerous, and pelitic components

Figure 5: Generalized stratigraphy of the Cuzco area (Aral et al., 2011). The Yuncaypata Group consists of evaporites, limestones, and pelitic formations.

formed from eroded marine components (turbidites, muds, limestones, evaporites, etc.). The Yuncaypata halite layer dates to ~ 110 Ma when the region

was likely covered by the sea prior to the Andean orogeny. Little further research has been done on the Maras salterns, though the pools were featured in a survey comparing the diversity of extremophile microbiota (Maturrano et al., 2006).



References

- Aral, H., M.I. Pownceby, and P. Moreno (2011), Artisanal salt mining in Maras-Urubamba, Cuzco, Peru, *Canadian Institute of Mining, Metallurgy, and Petroleum Journal*, 2 (4), 210-217.
- Hazma, V.M. and F.J.S. Silva Dias (2003), Functional representation of regional heat flow in South America: implications for the occurrence of low-temperature geothermal sources, *Transactions – Geothermal Resources Council*, 1-8.
- Maturrano, L., F. Santos, R. Rosselló-Mora, and J. Antón (2006), Microbial diversity in Maras salterns, a hypersaline environment in the Peruvian Andes, *Applied and Environmental Microbiology*, 72 (6), 3887-3895.

Richter, A., (2018), With growing demand geothermal energy is a real option for Peru's south, *ThinkGeoEnergy*, <http://www.thinkgeoenergy.com/with-growing-demand-geothermal-energy-is-a-real-option-for-perus-south/>.

Turcotte, D.L. and G. Schubert (2002), *Geodynamics (Second Edition)*, Cambridge, UK, 456.

Vargas, V. and V. Cruz (2010), Geothermal map of Perú, *Proceedings World Geothermal Congress 2010*, 1-7.